LBL-24762
Preprint

Lawrence Berkeley Laboratory
UNIVERSITY OF CALIFORNIA

Materials & Chemical
Sciences Division

Submitted to Progress in Solid State Chemistry

Thermalization of Excitons

P.Y. Yu

January 1988

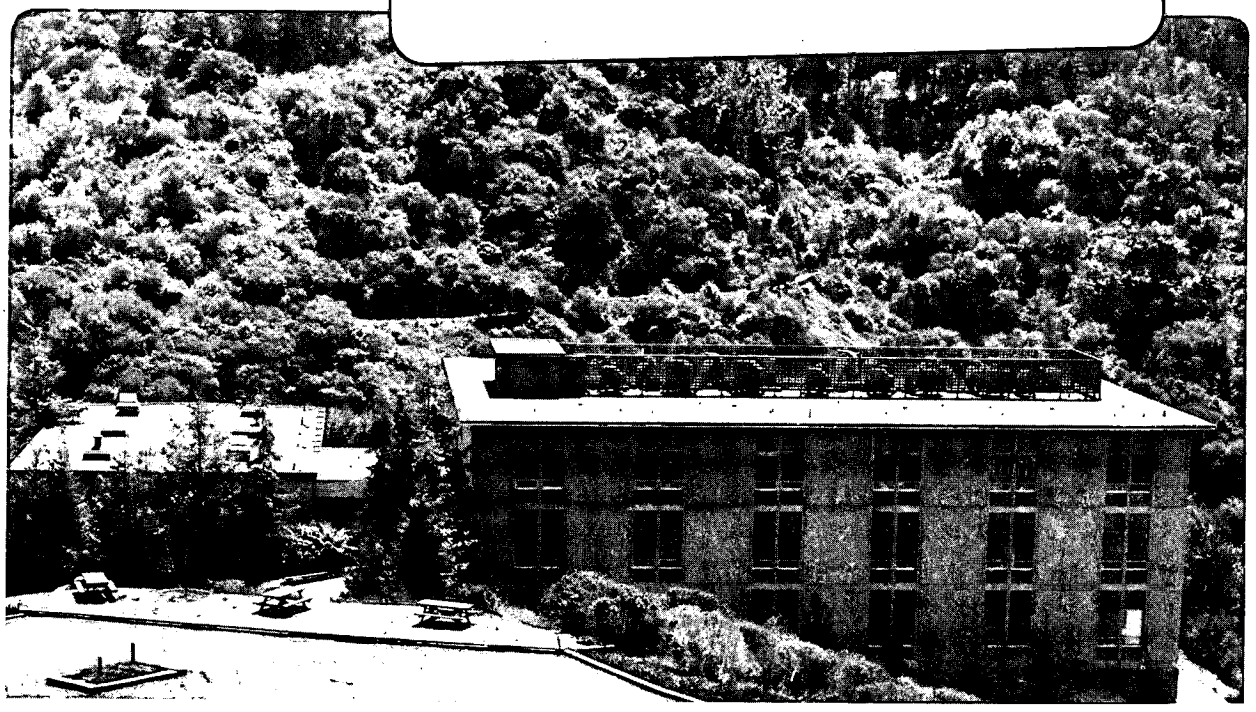

Prepared for the U.S. Department of Energy under Contract DE-AC03-76SF00098

DISCLAIMER

To be Published in Prog. in Solid State Chem.

THERMALIZATION OF EXCITONS

PETER Y. YU

Department of Physics, University of California, Berkeley,
and Materials and Chemical Sciences Division,
Lawrence Berkeley Laboratory, University of California,
Berkeley, California 94720

ABSTRACT

Recent studies of the thermalization of excitons by the use of picosecond time-resolved luminescence are reviewed. These studies have led to a better understanding of exciton-phonon interactions and the dynamics of exciton relaxation processes. Examples of experimental results have been selected from a variety of semiconductors ranging from semiconductors with forbidden or indirect bandgaps, alloy semiconductors to amorphous semiconductors.

PACS: 71.36.+C; 71.38.+i; 78.55. Ds

I. INTRODUCTION

Thermalization means the achievement of thermal equilibrium. In this article we will be interested in how physical systems achieve thermal equilibrium after optical excitation. Actually we are not always interested in how a system returns to true thermal equilibrium. Often we are interested only in how a part of the system attains thermal equilibrium and this is sometimes known as a quasi-equilibrium. However, for the sake of brevity, I will refer to all processes which enable a system or subsystem to relax towards thermal equilibrium or quasi-equilibrium as thermalization. The word "exciton" will also be used in this article in a broad sense. Exciton usually denotes a bound state of an electron and a hole in solids, I will consider mobile electrons and holes not bound to each other as continuum states of an exciton. This more general definition of excitons allows me to discuss the thermalization of electron-hole plasmas in semiconductors also.

The study of how systems relax and thermalize has been going on for years. This review article becomes necessary as a result of recent advances in short laser pulse technology. In solids there are typically a large number of electrons. In addition to electron-electron interactions, the electrons interact with lattice vibrations and with electromagnetic radiations. These interactions are often strong in solids and as a result excitons relax and thermalize in times varying from nanoseconds to femtoseconds. Such short time durations made a real time study of thermalization of excitons very difficult if not impossible in the past. Recent advances in short laser pulse technology made it possible for the first time to study these thermalization processes in condensed systems in real time. The purpose of this article is to review some of the recent time-resolved studies of thermalization of excitons in semiconductors. This article is not meant to be exhaustive and only representative examples have been chosen to illustrate the physical principles involved. In particular I want to point out some of the subtleties in the interpretation of the time-resolved photoluminescence experiments. It is hoped that by comparing the results in different systems this article will serve as a guide to understanding time-resolved studies of thermalization in less understood solids.

The organization of this article is as follows. In the next section I will survey the present status of experimental techniques available for performing time-resolved studies. Since many articles have already appeared on the generation of short laser pulses, the emphasis of that section will be on matching the detectors to the available light sources. As will be shown, the time resolution of an experiment is often not limited by the light source but rather by the detector. In Section III the theortical background for understanding relaxation processes in solids is reviewed. In the section following that the results in six different material systems are reviewed. That section has purposely been ordered in the following fashion. I will start out by considered crystals where excitons are not strongly coupled to radiation. The crystals involved either have indirect bandgaps or direct bandgaps with a forbidden electric dipole transition. Because these excitons are not strongly coupled to radiation their lifetimes are relatively long and they can achieve quasi-equilibrium. Next I will consider crystals where excitons couple strongly to radiation and their properties have to be understood within the framework of coupled modes known as polaritons. The formation of such coupled modes turns out to have profound effects on the thermalization of excitons. At low temperatures the polaritons do not achieve thermal equilibrium. Although this system is an example of a nonthermal equilibrium system, its dynamics is now fairly well understood. It serves as an introduction to semiconductor alloys whose dynamics are more complex. In semiconductor alloys, excitons do not reach thermal equilibrium at low temperatures also because when their energies decrease below the mobility edge, they become localized by the random crystal potential fluctuations. The alloys form a bridge to understanding the relaxation of excitons in completely disordered solids such as amorphous Si. Finally I will consider the case when the exciton density is high enough that they ionize to form electron-hole plasmas. The relaxations in these solid state plasmas occur on femtosecond time scale so they represent the frontier where further studies need to be carried out.

II. EXPERIMENTAL TECHNIQUES

In many solids excitons have recombination times of the order of nanoseconds. Quite often these excitons relax via exciton-exciton (e-e) or exciton-phonon (e-p) interactions. The rates for these interaction can vary from 10^{10} sec^{-1} for acoustic phonons to about 10^{13} sec^{-1} for longitudinal optical phonons. Thus to perform time-resolved studies in solids, it is necessary to have an experimental setup capable of generating and detecting optical pulses of picosecond (ps) and subpicosecond durations. This section will be divided into two parts: the first part is devoted to surveying the various lasers available for generating short laser pulses and the second part deals with techniques for detecting short pulses.

A) Generation of Short Pulses

Nowaday pulses of ps and fs durations are mostly generated by modelocked lasers.[1,2] Although there have been time-resolved experiments performed with subnanosecond incoherent light pulses,[3] the time resolution was much poorer than what could be achieved with lasers so I will not consider these incoherent sources here. Nowadays the most commonly used modelocked lasers are based on either dye molecules or Nd ions introduced into hosts such as glass or Yttrium Aluminum Garnet (YAG). Dye lasers have the advantages of being tunable and of being able to produce the shortest laser pulses (less than 10 fs duration).[4] The Nd:Glass laser is capable of producing pulses with the highest energy and of durations of several ps.[1] High energy fs pulses can be generated from modelocked dye lasers by amplification. Recently, it has been shown that, by using the technique of pulse compression, the output pulse of many laser systems can be compressed into the subpicosecond regime.[6-8] Thus the choice of available laser systems for time-resolved studies is wider than ever. I have summarized in Table 1 the characteristics of some common laser systems appropriate for time-resolved spectroscopies. This table is not meant to be complete. For example, I have omitted modelocked color center lasers[9] and semiconductor lasers[10] since these lasers have not been used in time-resolved spectroscopies as extensively as the other modelocked lasers. The advantages and disadvantages of individual systems are discussed in more detail below.

(1) Nd:glass and Nd:YAG Lasers

The advantage of the Nd:glass lasers is their high power. In the early days of picosecond laser spectroscopies, they were the only lasers with enough power to trigger optical Kerr cells. Their disadvantage is their low repetition rate. As a result, Nd:YAG lasers with repetition rates of up to about a hundred pulses per second have replaced the Nd:glass lasers for time-resolved experiments. The Nd:YAG lasers are also used to amplify the output of ps and fs dye lasers. The modelocked continuous wave (cw) Nd:YAG lasers, after frequency doubling, now compete with the modelocked cw Ar ion lasers as the pump for active modelocking of dye lasers. The modelocked Nd:YAG lasers have the advantage of producing shorter pulses than the modelocked Ar ion lasers. Furthermore the output of the modelocked Nd:YAG laser can be shortened to less than 1 ps by pulse compression.[11] When the Nd:YAG laser is frequency-doubled to pump dye lasers, considerable energy remains in the unconverted fundamental beam. This fundamental beam can be combined with the dye laser output to generate tunable picosecond uv pulses. These advantages make the Nd:YAG laser one of the most versatile laser for time resolved spectroscopies.

(2) Dye Lasers

With their wide gain bandwidth dye lasers have always produced the shortest pulse available. Dye lasers can be modelocked either passively or actively.[12] Dye lasers are modelocked actively by pumping the laser synchronously with another modelocked laser such as an Ar^+ laser or Nd:YAG laser. Such systems have been available commercially for some time.[13] They are now tunable over a wide range of wavelengths from near infrared to visible. Their other advantages are their high repetition rate ($>10^7$ Hz) which allows phase-sensitive detection and other signal averaging techniques. In the past actively modelocked dye lasers produce pulses of several ps long, so to produce subpicosecond pulses, either passive modelocking or a hybrid system of synchronous pumping combined with a saturable absorber would have to be used.[14] By using pulse compression the output of actively modelocked dye lasers can now be shortened into subpicosecond duration.

The shortest pulses are still generated by passively modelocked dye lasers. In such lasers there are typically two dye jets, one containing the lasing dye and the other a saturable absorber. By using a ring cavity instead of the usual linear cavity, Shank et al.[15] produced for the first time laser pulses of less than 100 femtosecond duration. Since then their colliding pulse modelocked (CPM) dye laser has been refined to produce pulses as short as 60 fs. Using pulse compression, the pulses can be shortened further to as little as 8 fs.[4] Beside this ability to produce shorter pulses, the CPM lasers have the advantage of being more stable in output power and pulse length since their performance is not sensitive to the laser cavity length. Their main drawback is that their output wavelengths are tunable over a very narrow range around 6200 A. One way to overcome this limitation is to first amplify the femtosecond output of the CPM laser to energy levels of mJ per pulse. Then the laser is focused into a liquid, typically water, to generate a white light cotinuum.[16,17] This weaker continuum, which is also of femtosecond duration, can be used directly to probe the sample. Or else a narrow band filter at the desired wavelength is used to select a part of this continuum for further amplification to form an intense femotosecond coherent pulse. At the time this article was written, CPM lasers were not available commercially. Most researchers fabricated their own CPM laser using information provided generously by Shank's group at the AT&T Bell Laboratories, Holmdel, New Jersey. A schematical diagram of the CPM laser is shown in Fig. 1.

B. Detection of Fast Signals

The technology of detecting short pulses has not kept up with the technology of generating short pulses. To make matters worse, the electrical signals produced by optical pulses from samples can be very weak and require amplification. Electronic amplifiers often do not have response times as short as the incident laser pulses. Thus the most difficult part of a time-resolved picosecond and subpicosecond experiment is the selection of an appropriate detection scheme. In addition, the experiment may involve dispersing the signal spectrally. In doing so the pulses may be broadened temporally due to the uncertainty principle.[18] In most cases the best way to plan a time-resolved experiment is to decide first the spectral resolution required and then use the uncertainty

principle to figure out the appropriate time resolution. The time resolution will decide the detection schemes and laser sources required for the experiment.

I will summarize below the various detection schemes most commonly used for studying thermalization of excitons. The techniques are presented roughly in the order of increasing time resolution. Since the faster detection techniques tend to have lower sensitivity, the techniques are presented in order of decreasing sensitivity.

(1) Time-Delayed Coincidence Photon Counting.[19-21]

This technique is similar to conventional photon counting systems used in most light scattering experiments. The signal from the sample is amplified in a photomultiplier tube (PMT) and the output pulse from the PMT are converted to logic pulses by a discriminator and counted by a counter. It is different from the ordinary photon counting system in that the time delay between the excitation pulse and the signal pulse from the sample is also measured. This time delay is determined by splitting part of the incident laser pulse train to trigger a fast photodiode. The output of the photodiode is also converted into logic pulses by a fast discriminator. The time delay between the photodiode output and the PMT output is determined with a time-to-amplitude converter (TAC). The TAC produces a pulse whose height is proportional to this time delay. By analyzing the height of the pules produced by the TAC with a multichannel analyzer, a histogram of the time dependence of the radiation emitted by the sample is obtained. A schematic diagram of an experimental setup for determining time dependence of photoluminescence based on this photon counting system is shown in Fig. 2.[22]

The obvious advantage of this system is its ability to detect individual photons so it is most useful in experiments where the quantum efficiency of emission is very low, such as less than one photon per incident laser pulse. If the samples emits more than one photon per pulse, the resulting spectrum has to be corrected for this "pulse pileup".[23] Since the quantum efficiency of emission is less than one photon per pulse, the excitation laser must have a high repetition rate. Thus this system is most compatible with the synchronously pumped modelocked dye lasers because of their high repetition rates and low pulse energy. The disadvantage of this system is its time resolution. This is limited essentially by the transit time spread of electrons inside the PMT. Using the fastest

microchannel-plate based PMT available, this system will produce peaks of about 100 ps in width from input optical pulses of zero width.[20] The decay of the emission from the sample can be determined with a precision of better than 100 ps by deconvolving the signal with the system response curve. If the emission from the sample is strong enough to produce a histogram with a good signal-to-noise ration, decay times as short as about 30 ps can be determined with this technique.[24]

(2) Streak Cameras.[1,25,26]

In principle, streak cameras offer the best combination of versatiltiy, time resolution and sensitivity for time resolved experiments. They can be used with both low repetion rate lasers and high repetition rate lasers. Using image intensifier tubes, their sensitivity can be comparable to PMT. They are commercially available and the fastest units have time resolution of about 1 ps. Their biggest drawback is their relatively high price tags which make them beyond the budget of most laboratories. Also it is unlikely that their time resolution can be shortened into the subpicosecond regime in the near future. This limits their usage in femtosecond experiments.

(3) Optical Gating.

When a modelocked laser is powerful enough it can be split into two beams: one is used to excite the sample while the other is delayed and used to "gate" the detector. In this way the detector can have a very slow time response. The time information is obtained by varying the time delay between the excitation pulse and the gating pulse. Various ways of gating the detector have been proposed. Figure 3 shows a "Kerr shutter" operating on the principle that an intense optical pulse can induce an ac Kerr effect in a liquid such as CS_2.[2,27] In the absence of the strong gating beam the signal cannot pass through the two crossed polarizers. In the presence of the gating beam the signal becomes elliptically polarized on passing through the liquid and is subsequently partially transmitted by the analyzer. A different scheme was proposed by Mahr and coworkers.[28,29] In this case the emission from the sample was mixed with a properly delayed excitation beam inside a nonlinear crystal to form the sum frequency. By measuring the sum frequency signal as a function of delay, the emission spectra could again be determined as a function of time. The disadvantage of this scheme is that the emission has to be relatively strong in order to generate a significant amount of sum frequency so the sample must have very

high quantum efficiency. In a recent variation of this technique the strong laser beam is used to pump an optical parametric amplifier to amplify the signal.[30]

The basis of the optical gating techniques is a nonlinear interaction between the signal from the sample and a part of the excitation laser which has been delayed inside some nonlinear optical media. As a result the time resolution of this technique is limited by the response time of the nonlinear medium and by pulse broadening which can occur in the medium due to dispersion effects. These effects limit the time resolution of optical gating methods to the picosecond range. For example, in the method of Mahr using sum frequency generation,if the pulse is of femtosecond duration, dispersion of the nonlinear susceptibility makes it impossible to achieve phase matching over the entire spectral bandwidth of the pulse. If only part of the incident pulse is phase matched, the spectral width of the output pulse will be narrowed and correspondingly the pulse will broaden temporally. One way to avoid this problem is to use a very thin crystal to avoid the phase matching requirement, but this will also decrease the sensitivity drastically. Recently Shah et al.[31] have improved the time resolution of this technique to the subpicosecond regime but it will be difficult to extend this method to fs and still retain good sensitivity.

(4) Excite and Probe Techniques.

One way to overcome the limitation of the optical gating technique is to use the sample as the nonlinear optical medium. In this technique one part of incident laser pulse is split off to excite the sample while the remaining part is time-delayed and used to probe the change in the sample. The excitation pulse must be strong enough to cause some change in the optical properties of the sample. The changes induced by pump pulse can be in the absorption coefficient,[32] reflectivity,[33] luminescence[34] or Raman spectra[35] of the sample. There are several variations of this straight forward excite-and-probe technique. In the transient grating technique,[36] the incident laser is split into three beams (see Fig.4). Two of the beams are focused at an angle on the sample to form an interference pattern; this interference can give rise to either a population grating or a phase grating. The delayed third beam is then deflected by the grating formed by the other two beams. In this way the decay time of the transient grating due to exciton decay or diffusion can be measured. In another

technique known as the equal pulse correlation technique,[37] the pump and probe beams are of equal intensity. As a result of this symmetry between the two beams, the resultant spectra are completely symmetric about the zero time delay. As pointed out by Erskine et al.,[38] this technique is particularly useful for observing a fast decay process overlapping with a much slower decay process. When a fast process is superimposed on a slow process, the slow process will form only a constant background while the fast process will produce a sharp symmetric peak in the equal pulse correlation spectra. Using this technique and deconvolution, Erskine et al.[38] have determined decay times even shorter than the length of the incident laser pulses.

III. THEORY

In this section I will review the theory of excitons and of their interactions with photons and phonons. Armed with the knowledge of these interactions, one can write down rate equations describing the time evolution of the exciton population as it relaxes towards thermal equilibrium. Such rate equations are usually difficult to solve analytically except for the simplest cases. However, nowadays even personal computers are often powerful enough to solve these rate equations numerically.

A) Excitons

Excitons represent the simplest excitations which can be optically excited in an insulator. In this article I will not consider more complicated excitations such as biexcitons or exciton droplets. Let us assume that the electronic band structure of the semiconductor can be represented by two parabolic bands: a band filled with electrons labelled as the valence band and an empty band labelled as the conduction band (see Fig. 4). An incident photon can excite an electron from the valence band to the conduction band, leaving a hole behind. This electron-hole pair will be attracted to each other via Coulomb interaction V(r). Due to the presence of other valence electrons present in the solid, this Coulomb interaction is screened. In semiconductors with band gaps of about 1 or 2

eV or less this screening greatly weakens the Coulomb attraction between the electron and the hole so that V(r) in the solid is given by:

$$V(r) = - e^2/(\epsilon r) , \qquad (1)$$

where e is the electronic charge, r is the distance between the electron and the hole and ϵ is the dielectric constant of the solid. The diagonalization of the electron Hamiltonian including this Coulomb interaction has been studied extensively in the past. The eigenstates consist of correlated electron-hole pairs known as excitons.[39,40] Traditionally excitons are classified as Frenkel excitons or Wannier excitons according to some ill-defined rules. Roughly, if the exciton size (such as given by the Bohr radius in case of Wannier excitons) is smaller or comparable to the interatomic distance the exciton is considered localized around the atoms and is known as a Frenkel exciton. Otherwise the exciton is referred to as a Wannier exciton. In most crystalline semiconductors, such as Si and GaAs, the dielectric constant is of the order of ten while the exciton reduced mass is less than the free electron mass m_o, so the exciton Bohr radii are much larger than the lattice constants. The excitons we will be studying are all Wannier excitons.

In this article I will use the second quantization notation to denote the exciton Hamiltonian:[40]

$$H_x = \sum_{n,k} E_n(\mathbf{k})[a_n^+(\mathbf{k})a_n(\mathbf{k})+1/2] \qquad (2)$$

where $E_n(\mathbf{k})$ denotes the eigenvalue of the exciton in bound state n and with wavevector $\mathbf{k}$, a_n and a_n^+ are the annihilation and creation operators for the exciton. For Wannier excitons, the eigenvalues $E_n(\mathbf{k})$ can be obtained within the effective mass approximation. $E_n(\mathbf{k})$ is given by the expression:[41]

$$E_n(\mathbf{k}) = E_g - \frac{\mu R}{n^2 \epsilon^2 m_o} + \frac{\hbar k^2}{2M} \qquad (3)$$

In Eq. (3) Eg is the energy gap between the conduction and valence band, R is the Rydberg constant (=13.6 eV), μ is the reduced mass of the exciton, and M is the total mass of the exciton. In terms of the effective masses m_e and m_h of the electron and hole, μ and M are given by:

$$(\mu)^{-1}=(m_e)^{-1}+(m_h)^{-1} \text{ and } M = m_e+m_h. \qquad (4)$$

So far I have assumed that the electron and hole band extrema occur at the same point in the reciprocal lattice space (or k-space) so the exciton is said to be direct. When the electron and hole band extrema occur at different points in k-space, the exciton is said to be indirect. Optical transitions of indirect excitons require the cooperation of lattice vibrations (phonons) to conserve quasimomenta.

B) Bound Excitons.

Both direct and indirect excitons are eigenstates of the crystal potential so they can travel throughout the crystal. They are referred to as free excitons as distinct from bound excitons which are localized around defects. Excitons can be trapped by both neutral and charged impurities[42], and by potential fluctuations in alloys.[43] Bound excitons relax their energy in a way different from free excitons. Excitons bound to neutral or charged impurities (such as donors, acceptors or isovalent centers), tend to have very well-defined energies and lifetimes. For example, in case of excitons bound to neutral donors or acceptors the binding energy of the exciton is about one tenth of the corresponding free exciton binding energy (Hayne's Rule).[44] The decay of these bound excitons is dominated by radiative recombination or Auger processes. In Auger processes, the exciton recombines nonradiatively, leaving the impurity in an excited state.[44] The crystal potential in alloys fluctuates randomly about some average value so that it can bind excitons with a range of binding energies rather than a well-defined energy. Based on the Anderson[45] model of localization of electrons, Lai and Klein[43] have argued that, for large enough fluctuations, there should exist a well-defined energy, known as the mobility edge, such that excitons with energy above the mobility edge are delocalized while those below the mobility edge are localized. Thus excitons above the mobility edge can relax rapidly into lower energy states. But excitons below the mobility edge are localized and, in order to relax, they have to tunnel through space to reach the lower energy states. Since the lower energy states correspond to deeper potentials which tend to be farther separated in space, one expects the relaxation

rate of such bound excitons to depend on energy. Each bound exciton can relax into a distribution of lower energy states with a distribution of relaxation rates, so the exciton population does not decay exponentially in time.

C) Exciton Interaction with Radiation and Polaritons

In the presence of electromagnetic radiation the Hamiltonian describing our system will be given by:[46]

$$H = H_x + H_{rad} + H_{x\text{-}rad} \tag{5}$$

where the two new terms represent the Hamiltonians for the photon and for the interaction betwen excitons and photons. H_{rad} is given by:

$$H_{rad} = \sum_k (\hbar kc/\sqrt{\epsilon})[b_k^+ b_k + 1/2] \tag{6}$$

where b_k^+ and b_k are the photon creation and annihilation operators. $H_{x\text{-}rad}$ is given by:

$$H_{x\text{-}rad} = \sum_k \Big\{ iA(b_k a_k^+ - b_k^+ a_k + b_k a_{-k} - b_k^+ a_{-k}^+) + [\pi\beta E_n(0)^2/(\hbar kc/\sqrt{\epsilon})](a_k a_k^+ + a_k^+ a_k + a_k a_{-k} + a_k^+ a_{-k}^+) \Big\} \tag{7}$$

The constant A in Eq.(7) can be expressed as:

$$A = [\pi \beta^2 E_n(0)^2 E_n(k)/(\hbar kc/\sqrt{\epsilon})]^{1/2} \tag{8}$$

where β is the polarizability of the exciton. The way to diagonalize H depends very much on the strength of $H_{x\text{-}rad}$. For indirect excitons or electric-dipole (ED) inactive excitons, $H_{x\text{-}rad}$ is very weak and can be treated by perturbation theory. In ED allowed excitons the situation is much more complicated.

ED allowed Wannier excitons are polarization waves travelling in the crystal and their properties are similar, in many ways, to optical phonons.[47] Like infrared-active phonons, they are split into transverse

and longitudinal modes by the longitudinal electric field produced by the longitudinal oscillation. If this splitting is denoted by E_{lt}, the dispersion of the transverse exciton E_t is given by Eq.(3) while the dispersion of the longitudinal exciton is given by:

$$E_l(k) = E_t(k) + E_{lt} . \tag{9}$$

E_{lt} is related to the exciton polarizability β by:[46]

$$E_{lt} = (2\pi\beta/\epsilon)\, E_t(0)$$

The exciton dispersion curves are shown as broken lines in Fig.5. If we neglect $H_{x\text{-}rad}$, the dispersion of the photon is shown by the dot-dashed line in Fig.5. Near the region where the photon curve intersects the exciton curves, the photon and exciton energies are degenerate and H must be diagonalized exactly. The resultant eigenmodes are now coupled transverse exciton-photon modes known as exciton-polaritons, to be abbreviated as polaritons in this article. Equation (5) has been diagonalized by Hopfield.[46] The polariton annihilation operator he introduced will be denoted by:

$$\alpha_{kj} = C_{j1}\, a_k + C_{j2}\, b_k + C_{j3}\, a^{+}_{-k} + C_{j4}\, b^{+}_{-k} \tag{10}$$

where the definition of the constants C_{jn} can be found in Ref.46. The corresponding polariton dispersion is given by the following implicit equation:

$$\epsilon(k,E) = \frac{\hbar^2 k^2 c^2}{E^2} = \epsilon_0 + \frac{4\pi\beta E_t^2(k)}{E^2(k) - E^2} \tag{11}$$

where $\epsilon(k,E)$ is the dielectric function. The two solutions of Eq.(11) corresponding to the two transverse propagating modes, which will be referred to as polariton branches, are shown as solid curves in Fig.5. The curves shown in Fig.5 are appropriate for the lowest energy exciton in CdS.[48] A phenomenological damping constant Γ can be introduced into Eq.(11) to take care of the damping of the exciton due to its interaction with phonons and trapping by defects.[49] For simplicity Γ will be assumed to be a constant independent of the exciton energy. As we will see, this is not true in most cases.

Equation (11) describes a spatially dispersive medium which allows two modes with the same energy $E>E_1$ to propagate in it. This gives rise to several problems. One problem involves the calculation of the transmission and reflection coefficients of light at the surface of the medium. The two normal boundary conditions from the Maxwell's Equations are insufficient to calculate the three unknowns in the problem:one reflected wave and two transmitted waves inside the medium. Extensive literatures exist on how to resolve this problem by introducting additional boundary conditions (ABC). The ABC mainly affect the calculation of the radiative lifetime of polaritons so they will not be discussed in detail in this article. Interested readers should consult ref. 50 for further details. A more important problem of polaritons relevant to this article is their dispersion. From Fig.5, one notes that the minimum energy of the lower polariton branch is zero. In principle polaritons should thermalize down to the zero energy state. Toyozawa[51] has pointed out that the lower polariton lifetime has a maximum near the transverse exciton energy which he labelled the polariton bottleneck'. If the interaction time between polaritons and phonons is short compared to the polariton lifetime at the bottleneck then the polariton can reach a quasiequilibrium near the bottleneck. The existence of this bottleneck can be understood from these arguments. Polaritons with energies much higher than the longitudinal exciton energy are mostly exciton-like. Their relaxation is dominated by scattering with phonons. Polaritons with energies close to the transverse exciton energy $E_t(0)$ become more and more photon-like and since photons interact very weakly with phonons in this region, the relaxation rate of polaritons should decrease. Polaritons with energies well below $E_t(0)$, on the other hand, are photon-like. As a result, they have high probabilities of escaping from the sample. These low energy polaritons again have fast relaxation rates due to radiative decay. Thus polaritons with energies in the vicinity of $E_t(0)$ should have the smallest relaxation rate and hence the longest lifetime.

D) Exciton Interaction with Phonons

Interaction between excitons and phonons can be included in our model by introducing additional terms H_{ph} and H_{x-ph} in Eq.(5). The phonon is described by the Hamiltonian:

$$H_{ph} = \sum_{q} \hbar \omega_{ph} (c_q^+ c_q + 1/2) \qquad (12)$$

where ω_{ph} is the phonon frequency, and c_q^+ and c_q are the phonon creation and annihilation operators. The Hamiltonian H_{x-ph} is defined by:[51]

$$H_{x-ph} = \sum_{k,q} iV_{x-ph} a_k^+ a_{k'} c_q^+ \delta_{k-k',-q} \qquad (13)$$

where the exciton-phonon matrix element V_{x-ph} describes the scattering of an exciton with wavevector k' to k with emission of a phonon with wavevector q. It is given by:

$$V_{LA}(1s,q) = [\hbar q D^2/(2V_c \rho u)]^{1/2} \qquad (14)$$

for the scattereing of an exciton in the 1s state by longitudinal acoustic (LA) phonons. In Eq.(14) D is the deformation potential for the exciton, V_c is the volume of the crystal, ρ is the density and u is the acoustic phonon velocity (sound velocity). For most Wannier excitons this exciton-phonon interaction is weak and can be treated by perturbation theory. The corresponding exciton-phonon matrix element for the longitudinal optical (LO) phonon is given by:[51]

$$V_{LO} = \left|[2\pi\hbar\omega_{LO} e^2/(V_c q^2)](\epsilon_\infty^{-1} - \epsilon_o^{-1})\right|^{1/2} (p_e - p_h) \qquad (15)$$

where ϵ_o and ϵ_∞ are the static and optical dielectric constants, p_e and p_h are defined in Ref. 51. This exciton-LO phonon interaction is also known as the Fröhlich interaction.[52]

E) Rate Equations

Most time-resolved experiments have been analysed by comparison with a model calculation involving the solution of some rate equations for the exciton populations. Let N_i denote the population of excitons or polaritons in state i where i can stand for the exciton band index or wavevector. Usually spatial diffusion of excitons is neglected to keep the problem simple, so N_i depends on time only. The time evolution of Ni is assumed to be given by a Boltzmann-type of rate equation:[52]

$$(dN_i/dt) = (\partial N_i/\partial t)_{in} - (\partial N_i/\partial t)_{out} \qquad (16)$$

$(\partial N_i/\partial t)_{in}$ denotes the rate at which excitons in state i are populated by processes such as absorption of external radiation and decay of excitons from another state j. $(\partial N_i/\partial t)_{out}$ denotes the rate at which excitons in state i are depopulated by processes such as radiative and nonradiative recombinations, scattering by phonons into other exciton states and trapping by defects. The scattering of excitons by phonons causes all the exciton states to be coupled together, so Eq.(16) represents really a system of coupled differential equations. In most cases the rate equations can be solved only numerically. This is not a serious drawback since, nowadays, these rate equations can often be solved with desktop computers.

To obtain a qualitative feeling as to what kinds of solutions one can expect from Eq. (16), I will consider some very simple models where Eq.(16) can be solved analytically. Some of these models have been applied to analyse experimental results to be discussed later.

a) One exciton level model.

If we assume there is only one exciton state and it is populated at the rate G(t) and depopulated at the constant rate Q. The rate equation for the population N is simply:

$$dN/dt = G(t) - QN. \qquad (17)$$

Assuming further that the initial condition is N=0 at t=0, N(t) can be shown to be given by:

$$N(t) = \exp(-Qt)\int_0^t \exp(Qt')G(t')dt' \qquad (18)$$

If the generation rate can be approximated by a delta function (such as in case of excitation by short laser pulses) then N(t) is a simple exponential function. In many cases the exciton state is not directly excited by a short laser pulse but is populated instead by relaxation of some other excitons. Let us assume the other exciton decays exponentially so that $G(t)=g\exp(-Q't)$. Substituting G(t) into Eq.(18) and solving for N(t) one obtains:

$$N(t) = g[\exp(-Q't)-\exp(-Qt)]/(Q-Q'). \qquad (19)$$

Notice the symmetric role of Q and Q' in Eq.(19). In this case the decay of N is not a simple exponential function except for time long compared to both 1/Q and 1/Q'. Also contrary to intuition the risetime and falltime of N are not necessarily given by Q' and Q respectively. Rather the risetime is given by the smaller of 1/Q and 1/Q'.[54]

b) Two exciton levels model.

Next we assume there are two exciton levels N_1 and N_2 which can scatter into each other with rates W_{12} and W_{21} respectively. In addition they can decay into states besides themselves with constant rates R_1 and R_2 respectively. They also have generation rates $G_1(t)$ and $G_2(t)$. Their rate equations are given then by:

$$dN_1/dt = G_1(t) + W_{21}N_2 - W_{12}N_1 - R_1N_1 \tag{20}$$

and

$$dN_2/dt = G_2(t) + W_{12}N_1 - W_{21}N_2 - R_2N_2 \,. \tag{21}$$

If the scattering mechanisms responsible for W_{21} and W_{12} are the same, such as exciton-phonon interactions, W_{12} and W_{21} are related by the equation:

$$W_{12} = W_{21}\exp(-E_{21}/K_bT) \tag{22}$$

because of the principle of detailed balancing. In Eq.(23) E_{21} is the energy separation between exciton levels 1 and 2, K_b is the Boltzmann constant and T is the lattice temperature. By assuming that the generation rates G_1 and G_2 are both delta functions and that $W_{12} \ll (R_1 \text{ and } R_2) < W_{21}$ the solutions for N_1 and N_2 are given approximately by:

$$N_2(t) = N_2(0)\exp[-(W_{21}+R_2)t] + (W_{12}/W_{21})[N_1(0)+N_2(0)]\exp(-R_1t) \tag{23}$$

and

$$N_1(t) = -N_1(0)(W_{21}/W_{21}+R_2)\exp[-(W_{21}+R_2)t] + [N_1(0)+N_2(0)]\exp(-R_1t) \tag{24}$$

The interpretation of $N_1(t)$ and $N_2(t)$ are actually quite simple. Keeping in mind that W_{21} is the largest rate and R_1 is the smallest, we note that N_2 decays at short times ($t \ll 1/R_1$) approximately exponentially with time constant $1/(W_{21}+R_2)$ due to the first term in Eq.(23). At long times ($t \gg 1/(W_{21}+R_2)$) N_2 again decays exponentially but now with time constant $1/R_1$ due to the second term in Eq.(23). On the other hand N_1 first increases with a risetime given approximately by $1/W_{21}$ due to decay of excitons from level 2 into level 1. At long times N_1 also decays exponentially with time constant $1/R_1$. As t approaches infinity both N_1 and N_2 decay exponentially with time constant $1/R_1$ and their population ratio N_2/N_1 is given by $\exp(-E_{21}/K_b T)$. This indicates that N_1 and N_2 are in thermal equilibrium at long times. That the decay time constants of any two levels are equal is an indication that the two levels have reached thermal equilibrium.

IV. EXPERIMENTAL RESULTS

A) Forbidden Excitons in Cu_2O

Cu_2O has always been the classic material for studying excitons because it has both allowed and forbidden excitons.[56] The two lower energy exciton series, known as the yellow and green series, are ED forbidden. The two higher energy series, known as the blue and indigo series, are ED allowed. All four series show many well-defined peaks obeying the Rydberg formula (Eq. (3)) and have been studied extensively by absorption,[57,58] photoluminescence[59,60] and resonant Raman scattering.[61,62] Information on the relaxation of excitons between these series have been obtained from cw measurements. For example, it is known from resonant Raman scattering that the higher energy exciton states relax to the 1s yellow exciton via emission of optical phonons.[61] The 1s excitons thermalize via exchange of LA phonons.[63] The yellow exciton is formed from zone-center conduction and valence bands with the same parity, so optical transitions are ED forbidden without assistance of phonons. Due to the exchange interaction between the electron and hole spins (both equal to 1/2) the 1s exciton is split into a triplet (S=1) orthoexciton state with Γ_5^+ symmetry and a singlet (S=0) paraexciton state with Γ_2^+ symmetry.[64] Assuming that both states decay predominantly by

phonon-assisted recombination their lifetimes are expected to be fairly long like indirect bandgap semiconductors such as Si. Photoluminescence spectra have indicated that the 1s yellow excitons are thermalized.[59] Figure 6 shows a luminescence spectrum of the yellow exciton in a high quality Cu_2O crystal at 26 K.[22] The sharp peak around 16,400 cm^{-1} has been identified[2] as the no-phonon emission peak of the orthoexciton via electric-quadrupole transition. The lower energy peak labeled as ortho-Γ_{12}^- is due to radiative recombination of the orthoexciton with simultaneous emission of a Γ_{12}^- optical phonon. Similarly the peak labeled as para-Γ_{25}^- is due to recombination of the paraexciton with emisssion of a Γ_{25}^- phonon. The lineshape $I(\hbar\omega)$ of these phonon-assisted peaks is consistent with a thermalized Maxwell-Boltzmann distribution:

$$I(\hbar\omega) = (\hbar\omega - \hbar\omega_{1s} - \hbar\omega_p)^{1/2} \exp[-\hbar(\omega - \omega_{1s} - \omega_p)/K_b T] \qquad (25)$$

where $\hbar\omega$ is the photon energy and $\hbar\omega_{1s}$ is the k=0 exciton energy appropriate for the ortho- or paraexcitons respectively and $\hbar\omega_p$ is the appropriate phonon energy.

In spite of extensive studies of the properties of the 1s excitons in Cu_2O several questions concerning their relaxations remained. Measurements of the orthexciton lifetime in Cu_2O with nanosecond laser pulses indicated that the orthoexciton lifetime was shorter than one nanosecond and therefore determined by nonradiative decays.[65] The variation of the orthoexciton luminescence intensity with temperature (see Fig. 7) was rather unusual.[60] As the temperature was increased, the intensity first decreased, reached a minimum around 20 K and started to increase exponentially with temperature. Kreingol'd and coworkers[60] proposed that this exponential increase in intensity with temperature could be explained by thermalization between the ortho- and paraexciton above 30 K.

Recently Weiner et al.[66] have used subnanosecond time-resolved emission measurements to study the interaction between the ortho- and paraexcitons in Cu_2O and to clarify its role in determining the temperature dependence of the orthoexciton luminescence intensity. Using a modelocked dye laser synchronously pumped by an Ar ion laser and a time-delayed coincidence photon counting system, Weiner et al. measured the time decay of the ortho- and paraexciton populations in Cu_2O as a function of temperature. Figure 8 shows the resultant spectra at three

different temperatures. At low temperatures (Fig. 8(a)) the orthoexcitons and the paraexcitons both decayed exponentially but with quite different lifetimes. As the temperature was increased the paraexciton decay remained unchanged while the orthoexciton decay became quite different. The orthoexciton decay appeared to be biexponential with a fast and a slow decaying component. The slow component has a decay constant approximately equal to that of the paraexciton. This is shown in Fig. 8(b) for T=35 K. As the temperature was increased further the amplitude of the fast decaying component decreased while its decay rate became larger. Eventually at high enough temperature the orthoexciton decay became exponential again but now dominated by the slow component. At T=48 K (Fig. 8(c)) both excitons decayed with the same rate indicating that they have thermalized with each other.

Weiner et al.[66] used the two excitons model discussed in the last section to analyze the time decays of the ortho- and paraexciton in Cu_2O. The orthoexciton and paraexciton were identified with exciton levels 1 and 2 respectively. The fast decaying component of the orthoexciton was identified with the rate $(W_{21}+R_2)$ while the paraexciton decay was identified with the rate R_1. The paraexciton decay rate was found experimentally to vary from sample to sample and so was determined presumably by defect-related processes. The surprising result was the strong temperature dependence of the orthoexciton decay rates $(W_{21}+R_2)$ shown by the open circles in Fig. 9. The experimental results were found to fit the expression: $A+BT^{3/2}$ with $A=4\times10^{8}$ sec^{-1} and $B=0.3\times10^{8}$ sec^{-1} K$^{-3/2}$. Since the rate R_2 was determined presumably by defects and hence temperature independent, Weiner et al. concluded that the orthoexciton to paraexciton conversion rate W_{21} varied as $T^{3/2}$. They found no satisfactory explanation for this temperature dependence after considering several different mechanisms, such as two-phonon scattering. Thus the time-resolved results showed conclusively that the orthoexcitons in Cu_2O decayed nonradiatively into paraexcitons. At T<30 K this decay occurred in a few ns, a time comparable to the paraexciton lifetime. As a result at T<30 K the orthoexcitons were not in thermal equilibrium with the paraexcitons. The decay rate increased rapidly with temperature so that at T>40 K the decay occurred in a time shorter than the paraexciton lifetime and the two exciton systems reached thermal equilibrium as suggested by Kreingol'd and coworkers.[60]

In the above photoluminescence experiments orthoexcitons with large kinetic energies were excited by radiation. These excitons thermalized via emission of optical and acoustic phonons to the bottom of the exciton band. While the ortho- to paraexciton conversion occurred in ns the phonon relaxation processes occurred in less than one ns, making them more difficult to study. Yu and Shen[61,63] have studied these orthoexciton relaxation processes with cw resonant Raman scattering (RRS). From these studies they concluded that at low temperatures the orthoexcitons thermalized predominantly via scattering with LA phonons. Using Eq. (13) and (14) they predicted that the LA phonon scattering rate would increase linearly with the exciton kinetic energy. This has been verified by Weiner and Yu using time-resolved RRS in Cu_2O.[67]

The two-phonon RRS process studied by Weiner and Yu is shown schematically in the inset of Fig. 9(a). It involves the excitation of orthoexcitons by Γ_{12}^- phonon-assisted ED transitions. Because of phonon participation, excitons with non-zero quasi-mementa can be excited. The exciton kinetic energy is determined uniquely by the equation:

$$E = \hbar[\omega - \omega_{1s} - \omega_{12}], \tag{26}$$

where $\hbar\omega_{12}$ is the energy of the dispersionless Γ_{12}^- phonon. In the $2\Gamma_{12}^-$ Raman process the orthoexciton decays radiatively via another Γ_{12}^- phonon-assisted ED transition producing the scattered photon. In the inset of Fig. 9(a) the arrows labeled LA represent possible relaxation of the orthoexcitons by emission of LA phonons. Figure 9(a) shows a typical time-integrated Raman spectrum of Cu_2O, when resonantly excited at 2 K by a dye laser with frequency equal to 16,510 cm^{-1}. The sharp peak at about 16,292 cm^{-1} is the $2\Gamma_{12}^-$ Raman peak. It is superimposed on a broader peak due to Γ_{12}^- phonon-assisted radiative decay of the thermalized orthoexcitons (same as the peak labelled ortho- Γ_{12}^- in Fig. 6).

Figure 10 shows the time dependence of the $2\Gamma_{12}^-$ phonon Raman peak for three incident laser frequencies. The system response is represented by the curve labeled laser in Fig. 8. From Eq.(26), these three incident laser frequencies corresponded to excitation of orthoexcitons with kinetic energies: 1, 4 and 7 cm^{-1} respectively. Weiner and Yu[55] have interpreted these time decay curves as the sum of two components: a resonant Raman peak with time constant equal to the relaxation time of the orthoexciton and a luminescence background which decayed with the lifetime

of the thermalized orthoexciton population. This interpretation was based on the fact that the lifetime of the thermalized orthoexcitons was independent of the laser frequency and was known from the ortho- to paraexciton conversion rate to be 1.5 ns at 2 K. On the other hand the exciton-LA phonon scattering rate should increase with the laser frequency. The broken curve in Fig. 10 (iii) was a fit to the experimental curve by convolving the system response with the expression: $[\exp(-t/0.26\text{ns})+0.126\exp(-t/1.5\text{ns})]$. As the orthoexciton energy increased in going from curve (i) to curve (iii), the magnitude of the RRS decreased while its decay rate increased. On the other hand the luminescence background remained constant. From these results Weiner and Yu determined that the orthoexciton-LA phonon scattering rate increased from $(1.0\pm0.4)\times10^{9}$ sec^{-1} to $(2.8\pm0.7)\times10^{9}$ sec^{-1} as the exciton energy was increased from 4 to 7 cm^{-1}. The corresponding LA phonon scattering rates calculated from the known deformation potential and properties of Cu_2O were 1.8×10^{9} sec^{-1} and 3.3×10^{9} sec^{-1} respectively.[67] The agreement with experiment is quite good considering the uncertainties in both the experimental and theoretical values.

From the above results it can be concluded that in Cu_2O the orthoexciton lifetime is dominated by scattering with LA phonons except for excitons with almost zero kinetic energy. The exciton lifetime decreases with energy so, when the exciton energy is larger than 7 cm^{-1}, the exciton relaxation times are of the order of 0.1 ns and cannot be resolved by coincidence photon-counting techniques. To observe the thermalization of the orthoexciton in real time, it is necessary to keep the lattice temperature low and to excite low energy excitons resonantly. It has been suggested by Habiger and Compaan[68] that orthoexcitons with zero kinetic energy would be scattered by absorption of LA phonons and from the known exciton and phonon dispersion curves the LA phonon absorbed should have a frequency of about 5 cm^{-1}. This means that a cold orthoexciton gas with $(K_b T/hc)<5$ cm^{-1} will thermalize by absorbing energy from the lattice!

To demonstrate this warming of a nonequilibrium exciton gas, Weiner and Yu[69] excited resonantly orthoexcitons in Cu_2O at 2 K by electric-quadrupole transition. The exciton population was monitored in real time via the Γ_{12}^{-} phonon-assisted recombination peak. The excitation and scattering processes involved are shown schematically in Fig. 9(b) together with the time-integrated emission spectrum. The time-

dependent decay curves were measured at each emission frequency and stored in a computer. From these decay curves the emission spectra at various time delays were reconstructed as three dimensional plots in Fig. 11(a) and (b). Since the decay curves were not deconvolved the time resolution was limited to about 0.3 ns by the system response. From these curves it can be deduced that the orthoexciton thermalization proceeded in this manner. First a peak appeared at about 5 cm^{-1} above the resonantly excited excitons within 0.5 ns. The maximum amplitude of this peak was about 5% of that of the main exciton peak. As time progressed both peaks decreased in magnitude while a broader background built up. After about 5 ns the spectrum reached a constant lineshape representative of a Maxwell-Boltzmann distribution.

To model the orthoexciton thermalization process Weiner and Yu[69] assumed that the time dependent emission lineshape $I(\omega,t)$ was related to the exciton distribution function $N(E,t)$ by:

$$I(\omega,t) = E^{1/2} N(E,t) \tag{27}$$

where $\hbar\omega$ was related to E via Eq. (26). The function $N(E,t)$ was obtained by solving the rate equation:

$$\frac{dN}{dt} = \left(\frac{\partial N}{\partial t}\right)_{in} - \left(\frac{\partial N}{\partial t}\right)_{out} - \left(\frac{\partial N}{\partial t}\right)_{nr} - \left(\frac{\partial N}{\partial t}\right)_{c} \tag{28}$$

$(\partial N/\partial t)_{in}$ and $(\partial N/\partial t)_{out}$ were the rates at which excitons were scattered into and out of the states with energy E. $(\partial N/\partial t)_{nr}$ was the nonradiative decay rate due to ortho- to paraexciton conversion. $(\partial N/\partial t)_{c}$ was the rate of exciton creation by the picosecond laser pulses and was assumed to be given by:

$$(\partial N/\partial t)_{c} = \delta(t)\exp[-E^2/W^2] \tag{29}$$

where W was the width of the zero-phonon absorption line. Experimentally W has been determined to be 0.4 cm^{-1}. All other parameters necessary for calculating the rates in Eq. (28) were known, so Eq.(28) could be solved numerically with no adjustable parameters. For comparison with the experimental spectra, the computed curves were convolved with Gaussian functions in frequency and time whose widths were chosen to be 1 cm^{-1} and 0.5 ns respectively to correspond to the experimental conditions. In

addition, to simulate the fact that the experimental laser pulses have a repetition rate of 80 MHz, a replica to the theoretical points delayed by 12.5 ns was added to the original computed points. The resulting theoretical spectra shown in Fig. 11 (c) and (d) reproduced quite well all the experimental features.

B) Indirect Excitons in AgBr

The silver halides crystallize in the zincblende structure. AgI is photosensitive and is an important photographic material. Of the three silver halides AgBr has been studied more extensively by optical techniques such as absorption,[70] emission,[71] RRS[72] and, more recently, time-resolved RRS.[73-75]

AgBr is an indirect bandgap semiconductor. Its band structure is shown schematically in Fig. 12. While its conduction band minimum occurs at the Brillouin zone center, its valence band maxima are at the L points. From crystal symmetry there are four such nonequivalent maxima. Optical transitions between the valence and conduction band extrema are ED allowed but require the assistance of phonons to conserve quasimomenta. As a result, the indirect excitons in AgBr are very similar to the forbidden excitons in Cu_2O in their relaxation properties. Figure 13 shows schematically the dispersion of the 1s exciton level in AgBr.[75] The top arrow labelled TO(L) represents optical excitation of the exciton with emission of a TO phonon at the L point of the Brillouin zone. Although other zone edge phonons can also participate in this transition, the TO(L) phonon was found to have the largest oscillator strength. As in the case of phonon-assisted optical excitations of the orthoexcitons in Cu_2O, the exciton kinetic energy E is determined by the photon energy $\hbar\omega$ by energy conservation via an equation similar to Eq.(26):

$$E = \hbar(\omega - \omega_{1s} - \omega_{TO(L)}) \qquad (30)$$

The excited exciton, labelled as β in Fig.13, can decay in four ways indicated by the arrows (a) to (d). Path (a) represents the radiative recombination of the exciton with emission of another TO(L) phonon. This process results in the resonant Raman scattering of a 2TO(L) mode similar to the $2\Gamma_{12}^-$ mode in Cu_2O. Path (b) corresponds to relaxation within

the same L valley by scattering with LA(Γ) phonons, while path (c) represents scattering to another nonequivalent L valley by emission of a TA(X) or LA(X) zone edge phonon. Finally path (d) represents nonradiative recombination involving defects. Except for path (c) the other three processes are similar to the corresponding processes in Cu_2O. AgBr has the advantage over Cu_2O in that both its exciton mass and deformation potential for scattering by the LA(Γ) phonons are about a factor of two smaller than the corresponding values in Cu_2O. As a result, its exciton-LA(Γ) relaxation rate increases less rapidly with exciton energy.

The exciton relaxation rates in AgBr have been measured by Stolz and von der Osten.[75] Similar to Weiner and Yu,[55] they excited the sample at low temperatures with a synchronously pumped, modelocked dye laser producing about 15 ps long pulses at 78 MHz repetion rate. The 2TO(L) RRS was detected in a time-resolved manner by using a delayed coincidence photon counting system. By using a fast photomultiplier tube containing microchannel plates and deconvolution techniques they were able to determine exciton relaxation times as short as 10-20 ps in AgBr. The decay constant of the 2TO(L) Raman mode was interpreted to be equal to the exciton decay rate in the same manner as in Cu_2O. The resultant exciton decay rates in AgBr are plotted as a function of the exciton energies in Fig. 14. The solid circles are the experimental points while the broken curves represent the calculated energy-dependent scattering rates due to the intravalley and intervalley processes shown in Fig. 13. The intervalley processes have abrupt onsets because the zone edge acoustic phonons have energies: 3.9 meV (TA) and 5.9 meV (LA) respectively. By fitting the experimental points with the theoretical curves Stolz and von der Osten were able to determine accurately the deformation potentials for the intervalley exciton-phonon interactions and the nonradiative lifetime of indirect excitons in AgBr. Their AgBr samples have nonradiative lifetimes of about 2 ns. On the other hand, the LA(Γ) scattering time was around 0.5 ns or longer. Thus at low temperatures the indirect excitons in their AgBr samples would not have enough time to thermalize before recombination. This conclusion was consistent with their time-resolved resonant Raman spectra shown in Fig. 15. In the lower set of curves the excitons were excited with energy 4.2 meV above the band minima. Within a time span of 10 ns none of the spectra showed a Maxwell-Boltzmann lineshape. In the upper set of curves the excitons were excited with 7.4

meV of kinetic enegy. These excitons decayed faster via intervalley scattering, producing the peaks labelled TA(X) and LA(X) and other unidentified peaks. Within a few ns these peaks showed appreciate broadening but their lineshapes deviated from a Maxwell-Boltzmann distribution even after 10 ns.

Similar nonthermalized emission spectra have also been observed in Cu_2O samples grown by oxidation of copper. Caswell et al.[67] have proposed a model to explain quantitatively the emission spectra in such Cu_2O samples. In their model the orthoexciton lifetimes were assumed to be reduced by defect trapping so that the excitons did not have enough time to thermalize. The experimental emission spectra were fitted by steady state solutions of Eq.(28), treating the term $(\partial N/\partial t)_{nr}$ as an adjustable parameter. They found that, in Cu_2O samples showing nonthermalized emission spectra, the nonradiative lifetime of the orthoexcitons was only 28 ps, almost fifty times shorter than the ortho- to paraexciton conversion time.

C) Polaritons in Direct Bandgap Semiconductors

Many intermetallic compounds formed from the Group III and Group V elements (such as GaAs) and from the Group II and Group VI elements (such as CdS and ZnSe) crystallize in the zincblende or wurtzite structure. Most of these compounds are direct bandgap semiconductors with their conduction and valence band extrema both occurring at the Brillouin zone center. Optical transitions from the top valence band to the conduction band minimum are ED allowed. In compounds with bandgaps larger than 1 eV the fundamental absorption edge is often dominated by excitonic effects. It has been found necessary to interpret the optical spectra of these compounds in terms of exciton-polaritons.

Polaritons represent the most fundamental excitation in any material that interacts with radiation. As a result, they have been studied extensively both theoretically and experimentally.[76] The theoretical work has concentrated on understanding their dispersion curves and the role of the additional boundary conditions (ABC)[77] in determining the optical spectra. The experimental work has been spurred by theoretical developments and advances in equipment. Much knowledge about polaritons were obtained by conventional reflection and absorption spectroscopies.

For example Hopfield and Thomas,[78] followed by many other groups,[79] showed that reflection anomalies in CdS and other semiconductors could be explained by invoking polaritons with the appropriate ABC and by assuming the presence of an exciton-free surface layer (nicknamed the dead layer). Gross et al.[79] found that the lineshapes of the luminescence spectra in high quality CdS and CdSe samples did not fit the Maxwell-Boltzmann distribution. Furthermore, the emission spectra showed two peaks instead of one as expected from one exciton band. Similar nonthermalized emission spectra were observed by Sell et al. in GaAs. Gross and coworkers attributed the nonthermalized lineshape to the unusual polariton dispersion and the presence of the second emission peak to a high probability for the polartions around the longitudinal exciton energy to escape from the sample. Sumi[53] developed a simple theoretical model which neglected the contribution of the upper polariton branch while assuming that the lower branch polaritons relaxed via scattering with LA phonons only. With this simple model he was able to explain the nonthermalized emission lineshape in CdS and to show that the emission peaked at the polariton bottleneck. Since he neglected the upper branch he could not explain the presence of the second emission peak. The appearance of narrow band tunable dye lasers made it possible to perform resonant Brillouin scattering (RBS) studies of polaritons first proposed by Brenig, Zeyher and Birman.[80] These authors showed that RBS is very powerful and direct method to study polariton dispersions and the ABC's. Experimental RBS spectra were first reported by Ulbrich and Weisbuch in GaAs.[81] Subsequent work by these authors[82] and others[76,83] established the usefulness of RBS for studying polaritons.

Although the above studies firmly established the validity of the polariton concept in interpreting optical spectra and provided very accurate measurement of polariton parameters, a few questions remain unresolved, such as the explanation of the second peak in the emission spectra[79,84] and the thermalization of polaritons. Wiesner and Heim[85] first reported a time-resolved luminescence study in CdS using a modelocked Ar ion laser. They found that at low temperatures ($T<2$ K) the polariton lifetime depended on energy indicating that polaritons did not thermalize before emission. However, the polariton lifetime did not reach a maximum as expected from the bottleneck theory of Toyozawa[51] but instead increased to a plateau. As temperature was increased the polariton decay became nonexponential. Finally

at temperatures above 30 K the polariton lifetime became independent of energy indicating that polaritons had thermalized. Thus Wiesner and Heim could only conclude that polaritons were not thermalized at low temperatures but became thermalized at higher temperatures. The existence of the bottleneck and its role in the thermalization of polaritons remained unclear. More recently these problem have been studied again in CdS and CdSe by Askary and Yu.[54]

Askary and Yu (to be referred to as AY) first extended the Sumi model by including the upper polariton branch and the appropriate ABC's.[86] The rate equations they used to calculate the relaxation of polaritons were identical to Eqs.(20) and (21) except N_1 and N_2 denoted the lower and upper polariton branches respectively. Also the polaritons formed bands so N_1 and N_2 were functions of the polariton energy E. Other modifications to the rate equations include the calculation of the rate coefficients W and R. In the model of AY polaritons could decay into the same branch or into another branch. The decay rate R consisted of two contributions: radiative decay and nonradiative decay. The nonradiative decay rate was assumed to be independent of polariton energy as was assumed also by Sumi. The radiative decay rate was determined by the probability of escape of the polariton out of the sample. In principle this is a very complex problem involving the spatial diffusion of polaritons towards the sample surface and the transmission coefficient of polaritons at the sample surface.[82] Askary and Yu avoided the transport problem by assuming that the polaritons were excited with high kinetic energies close to the surface. When these high energy polaritons relaxed towards the bottleneck region they also diffused into the sample to produce an uniform distribution near the surface. With this simplification the radiative decay rate was determined once the ABC's were specified.

Using this model they found that the calculated polariton distribution function always showed one broad structure while the emission spectra always showed two structures. Furthermore, the emission lineshape was more sensitive to the ABC than the distribution function (see Fig. 16).[86] Using the Pekar ABC[77] they were able to fit quantitatively most of the published polariton emission spectra, except those of GaAs (see Fig. 17). By comparing the polariton density-of-states with the emission spectra they concluded that all the emission originated from the lower branch because of its much higher

density-of-states. The main peak resulted from the high density of polaritons around the bottleneck whereas the higher energy structure resulted from a peak in the polariton transmission near the longitudinal exciton energy as proposed by Gross et al.[79]

Using their model AY also calculated the time-resolved polariton population in CdS as a function of temperature.[54] These theoretical results finally provided the basis for understanding the experimental results of Wiesner and Heim. First AY found that the calculated time-resolved polariton population of CdS showed single exponential decays both at low temperature (T< 2K) and at high temperature (T> 20K) in agreement with the experimental results. However there were important differences between the two cases. The decay constant at low temperature varied with the polariton energy while the decay constants at high temperature were independent of energy. The theoretical decay curves obtained by AY are reproduced in Fig. 18. From the low temperature decay curves AY found that the decay constant decreased as the polariton energy decreased towards the bottleneck as predicted by Toyozawa.[51] But, instead of showing a peak at the bottleneck, it leveled off into a plateau as observed experimentally first by Wiesner and Heim[85] (triangles in Fig. 19(a)). The explanation for this behavior hinged on the fact that at low temperatures polaritons were populated by relaxation from higher energy states via emission of LA phonons. At energies much higher than the longitudinal exciton energy polaritons were populated faster than they could decay so the decay constant of the population was equal to the rate of depopulation of the polariton states. As the polaritons relaxed toward the transverse exciton energy, their phonon emission rate decreased because the polaritons were becoming more photon-like. On the other hand their radiative decay rate increased as they became more photon-like. At the energy where their population rate via phonon scattering became smaller than their radiative decay rate, the decay constant equaled the smaller generation rate as shown in Eq. (19). The solid curve in Fig. 19(a) represents the calculated decay rate of the polariton as a function of energy. From the two curves in Fig. 19(a) it is clear that the decay rate shows a well defined maximum which can be identified as the bottleneck and the two curves are identical only for energies above the bottleneck. Thus when interpreted properly the results of Wiesner and Heim[85] have already demonstrated the existence of the polariton bottleneck.

The role of the bottleneck in the evolution of the polariton distribution from the nonthermalized lineshape at low temperature to the thermalized lineshape at high temperature was demonstrated by the theoretical decay curves at intermediate temperatures. Figure 20 shows two sets of theoretical decay curves for CdS at T=6 K for two different nonradiative recombination rates. These decay curves appear to consist of two exponential decays. By fitting these decay curves Askary[48] obtained a fast and a slow decay constant for CdS. His result for nonradiative recombination rate of 9×10^{8} sec^{-1} is reproduced in Figure 21. The interesting point to note is that the fast decay rate is energy dependent while the slow decay rate is energy independent. From the decay curves in Fig. 20 it can be seen that the relative amplitudes of these two components vary with energy. The fast component is dominant at higher energies while the slow component dominates at energies around and below the bottleneck. Furthermore the decay rate of the slow component is equal to that of the nonradiative rate. Nonexponential decay curves were mentioned by Wiesner and Heim[85] but they did not specify whether the curves were biexponential. As a result AY re-examined the time-resolved polariton decay curves in CdS and CdSe at 6 K using a delayed- coincidence photon counting system described in Section II.[54] They found that indeed the decay curves in both materials could be fitted quantitatively by the sum of two exponentials. The fast (τ_2) and slow (τ_1) decay time constants in CdS are plotted as a function of polariton energy in Fig. 22. The results in CdSe were similar and both were in good qualitative agreement with the theoretical results. In addition the experimental results also showed that the slow component became dominant at energies near the bottleneck.

The AY interpretation of these biexponential polariton decay curves is very similar to that of the biexponential decays of the orthoexciton in Cu_2O. The polaritons above the bottleneck relax down to the bottleneck via scattering with phonons so that the fast decay rate represents the time it takes the polaritons above the bottleneck to thermalize with the polaritons at the bottleneck. Once the polaritons reach thermal equilibrium the entire population decays at the rate determined by nonradiative recombination. At low temperatures this thermalization time is long compared to the polariton lifetime at the bottleneck so the polariton emission is nonthermalized. On the other hand at temperatures above 25 K the phonon scattering rate is so

large that polaritons thermalize almost instantaneously. Thus, interesting enough, the unusual temperature dependence of the orthoexciton luminescence intensity in Cu_2O[60] and of the decay rate of the polariton emission in CdS turns out to have the same simple explanation.

From Fig. 17 one sees that the model of AY fails to explain the shape and position of the higher energy emission peak typically found in GaAs[84] and a few other semiconductor such as ZnTe.[87] Subsequent work by Koteles and coworkers[88] and by Steiner et al.[24,89] showed conclusively that this higher energy peak resulted from the transport of polaritons to the sample surface. In studying the emission spectra of GaAs samples grown by molecular beam epitaxy Koteles et al.[84] noticed that this doublet structure was present only in samples with high donor concentrations (see spectra labelled MBE 3-3 in Fig. 23). The purer samples (MBE 3-14 and MBE 3-9) showed only one narrow peak in agreement with the model of AY. In studying the dependence of the polariton emission lineshape in GaAs on excitation wavelength, Ulbrich and Weisbuch[82] have already suggested that the transport of polariton to the sample surface played an important role in determining the polariton spectra. In particular they pointed out that the polariton group velocity could decrease by several orders of magnitude at the "knee" of the lower polariton branch. Such polaritons would have high probabilities of being scattered by impurities. Koteles et al.[88] proposed that elastic scattering of these polaritons by neutral donors resulted in decreased number of them reaching the surface and hence a dip in the emission curve. In other words, the salient feature of the GaAs emission spectra is not the existence of a second higher energy peak but rather the presence of a dip at the energy where a peak is expected. The strongest support for this explanation came from the time-resolved emission spectra obtained by Steiner et al.[89] on the same GaAs sample as in Fig. 23. The time-resolved spectra, measured with a delayed-coincidence photon counter, are shown in Fig. 24.[24] Note that the sample MBE 3-14 with an intermediate donor concentration showed only a single peak in the cw spectra. But at short delay times after excitation its emission spectrum developed a dip which disappeared completely after about 1 ns. This strongly suggests that polaritons with energies in the region of this dip take longer time to escape from the sample. Steiner[24] calculated the time-resolved polariton emission spectra in GaAs using a Boltzmann equation which included elastic

scattering by neutral donors. His results are reproduced in Fig. 25 and they reproduce qualitatively the experimental spectra in Fig. 24.

The above time-resolved studies have also led to explanation of other experimental results, such as the dependence of polariton emission spectra on sample surface quality, excitation intensity etc.[24] Thus one can conclude that polariton emission spectra in semiconductors are finally completely understood.

D) Localized Excitons in Semiconductor Alloys

In most semiconductors, emission from free excitons is not as strong as emission from excitons bound to neutral impurities. The reason is because free excitons are mobile and are often trapped rapidly at neutral donors or acceptors before they recombine radiatively. This is not always true in semiconductor alloys. In alloys often intense and broad emission peaks are found near free exciton energies. This is because excitons in the alloys are localized by random crystal potential fluctuations so their chance of being trapped at neutral impurities is greatly reduced. In addition excitons localized by potential fluctations often can recombine only radiatively. In contrast, excitons bound to neutral donors or acceptors can recombine nonradiatively via Auger processes.[44] In such Auger process the charges in the impurity atoms are excited from the ground state into the excited states. As pointed out by Lai and Klein,[43] nonradiatively Auger processes are not possible for excitons localized by potential fluctations in alloys, since the potential fluctations are not charged.

Because of the strength of their emission, localized excitons in alloys have been studied by techniques such as luminescence excitation spectroscopy,[90,91] and time-resolved spectroscopies.[92-95] Much of these work has been devoted to the determination of the exciton mobility edge (ME)[43,45] and to the study of exciton migration below the ME. In this section I will concentrate on the study of exciton energy relaxation in these alloys via time-resolved emission spectroscopies; in particular on how the thermalization of excitons in these alloys is affected by the ME. Semiconductor alloys are interesting because they form a bridge between the crystalline and the amorphous semiconductors.

The time dependence of exciton emissions in semiconductor alloys can generally be divided into two types, dependent on whether the alloy's bandgap is direct or indirect.[96]

The direct bandgap alloy studied most extensively is CdS_xSe_{1-x} for $0.3<x<0.95$. The cw emission spectra of CdS_xSe_{1-x} and their polarization have been studied by Permogorov et al.[91,92] as a function of the excitation photon energy. The solid curves in Fig. 26 show the cw emission spectra of two CdS_xSe_{1-x} samples at 2 K. In Fig. 26 (b) the largest emission peak is due to recombination of excitons localized by random alloy fluctuations while the two weaker peaks are its LO phonon sidebands. The lineshape of these peaks has been explained by Ablyazov et al.[98] using a model proposed by Baranovski and Efros.[99] The solid circles represent the degree of polarization of the LO phonon sideband as a function of the pump laser frequency. The polarization depends strongly on the excitation frequency. Permogorov et al.[91] argued that when the excitons were mobile they should dephase much faster than when they were localized. As a result they have identified the energy at which the polarization decreases to zero (about 2.104 eV in Fig. 26 (b)) as the ME.

The dynamics of exciton relaxation have been studied in $CdS_{0.53}Se_{0.47}$ by Kash, Ron and Cohen.[93] Using a delayed- coincidence photon counting system they have obtained time-resolved emission spectra of this alloy as a function of temperature. When excitons were excited above the bandgap, they found that the emission spectra as a whole shifted to lower energy as a function of time. In contrast, when the emission was excited below the bandgap, the luminescence remained unchanged in energy and only the amplitude decayed with time. These results are reproduced in Fig. 27. Kash et al. explained these results with a model first proposed by Cohen and Sturge.[100] When the excitons are excited above the bandgap, they relax rapidly by emission of acoustic phonons until they become localized. These localized excitons can tunnel into still lower energy states with assistance of acoustic phonons. However, the relaxation rate will decrease because the density of final states in the tunneling decreases exponentially with energy. When localized excitons are resonantly excited the lineshape of the emission becomes sharper and remains sharp since the probability of tunneling is now smaller than that of radiative recombination.[90] As a result, the localized exciton spectra decay in amplitude uniformly with time.

The above picture is also consistent with the observed time dependence of the decay. At low temperature Kash et al.[93] found that the localized excitons decayed nonexponentially. This is expected since each localized exciton will see a different environment and so will have a different probability of tunneling into a lower energy state. By defining an "effective lifetime" based on the average decay slope, Kash et al. obtained a plot of the energy dependence of this decay time shown in Fig. 28. The interesting result is the sudden increase in this effective lifetime at about 2.105 eV. Although Kash et al.[93] did not identify this energy as the ME, this energy is in good agreement with the ME determined by Permogorov et al.[97] in CdS_xSe_{1-x} alloys from the luminescence polarization. At higher temperatures, Kash et al. found that the luminescence decay became exponential and the decay rate became independent of emission energy. This suggested that above 40 K excitons could be thermally activated into extended states where thermal equilibrium can be attained. Thus the temperature dependence of luminescence of localized excitons in semiconductor alloys is very similar to that of exciton-polaritons.

The situation in semiconducting alloys with indirect band gaps, such as $Ga_xAl_{1-x}As$ with $x>0.43$, is quite different. At first we may expect the lifetime of localized excitons in these alloys to be dominated by nonradiative recombination rather than by radiative recombination. The reason is because radiative recombination in indirect band gap materials requires the participation of phonons to conserve momentum and hence the radiative recombination time will be longer. As pointed out by Klein, Sturge and Cohen[94], alloy fluctations relaxed the momentum conservation requirement in these materials and made radiative recombination the dominant decay mode for the localized excitons. Because each localized exciton sees a different environment, again the decay of the luminescence is expected to be nonexponential.

In this case an analytic expression describing the nonexponential decays has been derived by Klein et al.[94] These authors note that, in GaAlAs alloys, the conduction band minima (X_c) occur at the X point of the Brillouin zone while the valence band maximum (Γ_v) is at the zone center. The oscillator strength for the zero phonon optical transition is given by $|\langle \Gamma_v | p | \Gamma_c \rangle \langle \Gamma_c | V | X_c \rangle|^2$ where p is the electron

momentum operator, Γ_c is the lowest s-like conduction band minimum at Γ, V is the fluctuation in the crystal potential due to the alloying. In a normal optical transition the electron has to scatter from the Γ_c conduction band minimum to the X minima via phonons. In the alloy, V mixes the conduction band wavefunctions at Γ and X. In particular, if the wave vector of the conduction band minimum at X is K_x, the oscillator strength is proportional to the Fourier component, $|V(K_x)|^2$, of V. The distribution of radiative decay rates W is then determined by the distribution of $|V(K_x)|^2$. Klein et al.[94] assumed that the excitons in indirect bandgap GaAlAs alloys were not exactly located at the X point but instead have a 'camel back' structure as in GaP.[101] In this case V(K) would be complex and for a completely random potential the distribution in $|V(K)|^2$ could be shown to be an exponential function. Since W is proportional to $|V(K)|^2$ the distribution in W is also given by an exponential function:

$$p(W) = (W_m)^{-1} \exp(-W/W_m) \tag{31}$$

where W_m is the mean decay rate. Assuming that excitons can also decay at the rate W_c via nonrandom processes, such as phonon-assisted transitions and nonradiative recombinations, then the time dependence of the zero-phonon exciton luminescence after a delta-function pulse excitation is given by:

$$I(t) = (W_m)^{-1} \int_0^\infty W \exp[-(W_o + W_m)t] p(W) dW \tag{32}$$

$$= [1+W_m t]^{-2} \exp(-W_o t) \tag{33}$$

Whether the exciton decay is exponential or nonexponential depends on the relative magnitudes of W_o and W_m. For alloys, where the energy difference between the Γ_c and X minima is small, the Γ_c and X wave functions will be more strongly mixed by the potential V and hence W_m will be larger. Thus for GaAlAs alloys with Al concentration near the direct-indirect bandgap cross-over (at about 43 % of Al), one expects to see nonexponential exciton decays described by Eq.(33). Figure 29 shows the time dependence of the zero-phonon peak at 2 K in $Ga_{1-x}Al_xAs$ for x=0.48 and 0.445.[94]

The smooth curves were fits to the data points using these parameters: (a) $W_o = 6x10^5\ sec^{-1}$, $W_m = 4.6x10^6\ sec^{-1}$; and (b) $W_o = 10^6\ sec^{-1}$, $W_m = 3.7x10^7\ sec^{-1}$. The excellent agreement between theory and experiment strongly supports the stochastic nature of exciton recombination in these indirect bandgap semiconductor alloys.

E) Amorphous Hydrogenated Si

The compositional disorder in alloys leads to nonthermal equilibrium distribution for photoexcited excitons and to nonexponential luminescence decays. Amorphous semiconductors have structural disorder and one may expect this disorder to cause similar behaviors in their luminescence properties. This is only approximately true because the emission properties of amorphous semiconductors are more complicated than those of semiconductor alloys. There are two systems of amorphous semiconductors which have been studied extensively. One system consists of mainly chalcogenide glasses such as As_2S_3.[102] The other system consists of tetrahedrally bonded semiconductors such as amorphous silicon.[103]

One expects an amorphous material to contain more nonradiative recombination centers so their photoluminescence quantum efficiencies will be lower than the corresponding crystalline material and they will not be ideal candidates for photoluminescence studies. It turns out that hydrogenated amorphous silicon is an exception. The quantum efficiency of crystalline silicon is quite low (less than 1 %) because silicon is an indirect bandgap semiconductor. On the other hand, quantum efficiency in hydrogenated amorphous silicon (to be abbreviated as a-Si:H) has been found to be as high as 20 %.[104] This high quantum efficiency of a-Si:H makes them amenable to time-resolved photoluminescence studies and much information on the relaxation of electron-hole pairs in a-Si:H has been obtained from these studies. In this review I will consider the TRPL in a-Si:H only. Readers interested in corresponding results in chalcogenide glasses should consult References 105.

Before discussing the TRPL in a-Si:H it is necessary to briefly review some of its relevant properties. When a-Si was first studied in the sixties, the samples typically exhibited no photoluminescence and have very

poor transport properties. These observations were explained by the fact that a-Si contained high densities of dangling bonds which served as nonradiative recombination centers. In the late sixties Spear and coworkers[106] discovered that dangling bonds in a-Si:H could be passivated by hydrogen. Amorphous Si grown by decomposition of SiH_4 in a plasma glow discharge showed low density of dangling bonds in electron spin resonance and strong photoluminescence signals. From extensive studies of the transport and optical properties, the local electron density-of-states (shown schematically in Fig. 30) of a-Si:H have been deduced.[107] As in case of excitons in semiconductors alloys, it is believed that there are mobility edges E_c and E_v which separate the delocalized states from the localized states. The density-of-states below the mobility edge E_c, (referred to as the band tail states) resulted from disorder. They are usually assumed to have an exponential dependence on energy:[103,104]

$$g(E) \sim \exp[-(E_c - E)/K_b T_o] \qquad (34)$$

where T_o is about 300 K for electrons. For holes the corresponding T_o is about 500 K. The cw optical properties of a-Si:H are summarized in Fig. 31. For photon energies above $\sim$1.8 eV the absorption coefficient in a-Si:H can be fitted with a $(E-E_g)^{1/2}$ dependence as in a direct bandgap semiconductor with a bandgap E_g.[104] This leads to the definition of a pseudo-optical gap of approximately 1.7-1.8 eV in a-Si:H. On the other hand the energy of the PL peak is typically 1.4-1.5 eV.[104] This large difference in energy between the optical gap and the PL peak was first explained by the Franck-Condon shift in a strongly coupled electron-phonon system. Time-resolved PL measurements have since shown that this energy difference resulted from the relaxation of photoexcited electrons and holes into the band tail states.

Time-resolved PL has been studied in a-Si:H with time resolution ranging from ms to ps. It was pointed out by Street[103] that when a system has a wide distribution of relaxation times then the relaxation time measured in a particular experiment would always be determined by the time resolution of the experiment. Thus experiments with different time resolutions could be measuring different processes. So far time-resolved

PL experiments have been performed on a-Si:H on these time scales: (1) 50 ps-3 ns; (2) 0.5- 40 ns; and (3) 10 ns-1 ms. Experiments on even shorter time scales have been carried out using photoinduced absorption technique.[108] Based on these measurements the following picture has emerged on the time evolution of an electron-hole pair in a-Si:H excited by photons with energies above the pseudo-optical gap. I should point out that this picture is only valid for high quality a-Si:H samples with PL efficiencies of at least 10 % or more at low temperatures.

First the photoexcited electrons and holes relax via emission of phonons toward their respective mobility edges. From photoinduced absorption[108] the energy relaxation rate has been determined to be about 0.1 eV/ps. If the excitation photon energy is about 2 eV and the optical gap is assumed to be 1.8 eV, the electron-hole pair will be localized within 2 ps. Thus all TRPL experiments performed so far on a-Si:H measure only the relaxation of electrons and holes within the band tail states. Furthermore it is generally believed that the holes are less mobile than the electrons in the localized states so these experiments monitor mainly the relaxation of the electrons. Electrons relax within these band tail states by hopping into states with lower energies. As their energies are lowered the density of final states they can relax into decreases exponentially. Competing with these energy relaxation processes are radiative and nonradiative recomination processes. During the hopping processes the electron will every now and then hop onto a site containing the hole and recombination occurs. Thus the radiative recombination rate is determined by the distance between the electron and hole separation during the relaxation. In a-Si:H samples with high quantum efficiencies the maximum radiative lifetime was found to be about 10 ns. This time represents the recombination time of the closest pairs. For the more distant pairs the recombination will be slower so there is a large range of recombination times. During all these hopping processes the electrons will also relax in energy so the peak of PL shifts to lower frequency with time. In many respects the behavior of the PL peak in a-Si:H between 10 ns and 0.1 ms is very analogous to the donor-acceptor pair recombination peak in semiconductors such as GaP. As the electron-hole pairs relax their average separation also increases. If the initial density of e-h pairs is less than 10^{18} cm^{-3} which is typical of most PL experiments the

electron will be closer to the hole it left behind than to other e-h pairs. Thus in early times the electron can recombine only with the original hole with which it is created together by the photon. This kind of recombination is referred to as geminate recombination. In crystalline semiconductors, recombination of electrons and holes is usually nongeminate. For long times, such as on ms time scale, one may expect that electrons and holes may have wandered far enough from each other for nongeminate recombination to dominate.[109]

I will now examine the experimental results based on which the above picture has been obtained.

Orlowski and Scher[110] have utilized a passively modelocked Nd:Glass laser and streak camera to measure the time dependence of the high energy emission (1.5-2.1 eV) in a-Si:H between 10 ps and 4 ns. A typical time dependent decay curve of the PL at low temperature is shown in Fig. 31. The solid curve represent a fit to the decay with a power law dependence: $I(t)=t^{-\gamma}$. Orlowski and Scher found that γ increased linearly with sample temperature from about 0.5 at 20 K to about 1 at 180 K. Such power law decays are not unusual in the properties of amorphous materials. For example the transport properties of a-Si are also known to be dispersive with the mobility having a power law dependence on time: $\mu_e \sim t^{-(1-\alpha)}$ where α is usually referred to as the dispersion parameter. Models have been proposed to explain such dispersive transport in amorphous materials.[111] For example the multiple trapping model[112] predicts that $\alpha=T/T_o$ with $K_b T_o=50$ meV. The dependence on T of γ in this case is not consistent with the prediction of the multiple trapping model so Orlowski and Scher proposed a different model. Their model was the first comprehensive model of energy relaxation within the band tail states of an amorphous material. The model assumed that there were many clusters of sites embedded in a random distribution of additional sites. An electron could hop an arbitrary number of times between sites within a cluster but could hop only once to the sites outside the cluster. The probability W(r) of hopping to a site at distance r outside the cluster was given by:

$$W(r) = W_o \exp(-r/R) \qquad (35)$$

where W_o and R were estimated to be $\sim 10^{13}$ s^{-1} and 7 A respectively from the properties of donor electrons in crystalline Si. The probability $p(r, \Delta E)$ that an electron with energy E_1 (below the conduction band edge E_c) would find a site at distance r and with energy lowered by ΔE was assumed to be:

$$p(r,\Delta E) = g_o \exp[-(E_1-\Delta E)/K_b T_o] \qquad (36)$$

where g_o and $K_b T_o$, the width of the band-tail states, were assumed to be about 4×10^{20} eV^{-1} cm^{-1} and 30 meV respectively. Furthermore the transition probability was assumed to be nonzero only for ΔE between $-\hbar\omega_o$ and $K_b T$. The energy $\hbar\omega_o$ could be considered an effective phonon energy as in the case of crystalline material. By assuming that each cluster contained only two sites and carrying out exactly the configuration average over all the remaining sites, Orlowski and Scher obtained a power law decay as observed experimentally. By fitting the experimental data (shown as the solid lines in Fig. 31) they deduced that $W_o = 3\times10^{13}$ s^{-1}, $\hbar\omega_o = 20$ meV and the initial electron energy E_1 to be 50 meV. Thus the smallest hopping time at the beginning of their experiment was about 60 psec at T=20 K. Since the time resolution of their experiment was about 100 ps this result was quite consistent with Street's argument. It was also clear that the multiple trapping model was not appropriate for the low temperatures in their experiment. For E_1=50 meV and T=20 K it would take about 10 s for the electron to tunnel out of a trap.

Time-resolved PL in a-Si:H in the range of about 0.3-100 ns has been studied by several groups.[3,113,114]

Wilson et al.[113] measured the time decay of the total luminescence intensity from a-Si:H and found an approximately exponential decay with time constant of about 8 ns within the first few ns. Since the energy relaxation processes discussed by Orlowski and Scher would only redistribute and not annihilate the electron and hole pairs, Wilson et al.[113] have interpreted this decay time as the radiative recombination time of electron-hole pairs in a-Si:H. They also concluded that this radiative lifetime was compatible with the picture of localized excitons although this interpretation was not unique. If ν represented the initial decay rate of PL in a-Si:H, Wilson et al. found that ν depends on temperature T as:

$$\nu = \nu_1 + \nu_o \exp(T/T_o) \qquad (37)$$

where $\nu_1 = 1.0 \times 10^8\ s^{-1}$, $\nu_o = 0.27 \times 10^8\ s^{-1}$ and $T_o \sim 95$ K. The temperature independent ν_1 was interpreted as the radiative recombination rate while ν_o as the nonradiative recombination rate. Several mechanisms, such as spatial tunneling, phonon-assisted local relaxation at internal surfaces, have been suggested to explain the exponential dependence of the nonradiative rate. Wilson et al. noted that Eq. (37) was very similar to the equation describing temperature quenching of cw PL in a-Si:H reported by Collins et al.:[115]

$$(I_{cw})^{-1} = (I_o)^{-1} + B\exp(T/T_1) \qquad (38)$$

although the temperature T_1 describing the cw PL was considerably smaller than T_o. Thus from the work of Wilson et al. one can conclude that, at low temperatures, after relaxating into the band-tail states photoexcited electron-hole pairs in a-Si:H recombine radiatively at the initial rate of about $10^8\ s^{-1}$. At higher temperatures nonradiative decays become activated and more important.

A comprehensive study of TRPL in a-Si:H has also been reported by Stearns.[3] Instead of using short laser pulses, as in most other experiments, Stearns used the subnanosecond pulses from the Stanford Synchrotron Radiation Laboratory to excite the PL. He used the tunability of the synchrotron radiation to vary the excitation photon energy. In addition he also studied the time decay of the PL as a function of the emission energy and temperature. Stearns fitted the nonexponential decay of the PL with a function different from the one used by Orlowski and Scher.[110] He found that all his time decay curves can be fitted very well by the single expression of the form:

$$I(t) = a_1 + a_2/(t+t_o) \qquad (39)$$

Stearns justified this expression on the ground that an amorphous material would have a distribution of relaxation times $F(\nu)$. If the distribution has an exponential dependence on the high frequency side beyond a cut-off frequency $\bar{\nu}$:

$$\nu_r F(\nu) = a_2 \exp(-t_o \nu) \qquad \bar{\nu} < \nu < \infty \qquad (40)$$

where ν_r is the average radiative recombination time, then I(t) will be given by Eq.(39) provided $(\bar{\nu})^{-1}$ is much longer than the time of the experiment. The constant a_1 is given by:

$$a_1 = \int_0^{\bar{\nu}} \nu_r F(\nu) d\nu \qquad (41)$$

Stearns suggested that a reasonable value for $\bar{\nu}$ would be $\S 10^6$ s^{-1}. Stearns interpreted to as the 'decay time cutoff' since it determined how fast the decay rate distribution would attenuated at ν larger than $\bar{\nu}$. Another way to understand t_o is that, when the time is much longer than t_o, I(t) simply decays as t^{-1}. The factor $S = a_1 t_o / a_2$ represents the fractional contribution to the early PL decay from the slow decay components ($\nu < \bar{\nu}$) in the decay rate distribution.

Stearns found that both t_o and S changed with temperature, excitation frequencies and emission frequencies. The changes were larger with temperature and emission frequencies. In particular $(t_o)^{-1}$ varied with T in the same way as ν in Eq.(37). For excitation energy of 2.07 eV and emission energy of 1.43 eV, ν_1 and ν_o were found to be equal to 6×10^6 s^{-1} and 2.7×10^8 s^{-1} respectively, and T_1 was equal to 24.5 K. Thus Stearns and Wilson et al. found the same temperature dependence in the initial decay rate of PL in a-Si:H but their values of ν_1, ν_o and the activation temperatures were quite different. As in most work on amorphous materials one can only account for the different results by the different samples used in the two experiments. Unfortunately the different results led to different conclusions. Wilson et al.[113] found the temperature independent radiative decay rate ν_o to be larger than the temperature dependent rate ν_1. As a result they concluded that the initial decay of electron-hole pairs in a-Si:H was dominated by radiative recombination. Stearns, however, found that the temperature dependent rate was much larger so he suggested an alternate explanation. This alternate model, proposed by Street and other workers,[104,116] is an analogue of the donor-acceptor pair recombination model.

The donor-acceptor model was used by Tsang and Street to explain their TRPL results in a-Si:H measured for decay times >10 ns. They found that the PL peak height and frequency both continued to decrease with time between 10^{-8} s and 10^{-5} s. Their picture of what was happening was that electrons and holes separated from each other in their initial relaxation into the band tail states. In these localized states radiative recombination occurred via tunneling of electrons to the hole traps. This tunneling rate depended strongly on the separation between the electrons and holes. The close pairs recombined first while the more distant pairs took longer time to recombine. Thus the decay of the PL intensity with time was caused, not so much by the decay of the electron-hole population, but rather by the decrease in the radiative recombination rate. The decrease in the emission peak frequency could also be explained in this model by the Coulomb interaction between the electron and the hole. This Coulomb attraction was larger for the closer pairs than for the distant pairs so, as the more distant pairs recombined in later times, the emission frequency also decreased. However some of Tsang and Street's conclusions were disputed by Wilson and Kerwin.[117] The latter authors repeated the experiment of Tsang and Street and found similar results, except when they changed the excitation frequency. They found that the decrease in emission peak frequency with time disappeared when the excitation frequency was decreased from 18790 cm^{-1} to 13170 cm^{-1}. Thus they concluded that the shift of the PL peak between 10^{-8} s and 10^{-5} s observed by Tsang and Street was not due to the Coulomb interaction between electrons and holes although the later time shifts ($t>10^{-4}$ s) was consistent with that mechanism. Instead they explained the emission peak shifts by the energy relaxation of the electron-hole pairs in the band tail states. If this explanation were correct then the energy relaxation processes of electrons and holes in a-Si:H would extend in time from ps to ms. This would be consistent with the expectation that electrons and holes never attained complete thermal equilibrium in highly disordered systems.

F) Electron-Hole Plasmas in GaAs

When the exciton density becomes large enough, electron wavefunctions in adjacent excitons will overlap. The electron-electron and hole-hole correlation can become more important than the electron-hole correlation. When this happens, the excitons will dissociate into a two-component plasma consisting of an electron gas moving relative to the heavier holes. The relaxation of such electron-hole plasmas (to be abbreviated as EHP) in some semiconductors, such as Si and GaAs, has been the subject of intensive studies. In case of Si, the relaxation processes of energetic EHP are important for understanding laser annealing. In GaAs these processes are relevant to hot electron devices, such as Gunn oscillators. As a result, both extensive experimental and theoretical studies have been devoted to understand the properties of EHP in these semiconductors. Also many review articles have been written on them.[118-122] However, because of the complexities arising from many-body effects, the details of some of these relaxation processes are still not completely understood. In this article I will concentrate on the recent experimental results in GaAs and related materials. My emphasis will be on what has been learnt about the relaxation of EHP in GaAs and on pointing out areas where further work are still needed.

Much of the earlier experimental and theoretical work on hot electron effects in GaAs and related semiconductors has been reviewed by Conwell[118] in her book. From these earlier transport experiments it is known that the relaxation of hot electrons depends on the carrier density N.

For relatively low density plasmas ($N<10^{16}$ cm^{-3}) electron-electron interaction is relatively unimportant compared to electron-phonon interactions.[123] When a nonequilibrium distribution of EHP is excited, for example by optical excitation, the electrons and holes relax predominantly by successive emission of LO phonons via the Frohlich interaction. The time required to emit one LO phonon is about 0.1 ps (see Fig. 32).[123,124] When the electrons do not have sufficient energy to emit LO phonons, they thermalize via scattering with acoustic phonons. The scattering time of electrons with acoustic phonons is of the order of 10 ps or more so the thermalization time of such low density EHP is of the order of 100 ps. When the experiment is performed at low temperatures, often the

temperature of the electrons (T_e) after thermalization is still higher than the lattice temperature (T_L). It takes nanoseconds for the electrons to cool to the lattice temrperature. It was not possible to measure the cooling rate before the advent of picosecond and femtosecond lasers. Ulbrich[125] was one of the first to use a modelocked, subnanosecond laser to study the cooling of a warm photoexcited electron gas by TRPL (see Fig. 33). At higher T_e, the electron cooling rate became faster and picosecond laser pulses have to be used. These faster cooling rates for electrons in GaAs have been determined by photoinduced absorption[126,127] and TRPL studies.[128,129] Figure 34 shows the cooling curve obtained by von der Linde and Lambrich.[127] Still the time resolution in these experiments were not faster enough to measure the electron distribution before thermalization. Only recently, with subpicosecond pulses generated by CPM dye lasers, it became possible to determine the time evolution of a nonequilibrium electron distribution.[130,131] Even then the electron energies were kept small enough so that electrons relaxed slowly by emission of acoustic phonons only. The fast relaxation of hot electrons by emission of LO phonons can be observed only indirectly. Instead of measuring the electron distribution, one can measure the LO phonon population by anti-Stokes Raman scattering.[124,132] From the risetime of the nonequilibrium LO phonon population, Kash et al. have determined the time required to emit one LO phonon in GaAs to be 0.165 ps.

The situation is much more complicated when the plasma density is higher than 10^{17} cm^{-3}. First the electron-electron, hole-hole and electron-hole interactions are now stronger than the electron-phonon interactions. As a result, the photoexicted electrons and holes will thermalize first and then cool towards the lattice temperature. However, the relative magnitudes of these carrier-carrier interactions are very poorly known both theoretically and experimentally. Since most experiments determine only the electron temperature, it is not known whether the electrons and holes are in equilibrium and what is the hole cooling rate. From the theoretical point of view the calculation of these carrier-carrier interactions including exchange and correlation is an extremely difficult many-body problem. Recently Lin et al.[133] have determined the relaxation of hot EHP in GaAs excited by 35 fs long dye laser pulses. They observed a fast component with relaxation times ranging

from 13 to 30 fs depending on the carrier density. They attributed this fast relaxation time to carrier-carrier scattering. Huang and Yu[134] have also estimated, from the lineshape of Raman spectra due to single particle scattering, that the electron scattering time (due to both electron-electron and electron-hole interactions) in an EHP of density 1×10^{18} cm^{-3} to be 70 fs for GaAs. These carrier-carrier scattering times are consistent with the theoretical estimate of ≥ 50 fs by Levi et al.[135] using the random phase approximation. Hulin et al.[136] have calculated the carrier-carrier interactions in high density EHP in Si. They concluded that the electron scattering time was dominated by electron-hole scattering. The scattering times of carriers in high density EHP are near the limit but still within the range of present measurement technology so one can expect that more precise determination of these scattering times will be available in the near future.

Another problem in understanding the relaxation of dense EHP was first noted by Leheny et al.[137] These authors found that the cooling rate of hot electrons in photoexcited EHP in GaAs could be explained satisfactorily by electron-phonon interaction provided N is less than 5×10^{17} cm^{-3}. For larger N they found that the initial cooling rate was significantly reduced. They explained this decrease in the cooling rate by the screening of the Frohlich interaction. An alternate explanation was offered by van Driel[138] who has also found anomalously long energy relaxation times for dense EHP in highly excited Ge. Instead, van Driel proposed that this slow down in the EHP cooling could be explained by hot phonons. The hot carriers relaxed by emitting optical phonons. These nonequilibrium optical phonons have to decay into acoustic phonons by the much slower anharmonic phonon interactions. Thus the optical phonons heated up and slowed down the cooling of the hot carriers. In other words, electrons would thermalize with optical phonons, and once the two reached the same temperature, the cooling rate of the electron would be determined by that of the optical phonons. Although recent calculations[139] and experiments[140] support the "hot phonon" explanation for the slow down of EHP cooling rates at high densities, a definitive experiment, such as one in which both the electron and phonon temperatures are monitored simultaneously, is still lacking.

The cooling of a dense EHP at later times are complicated by two other factors: spatical expansion of the EHP and radiative recombination. Several workers have reported anomalously fast expansion of hot dense EHP excited by ps laser pulses.[141] It has been proposed that the motion of the EHP in this case was not driven by diffusion. Instead the electrons were pushed apart by the so-called "Fermi pressure".[142] Such adiabatic expansion of the EHP should cool the plasma rapidly while at the same time decrease the plasma density. Since the Fermi pressure and the cooling of the EHP are both strongly density dependent, the dynamics of such hot dense EHP should be highly nonlinear and quite interesting.

The cooling of two-dimensional EHP in quantum well structures has also been studied with ps and subpicosecond lasers. The results are still controversial. While some groups[143,144] have found that the cooling rates of 2-D EHP were slower than the corresponding 3-D plasma at high densities, other group has found no difference between the cooling rates of 2D and 3D EHP.[145]

V. CONCLUSIONS AND ACKNOWLEDGEMENTS

In the last few years great strides have been made in understanding the thermalization of excitons via picosecond time-resolved studies. These experiments have been made possible by the availability of ps and subpicosecond laser pulses and ultrafast detection schemes. From these studies the roles of exciton-phonon interactions, exciton-radiation interaction and exciton-defect interactions in determination the thermalization paths of exciton have been elucidated. These studies have also demonstrated the wealth of information which could be derived from time-resolved emission spectra of a large varieties of solids.

I am indebted to my former students: J. W. Weiner, F. Askary and C. L. Collins, for much of this work is based on their these; and to many collaborators for their contributions to this article including: R. S. Berg, Yi-he Huang, N. S. Caswell, D. J. Erskine, and A. Mysyrowicz. In addition I have benefited from discussions and correspondences with many friends and colleagues: Y. R. Shen, H. Z. Cummins, E. Burstein, J. Kash, J. Shah, M. L. Thewalt, and E. S. Koteles, just to name a few. This work was supported by the Director, Office of Energy Research, Office of Basic Energy Sciences, Materials Sciences Division of the U. S. Department of Energy under Contract No. DE-AC03-76SF00098.

VI. REFERENCES

1. See for example article by D. J. Bradley in Ultrashort Light Pulses, ed. by S.L. Shapiro (Springer, Berlin, 1977) p.25.

2 E. P. Ippen and C. V. Shank, ibid, p.83.

3. D. G. Stearns, Phys. Rev. B30, 6000 (1984).

4. W. H. Knox, R. L. Fork, M. C. Downer, R. H. Stolen, C. V. Shank and J. A. Valdmanis, Appl. Phys. Lett. 46, 1120 (1985).

5. W. H. Knox, M. C. Downer, R. L. Fork and C. V. Shank, Opt. Lett. 9, 552 (1984).

6. D. Grischkowsky and A. Balant, Appl. Phys. Lett. 41, 1 (1982).

7. B. Nikolaus and D. Grischkowsky, Appl. Phys. Lett. 43, 228 (1983).

8. C. V. Shank, R. L. Fork, R. Yen, R. H. Stolen and W. J. Tomlinson, Appl. Phys. Lett. 40, 761 (1982).

9. L. Mollenauer, N, D. Vieira and L. Szeto, Opt. Lett. 7, 414 (1982).

10. R. S. Putnam, C. B. Roxlo, M. M. Salour, S. H. Groves and M. C. Plonko, Appl. Phys. Lett. 40, 660 (1982).

11. A. M. Johnson, R. H. Stolen and W. M. Simpson in Ultrafast Phenomenon IV, Springer Series in Chemical Physics, Vol. 38, ed. by D. H. Auston and K. B. Eisenthal (Springer-Verlag, Heidelberg, 1984) p.16; B. H. Kolner, J. D. Kafka, D. M. Bloom and T. M. Baer, ibid, p. 19.

12. C. V. Shank and E. P. Ippen, in Dye Laser, Topics in Applied Physics,Vol. 1, ed. by F. P. Schafer (Springer-Verlag, Heidelberg, 1971) p.121; A. Dienes, Opto-Electronics 6, 99 (1974).

13. Spectra-Physics, Inc. San Jose, CA 95134 and Coherent, Inc. Palo Alto, CA 94303.

14. G. W. Fehrenbach, K. J. Gruntz and R. G. Ulbrich, Appl. Phys. Lett. 32, 159 (1978).

15. R. L. Fork, B. I. Greene and C. V. Shank, Appl. Phys. Lett., 38, 671 (1981).

16. A. Penzkofer, A. Laubereau and W. Kaiser, Phys. Rev. Lett. 31, 863 (1973).

17. W. H. Knox, R. L. Fork, M. C. Downer, D. A. B. Miller, D. S. Chemla, and C. V. Shank, Phys. Rev. Lett. 54, 1306 (1985).

18. N. H. Schiller and R. R. Alfano, Opt. Commun. 35, 451 (1980).

19. R. Z. Bachrach, Rev. of Sci. Inst. 43, 734(1972);V. J. Koester and R. M. Dowben, Rev. of Sci. Inst. 49, 1186(1978).

20. B. Leskovar, C. C. Lo, Nuc. Inst. Meth. 123, 145 (1975).

21. K. Spears, L. E. Cramer and L. D. Hoffland, Rev. Sci. Instrum. 49, 255 (1978).

22. J. S. Weiner, Ph. D. Thesis, University of California, Berkeley, California (unpublished, 1984).

23. A. E. W. Knight and B. K. Selinger, Aust. J. Chem. 26, 1 (1973).

24. T. W. Steiner, Ph. D. Thesis, Simon Fraser University, (unpublished, 1986).

25. F. Heisel, Rev. Sci. Instrum. 52, 992 (1981).

26. N. Schiller in Semiconductors Probed by Ultrafast Laser Spectroscopy,Vol. 2, ed. by R. R. Alfano (Academic Press, New York, 1984) p.441.

27. G. Mayer and F. Gires, Compt. Rend. Acad. Sci.(Paris) 258, 2039 (1964).

28. H. Mahr and M. D. Hirsch, Opt. Commun. 13, 96 (1964).

29. T. Daly and H. Mahr, Solid State Commun. 25, 323 (1978).

30. D. Hulin, A. Migus, A. Antonetti, I. Ledonx, J. Baden, J. L. Oudar, and J. Zyss, Appl. Phys. Lett. 49, 761 (1986).

31. J. Shah, T. C. Damen, B. Deveaud and D. Block, Appl. Phys. Lett. 50, 1307 (1987).

32. C. V. Shank, R. L. Fork, R. F. Leheny and J. Shah, Phys. Rev. Lett. 42, 112 (1979).

33. A. V. Nurmikko, in Semiconductors Probed by Ultrafast Laser Spectroscopy, Vol. 2, ed. by R. R. Alfano (Academic Press, New York, 1984) p.509.

34. D. L. Rosen, A. G. Doukas, Y. Budansky and R. R. Alfano, Appl. Phys. Lett. 39, 935 (1981).

35. D. von der Linde, J. Kuhl, and H. Klingenburg, Phys. Rev. Lett. 44, 1505 (1980).

36. C. A. Hoffman, K. Jarasiunas, H. J. Gerritsen and A. V. Nurmikko, Appl. Phys. Lett. 33, 536 (1978).

37. D. J. Erskine, Ph. D. Thesis (Cornell University, 1984) unpublished.

38. D. J. Erskine, A. J. Taylor and C. L. Tang, Appl. Phys. Lett. 45, 54 (1984).

39. See for example R. S. Knox, Solid State Physics, Suppl. No. 5 (Academic Press, New York, 1963).

40. J. O. Dimmock, in Optical Properties of III-V Compounds, Semiconductors and Semimetals, Vol. 3, ed. by R. K. Willardson and A. C. Beer (Academic Press, New York, 1967) p.259.

41. See for example C. Kittel, Introduction to Solid State Physics, 6th Edition (J. Wiley & Son, Inc, New York, 1986) p.303.

42. J. J. Hopfield, in Proceedings of the Seventh International Conference on the Physics of Semiconductors, ed. by M. Hulin (Dunod, Paris, 1964) p.725.

43. S. Lai and M. V. Klein, Phys. Rev. Lett. 44, 1087 (1980).

44. See for example review article by P. J. Dean in Excitons, ed. by K. Cho (Springer-Verlag, Heidelberg, 1979).

45. P. W. Anderson, Phys. Rev. 109, 1492 (1958); N. F. Mott, Phil. Mag. 13, 989 (1966).

46. J. J. Hopfield, Phys. Rev. 112, 1555 (1958).

47. See for example M. Born and K. Huang, Dynamical Theory of Crystal Lattices, (Oxford University Press, Oxford, 1962) p.89.

48. Farid Askary, Ph. D. Thesis, University of California, Berkeley, California (unpublished, 1983).

49. W. C. Tait, Phys. Rev. B5, 648 (1972).

50. See for example F. Askary and P. Y. Yu, Phys. Rev. B 31, 6643 (1985) and references therein.

51. Y. Toyozawa, Progr. Theor. Phys. Suppl. 12, 111 (1959).

52. H. Frohlich, Adv. in Phys. 3, 325 (1954).

53. H. Sumi, J. Phys. Soc. (Japan) 41, 526 (1976).

54. F. Askary and P. Y. Yu, Phys. Rev. B 28, 6165 (1983).

55. J. S. Weiner and P. Y. Yu, Solid State Commun. 50, 493 (1984).

56. See for example review article by S. Nikitine in Optical Properties of Solids, ed. by S. Nudelman and S. S. Mitra (Plenum Press, New York, 1969).

57. P. W. Baumeister, Phys. Rev. 121, 359 (1961).

58. E. F. Gross and A. A. Kaplayanskii, Soviet Phys.-Doklady 5, 530 (1960).

59. Y. Petroff, P. Y. Yu, and Y. R. Shen, Phys. Rev. B12, 2488 (1975).

60. A. Compaan and H. Z. Cummins, Phys. Rev. B6, 4753 (1972); F. I. Kreingol'd and V.L. Makarov, Fiz. Tverd. Tela, 15, 1307 (1973) [Sov. Phys. Sol. State 15, 890 (1972)]; E. F. Gross, F. I. Kreingol'd and V. I. Makarov, ZhETF Pis Red. 15,383 (1972) [JETP Lett. 15, 269 (1972)].

61. P. Y. Yu and Y. R. Shen, Phys. Rev. B12, 1377 (1975).

62. A. Compaan and H. Z. Cummins, Phys. Rev. Lett. 31, 41 (1973); M. A. Washington, A. Z. Genack, H. Z. Cummins, R. H. Bruce, A. Compaan and R. A. Forman, Phys. Rev. B 15, 2145 (1977).

63. P. Y. Yu and Y. R. Shen, Phys. Rev. Lett. 32, 939 (1974).

64. R. J. Elliot, Phys. Rev. 108, 1384 (1957).

65. R. M. Habiger and A. Compaan, Solid State Commun. 18, 1531 (1976).

66. J. S. Weiner, N. Caswell, P. Y. Yu and A. Mysyrowicz, Solid State Commun. 46, 105 (1983).

67. N. Caswell, J. S. Weiner and P. Y. Yu, Solid State Commun. 40, 843 (1981); H. R. Trebin, H. Z. Cummins and J. L. Birman, Phys. Rev. B 23, 597 (1981); R. G. Waters, F. H. Pollak, R. H. Bruce and H. Z. Cummins, Phys. Rev. B 21, 1665 (1980).

68. R. M. Habiger and A. Compaan, Solid State Commun. 26, 533 (1978).

69. J. S. Weiner and P. Y. Yu in Proceedings of the XVII InternationalConference on the Physics of Semiconductors, ed. by J. D.Chadi and W. A. Harrison (Springer-Verlag, New York, 1985) p.1207.

70. See for example F. Wooten, Optical Properties of Solids (Academic Press, New York, 1972) p.146-148.

71. H. Stolz, W. von der Osten and J. Weber, in Physics of Semiconductors, Proceedings of the 13th International Conference, Rome, 1976, ed. by F. G. Fumi (Tipografia Marves, Rome, 1976) p.865.

72. J. Windscheif and W. von der Osten, J. Phys. C: 13, 6299 (1980).

73. H. Stolz and W. von der Osten, Solid State Commun. 49, 1035 (1984).

74. H. Stolz, E. Schreiber and W. von der Osten in Proceedings of the XVII International Conf. on the Physics of Semiconductors, ed. by J. D. Chadi and W. A. Harrison (Springer-Verlag, New York, 1985) p.1271.

75. H. Stolz and W. von der Osten, in Proceedings of the International Conference on Defeccts in Insulating Crystal, ed. by F. Luty (Gordon and Breach, New York, 1984).

76. See for example review articles in Excitons, ed. by K. Cho (Springer-Verlag, Heidelberg, 1979) and in Excitons, ed. by E. I. Rashba and M. D. Sturge (North-Holland Publishing Co., Amsterdam, 1982).

77. S. I. Pekar, Sov. Phys. JETP 6, 785 (1958); S.I. Pekar, Sov. Phys. JETP 7, 813 (1958).

78. J. J. Hopfield and D. G. Thomas, Phys. Rev. 132, 563 (1963).

79. F. Evangelisti, A. Grova and F. Patella, Phys. Rev. B 10, 4253 (1974); S. A. Permogorov, V. V. Travnikov and A. V. Selkin, Sov. Phys. Solid State 14, 3051 (1973); E. Gross, S. Permogorov, V. Travnikov and A. Selkin, Solid State Commun. 10, 1071 (1972).

81. C. Weisbuch and R.G. Ulbrich Phys. Rev. Lett. 39, 654 (1977).

82. C. Weisbuch and R.G. Ulbrich, J. of Lumin. 18/19, 27 (1979); R.G. Ulbrich and C. Weisbuch, in Festkorperprobleme (advances in Solid State Physics) volume XVIII, ed. by J. Treusch (Vieweg, Braunschweig, 1978) p.217.

83. See for example P. Y. Yu, in Light Scattering in Solids, eds. J. L. Birman, H. Z. Cummins, and K. K. Rebane (Plenum, New York, 1979) p.143.

84. D. D. Sell, S. E. Stokowski, R. Dingle and J. V. DiLorenzo, Phys. Rev. B 10, 4568 (1973).

85. P. Wiesner and U. Heim, Phys. Rev. B 11, 3071 (1975).

86. F. Askary and P.Y. Yu, Solid State Commun. 47, 241 (1983).

87. M. S. Brodin and M. G. Matsko, Solid State Commun. 35, 375 (1980).

88. E. S. Koteles, J. P. Salerno, W. Bloss, and E. M. Brody, Proceedings of the 17th International Conference on the Physics of Semiconductors, ed. by J. D. Chadi and W. A. Harrison (Springer-Verlag, New York, 1985) p.1247; E. S. Koteles, J. Lee, J. P. Salerno and M. O. Vassell, Phys. Rev. Lett. 55, 867 (1985); W.L. Bloss, E.S. Koteles, E.M. Brody, B. J. Sowell, J. P. Salerno and J.V. Gormley, Solid State Commun. 54, 103 (1985); J. Lee, E. S. Koteles, M. O. Vassell and J. P. Salerno, J. Lumin. 34, 63 (1985).

89. T. Steiner, M. L. Thewalt, E. S. Koteles and J. P. Salerno, Phys. Rev. B 34, 1006 (1986).

90. D. J. Wolford, B. G. Streetman and J. Thompson, in Proceedings of the 15th International Conference on the Physics of Semiconductors, ed. by S. Tanaka and Y. Toyozawa, J. of Phys. Soc. of Japan 49, Suppl. A (1980) p.223.

91. S. Permogorov, A. Reznitsky, S. Verbin, G. O Muller, P. Flogel and M. Nikiforova, Phys. Stat. Solidi 113, 589 (1982).

92. J. H. Collet, J. A. Kash, D. J. Wolford and J. Thompson, J. Phys. C 16, 1283 (1983).

93. J. A. Kash, A. Ron and E. Cohen, Phys. Rev. B 28, 6147 (1983).

94. M. V. Klein, M. D. Sturge and E. Cohen, Phys. Rev. B 25, 4331 (1982).

95. G. Gershoni, E. Cohen and A. Ron, Phys. Rev. Lett. 56, 2211 (1986).

96. E. Cohen, in Proceedings of the XVII International Conference on the Physics of Semiconductors, ed. by J. D. Chadi and W. A. Harrison (Springer-Verlag, New York, 1985) p.1221.

97. S. Permogorov, A. Reznitsky, S. Verbin and V. Lysenko, Solid State Commun. 47, 5 (1983).

98. N. N. Ablyazov, M. E. Raikh and A. L. Efros, Soviet Phys.-Solid State 25, 199. (1983).

99. S. D. Branovskii and A. L. Effros, Sov. Phys. Semicond. 12, 1328 (1978).

100. E. Cohen and M. D. Sturge, Phys. Rev. B 25, 3828 (1978).

101. P. Lawaetz, Solid State Commun. 16, 65 (1975); M. Altarelli, R. A. Sabatini, and N. O. Lipari, ibid. 25,1101 (1978).

102. R. Fisher, U. Heim, F. Stern and K. Weiser, Phys. Rev. Lett. 26, 1182 (1971).

103. R. A. Street, Adv. in Phys. 30, 593 (1981).

104. C. Tsang and R. A. Street, Phys. Rev. B 19, 3027 (1979).

105. G. S. Higashi and M. Kastner, Phys. Rev. B 24, 2295 (1981); J. Shah, Phys. Rev. B 21, 4751 (1980); B. A. Weinstein, T. E. Orlowski, W. H. Knox, T. M. Nordlund and G. Mourou, Phys. Rev. B 26, 4777 (1982); K. Murayama and M. A. Bosch, Phys. Rev. B 25, 6542 (1982).

106. See for example review article by P. G. Le Comber and W. E. Spear, Topics in Applied Physics, Vol. 36, (Springer-Verlag, Heidelberg, 1979) p.251.

107. See for example P. G. Le Comber in Fundamental Physics of Amorphous Semiconductors, Springer Series in Solid State Sciences, Vol. 25, ed. by F. Yonezawa (Springer-Verlag, Heidelberg, 1981) p.46.

108. D. E. Ackley, J. Tauc and W. Paul, Phys. Rev. Lett. 43, 715 (1979); Z. Vardeny and J. Tauc, Phys. Rev. Lett. 46, 223 (1981); Z. Vardeny, J. Strait, D. Pfost, J. Tauc and B. Abeles, Phys. Rev. Lett. 48, 1132 (1982).

109. D.J. Dunstan, Philos. Mag. B 46, 579 (1982).

110. T. E. Orlowski and H. Scher, Phys. Rev. Lett. 54, 220 (1985).

111. See for example references in review article by G. Pfister and H. Scher, Adv. in Phys. 27, 747 (1978).

112. J. Orenstein and M. Kastner, Phys. Rev. Lett. 46, 1421 (1981).

113. B. A. Wilson, P. Hu, T. M. Jedju and J. P. Harbison, Phys. Rev. B 28, 5901 (1983); B. A. Wilson, P. Hu, J. P. Harbison, and T. M. Jedju, Phys. Rev. Lett. 50, 1490 (1983).

114. P. Y. Yu and R. S. Berg, Bull. Am. Phys. Soc. 28, 259 (1983).

115. R. W. Collins, M. A. Paesler, and W. Paul, Solid State Commun. 34, 833 (1980).

116. See for example review article by P. J. Dean in Progress in Solid State Chemistry, Vol. 8, ed. by J. O. McCaldin and G. Somorjai (Pergamon Press, Oxford, 1973) p.1.

117. B. A. Wilson and T. P. Kerwin, Phys. Rev. B 25, 5276 (1982).

118. E. M. Conwell, High Field Transport in Semiconductors, Solid State Physics Suppl. 9, ed. by F. Seitz, D. Turnbull and H. Ehrenreich (Academic Press, New York, 1967).

119. R. Ulbrich, Solid State Electronics 21, 51 (1978).

120. E. J. Yoffa, Phys. Rev. B 23, 1909 (1981).

121. See articles in Semiconductors Probed by Ultrafast Laser Spectroscroscopy, Vol. 1 and 2, edited by R. R. Alfano (Academic Press, New York, 1984).

122. S. A. Lyon, J. of Lum. 35, 121 (1986).

123. E. M.Conwell and M. O. Vassell, IEEE ED-13, 22 (1966).

124. C. L. Collins and P. Y. Yu, Phys. Rev. B 30, 4501 (1984).

125. R. Ulbrich, Phys. Rev. B 8, 5719 (1973).

126. C. V. Shank, R. L. Fork, R. F. Leheny and J. Shah, Phys. Rev. Lett. 42, 112 (1979).

127. D. von der Linde and R. Lambrich, Phys. Rev. Lett. 42, 1090 (1979).

128. E. O. Goebel and O. Hildebrand, Phys. Stat. Sol. **b** 88, 645 (1978).

129. K. Kash and J. Shah, Appl. Lett. 45, 401 (1984).

130. J. L. Oudar, D. Hulin, A. Migus, A. Antonetti and F. Alexandre, Phys. Rev. Lett. 55,2074 (1985).

131. W. H. Knox, C. Hirlimann, D. A. B. Miller, J. Shah, D. S. Chemla, and C. V. Shank, Phys. Rev. Lett. 56, 1191 (1986).

132. J. A. Kash, J. C. Tsang, and J. M. Hvam, Phys. Rev. Lett. 54, 2151 (1985).

133. W. Z. Lin, L. G. Fujimoto, E. P. Ippen and R. A. Logan, Appl. Phys. Lett. 50,124 (1987); ibid, 51,161 (1987).

134. Y. Huang and P. Y. Yu, Solid State Commun. 63, 109 (1987).

135. A. F. J. Levi, J. R. Hayes, P. A. Platzman and W. Wiegmann, Phys. Rev. Lett. 55, 2071 (1985).

136. D. Hulin, M. Combescot, J. Bok, A. Migus, J. Y. Vinet and A. Antonetti, Phys. Rev. Lett. 52, 1998 (1984).

137. R. F. Leheny, J. Shah, R. L. Fork, C. V. Shank and A. Migus, Solid State Commun. 31, 809 (1979).

138. H. M. van Driel, Phys. Rev. B 19, 5928 (1979).

139. P. Lugli, C. Jacoboni, L. Reggiani and P. Kocevar, Appl. Phys. Lett. 50, 1251 (1987).

140. J. Shah, A. Pinczuk, A. C. Gossard, and W. Wiegmann, Phys. Rev. Lett. 54, 2045 (1985).

141. K. M. Romanek, H. Nather, and J. Fisher, J. of Lum. 24/25, 585 (1981); C. L. Collins and P. Y. Yu, Solid State Commun. 51, 123 (1984); A. Cornet, J. Collet, T. Amand, M. Pugnet, M. Brousseau and R. S. Razabirin, J. of Lum. 24/25, 609 (1981).

142. M. Combescot and J. Bok, J. of Lum. 30, 1 (1985).

143. Z. Y. Xu and C. L. Tang, Appl. Phys. Lett. 44, 692 (1984).

144. J. F. Ryan, R. A. Taylor, A. J. Turberfield, A. Maciel, J. M. Worlock, A. C. Gossard and W. Wiegmann, Phys. Rev. Lett. 53, 1841 (1984).

145. C. V. Shank, R. L. Fork, R. Yen, J. Shah, B. I. Greene, A. C. Gossard, and C. Weisbuch, Solid State Commun. 47, 981 (1983).

TABLE 1 SUMMARY OF CHARACTERISTICS OF COMMON LASER SYSTEMS GENERATING PICOSECOND OR SUBPICOSECOND PULSES

LASER SYSTEM	PULSE DURATION	PHOTON ENERGY	REPETITION RATE	ENERGY/ PULSE
(a) Modelocked Pulse Nd:glass	>10 ps	1.17 eV or 2.34 eV	1 Hz	>1 mJ
(b) Modelocked Pulse Nd:YAG	<100 ps	ditto	>100 Hz	>1 mJ
(c) Modelocked cw Nd:YAG	<100 ps	ditto	$<10^8$ Hz	<100 nJ
(d) Modelocked cw Ar ion	>150 ps	2.4-2.7 in steps	$<10^8$ Hz	<10 nJ
(e) Dye Laser Synchronously pumped by modelocked Nd:YAG	>1 ps	1-2.3 eV	$<10^8$ Hz	<10 nJ
(f) Dye Laser Synchronously pumped by modelocked Ar ion	>1 ps	1-2.3 eV	$<10^8$ Hz	<1 nJ
(g) Colliding Pulse passively modelcked dye laser	<0.1 ps	2 eV	$<10^8$ Hz	<1 nJ

VII. FIGURE CAPTIONS

FIG.1 Schematic diagram of the construction of a colliding pulse modelocked dye laser.

FIG.2 Schematic diagram of an experimental setup for determining the time dependence of emission from a sample using a synchronously pumped modelocked dye laser as the excitation source and the time-delayed coincidence photon counter as the detecting system. The notations are: CFD-Constant Fraction Discriminator; TAC- Time-Amplitude Converter; PHA- Pulse Height Analyser. (From Ref. 22).

FIG.3 Schematical diagram of a optical Kerr shutter.

FIG.4 Two-band models of exciton for: (A) a direct bandgap semiconductor and (B) an indirect bandgap semiconductor.

FIG.5 Dispersion curves of photon (dot-dashed line), exciton (broken curve) and polariton (solid curve) for the lowest energy exciton for CdS. (From Ref. 48).

FIG.6 Photoluminescence spectrum of Cu_2O showing the no-phonon peak of the 1s exciton (labelled ORTHO(EQ)) and the phonon assisted peaks of the orthoexciton and of the paraexciton. (From Ref. 22).

FIG.7 Dependence of the orthoexciton luminescence intensity on temperature. (From Ref. 66).

FIG.8 The time decay of the orthoexciton and paraexciton luminescence intensity at three different temperatures:(a) T=2.5 K; (b)35 K and (c)48 K. (From Ref. 66).

FIG.9 Luminescence spectra of Cu_2O excited at two different frequencies. The insets show schematically the excitation, relaxation and emission processes of the orthoexciton in Cu_2O for the two

different excitation frequencies. The arrows labelled LA and Γ_{12} represent relaxation of the orthoexciton via emission of LA phonons and Γ_{12} phonons respectively. (From Ref. 55).

FIG.10 Decay of the $2\Gamma_{12}$ phonon Raman peak in Cu_2O for three different incident laser frequencies. These laser frequencies correspond to excitation of orthoexcitons with kinetic energies: (a) 1 cm^{-1}; (b) 4 cm^{-1}; and (c) 7 cm^{-1} respectively. The broken curve is a fit to the experimental curve with a biexponential decay: exp(-t/0.26 ns)+exp(-t/1.5 ns). (From Ref. 55).

FIG.11 (a) and (b) Experimental time dependent luminescence spectra of the Γ_{12} phonon sideband of the orthoexciton in Cu_2O. (c) and (d) Corresponding computed time dependent emission spectra using the model described in Ref. 69.

Fig.12 Schematic band structure of AgBr reproduced from Ref. 75.

Fig.13 Schematic exciton band diagram of AgBr showing the intervalley and intravalley scattering of excitons by various phonons.

FIG.14 Scattering rate of the indirect exciton in AgBr as a function of its kinetic energy. The broken curves show the calculated contributions to the total scattering rate (solid curve) due to scattering by the different phonons. The solid points are experimental data. (From Ref. 75).

Fig.15 Time-resolved resonant Raman scattering spectra in AgBr excited at two different laser energies: 2.700 eV (top spectra) and 2.6968 eV (bottom spectra). (From Ref. 75).

Fig.16 Computed polariton density of states (a) and emission spectra (b) in CdS using two different additional boundary conditions: broken curves-Pekar's ABC (Ref. 77); solid curves-ABC from C. S. Ting, M. J. Frankel and J. L. Birman, Solid State Commun. 17, 1285 (1975). E_L and E_T denote respectively the energies of the longitudinal and transverse excitons in CdS. (From Ref. 86).

Fig.17 Experimental and computed polariton emission spectra in four different semiconductors reproduced from Ref. 86.

Fig.18 Computed decay profiles of the lower branch polaritons in CdS. The three coordinate axes are: x- energy in cm^{-1}; y- time in ns; and z- log of the polariton population in arbitrary units. The peak populations for each curve have been normalized to facilitate comparison of decay rates. Sample temperatures for the four sets of curves are: (a) 0 K; (b) 1.6 K; (c) 4 K; (d) 25 K.

Fig.19 A comparison between the theoretical inverse loss rates (solid curve) and the decay times (triangles) of the polariton in CdS. The decay times were obtained by single exponential fits to the calculated decay profiles in Fig. 18 (a) and (d). The temperatures for the two sets of curves are (a) 0 K; (b) 25 K.

Fig.20 Effect of impurity trapping rate on the computed decay profiles of CdS at 6 K. The x and y coordinate axes are same as in Fig. 18. The z axes in (a) and (b) are linear in the polariton population while the z axes in (c) and (d) are logarithmic in the the population. The impurity trapping rates are: $3\times10^{8}\ s^{-1}$ for curves in (a) and (c); $9\times10^{8}\ s^{-1}$ for (b) and (d).

Fig.21 Comarison of the inverse loss rates (solid curve) and the two decay times obtained by fitting the calculated decay profiles in Fig. 20 (d) with a biexponential decay. The triangles represent the longer decay time and the crosses the shorter decay time.

Fig.22 Summary of the experimental results on the time decay of polaritons in CdS obtained at 6 K by Askary and Yu (Ref. 54). The triangles and crosses represent respectively the long and short decay times as in Fig. 21. The open circles represent the fractional amplitude of the longer decay time component in the decay profiles.

Fig.23 The steady state emission spectra of three GaAs samples grown by molecular beam epitaxy (MBE). The lower curves have progressively lower donor concentrations as shown by the progressively weaker

bound exciton peaks (D^o,X) and (D^o,h) as compared with the polariton (X) peak.

Fig.24 A series of experimental time resolved emission spectra for the three MBE GaAs samples in Fig. 23. In the sample MBE 3-14 notice how the dip in the sample evolved into a peak at longer times. The photon energy scales are identical for the three samples.

Fig.25 A series of computed time resolved emission spectra for the polariton in GaAs. The model assumes polariton are scattered by neutral donors and the donor concentrations (N_D)in the three series of curves have been adjusted to approximately reproduce the experimental spectra in Fig. 24. (From Ref. 24).

Fig.26 Excitation spectra of the degrees of polarization in $CdS_{1-x}Se_x$ with x=0.1 (a); and x=0.49 (b). The energy scales are that of the exciting laser. Solid circles represent the maximum values of the degree of polarization in the LO_1 phonon replica at a given excitation energy. Open circles show the energy dependence of the narrow LO_1 line intensity relative to the LO_1 wing intensity. The solid curves show the luminescence at bandgap excitation. The reflectivity spectrum for the x=0.1 sample is shown in the inset. (From Ref. 91).

Fig.27 A series of time resolved emission spectra in $CdS_{0.53}Se_{0.47}$ excited by different laser energies at 2 K. The luminescence in (b) and (c) is monitored in the LO phonon replica and the energy scale is shifted from (a) by the corresponding phonon energy of 25.5 meV (From Kash, Ron and Cohen, Ref. 93).

Fig.28 Effective lifetimes (solid circles) of excitons bound by potential fluctuations in $CdS_{0.53}Se_{0.47}$ at 2 K. The solid curve is the time integrated luminescence spectrum. The vertical broken line indicates the position of the peak in the reflectivity spectrum.

Fig.29 Experimental time decay (solid circles) of photoluminescence in two $Ga_{1-x}Al_xAs$ samples, (a) x=0.48 and (b) x=0.445, obtained by

Klein, Sturge and Cohen (Ref. 94). The solid curves are theoretical fits to the experimental points with Eq. (33) with these parameters: (a) $W_o = 6 \times 10^5\ s^{-1}$, $W_m = 4.6 \times 10^6\ s^{-1}$; (b) $W_o = 10^6\ s^{-1}$, $W_m = 3.7 \times 10^7\ s^{-1}$.

Fig.30 Model Density of States of a-Si determined from field effect measurements. Curves 1 and 2 are hydrogenated samples grown in glow discharge on substrates with two different temperatures. Curve 1: 550 K and Curve 2: 350 K. Curve 3 represents evaporated or sputtered films. (From Ref. 107).

Fig.31 Time decay of photoluminescence in a-Si:H obtained by Orlowski and Scher (Ref. 110) at 20 K. The solid curves are least-squares fits to the decay curves with a power law of the form: $t^{-\gamma}$.

Fig.32 The calculated intravalley (τ) electron-phonon scattering times of GaAs for the acoustic phonon (τ_{ac}) and the LO phonon (τ_{po}) as a function of the kinetic energy of the electron either in units of eV or relative to the LO phonon energy. The broken curves represent the Γ- X intervalley scattering times. (From Ref. 123).

Fig.33 The cooling curve of a "warm" EHP excited in GaAs with a lattice temperature (T_L) of 4.2 K by a modelocked ion laser. The open circles are experimental points while the solid curve is obtained by a theoretical calculation assuming only electron-acoustic phonon scattering. (From Ref. 125).

Fig.34 The cooling curve of a EHP excited by picosecond laser pulses. The solid and broken curves are obtained from theoretical calculations.

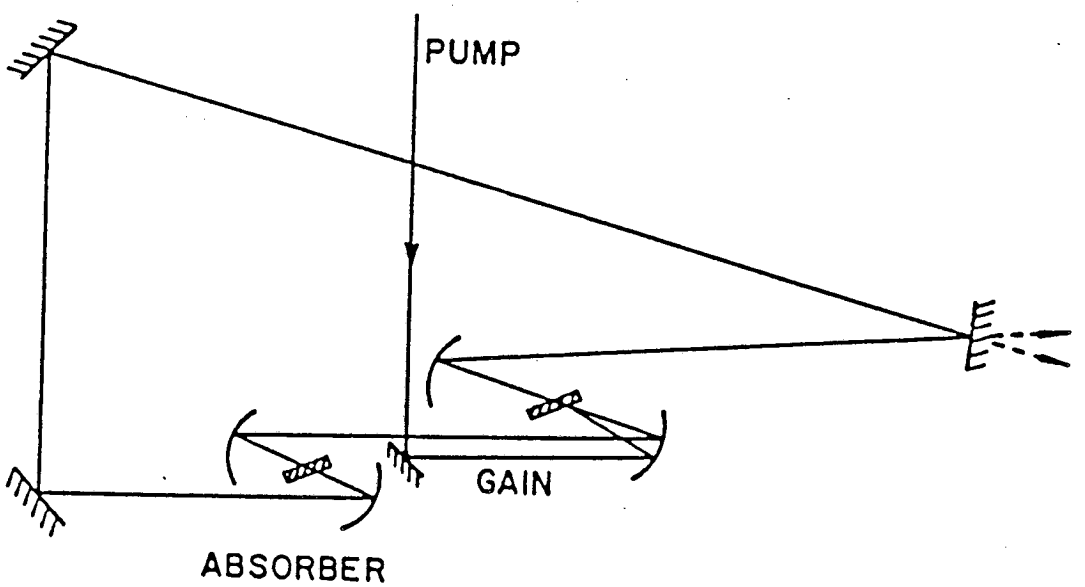

Fig. 1

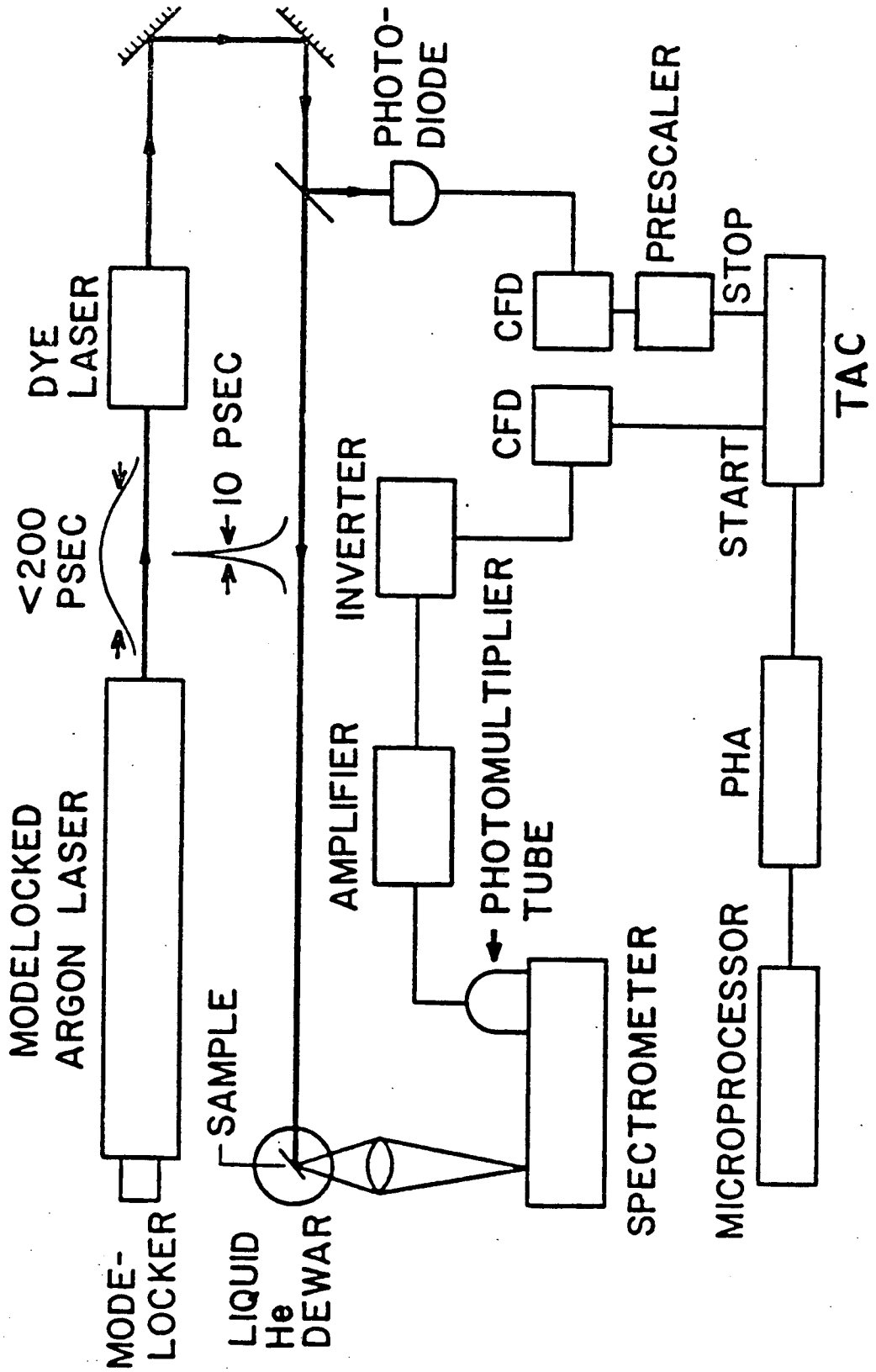
MODELOCKED ARGON LASER
MODE-LOCKER
DYE LASER
<200 PSEC
10 PSEC
SAMPLE
LIQUID He DEWAR
PHOTO-DIODE
INVERTER
AMPLIFIER
PHOTOMULTIPLIER TUBE
SPECTROMETER
CFD
CFD
PRESCALER
START
STOP
TAC
PHA
MICROPROCESSOR

Fig. 2

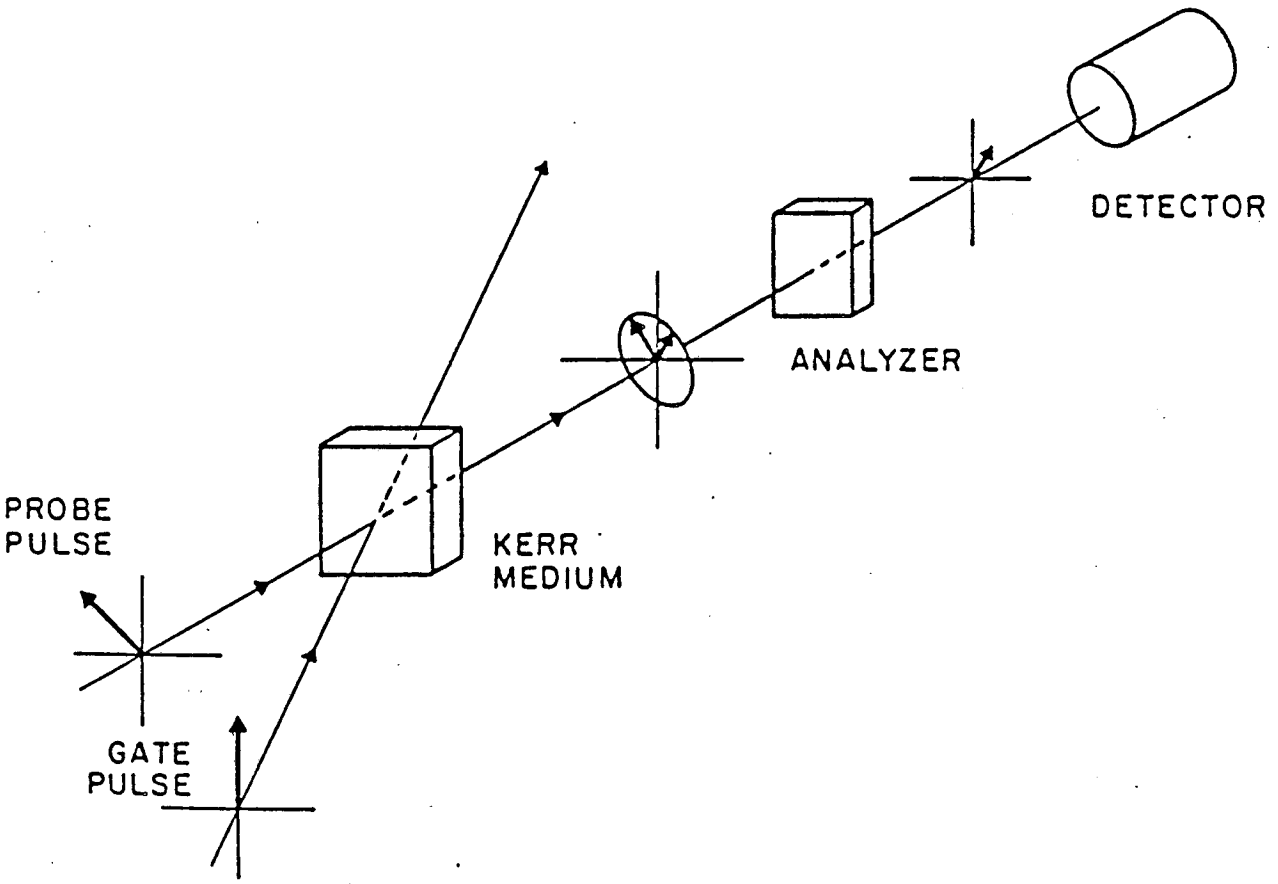

Fig. 3

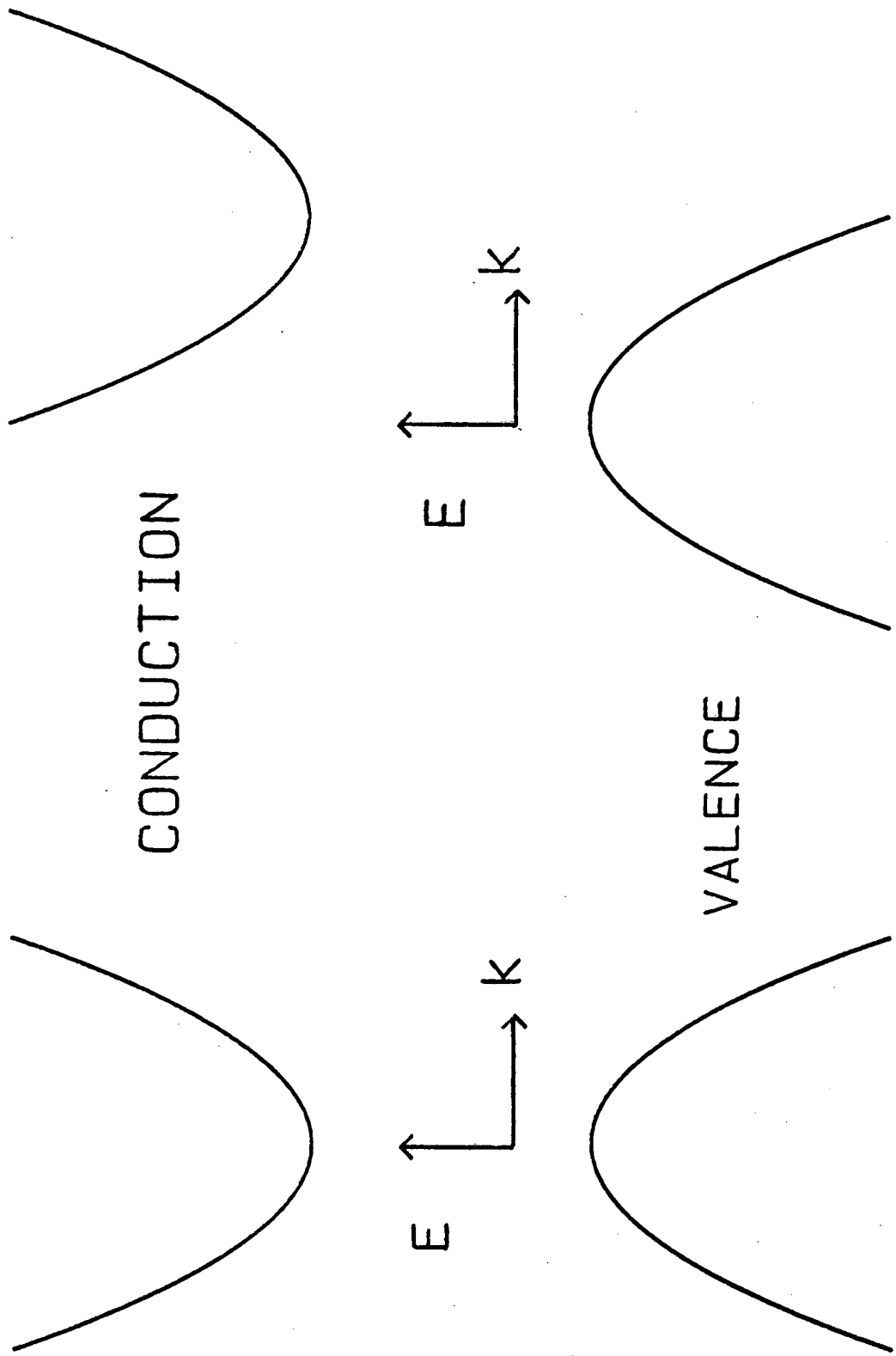

Fig. 4

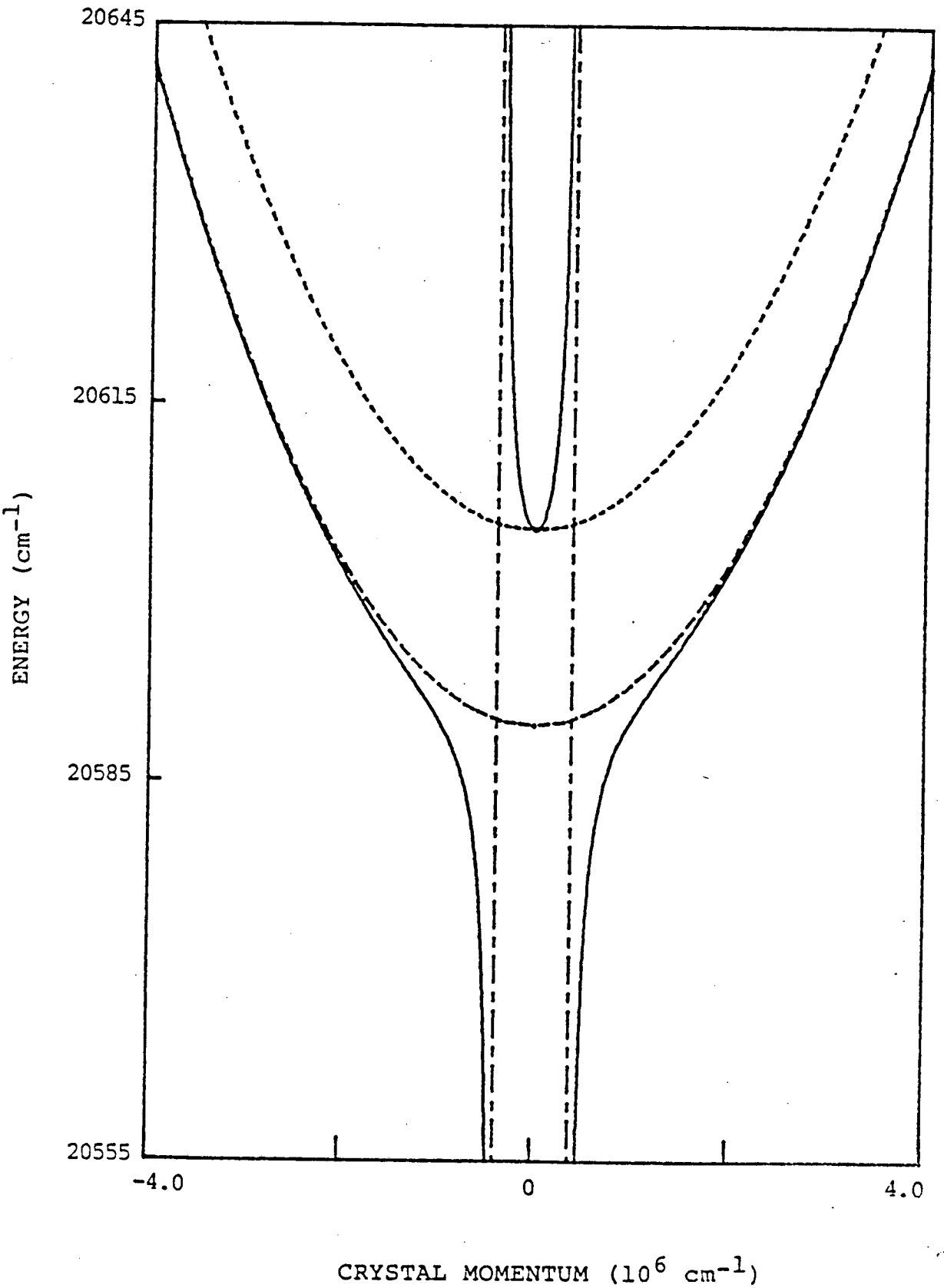
20645
20615
20585
20555
ENERGY (cm^{-1})
-4.0
0
4.0
CRYSTAL MOMENTUM (10^6 cm^{-1})

Fig. 5

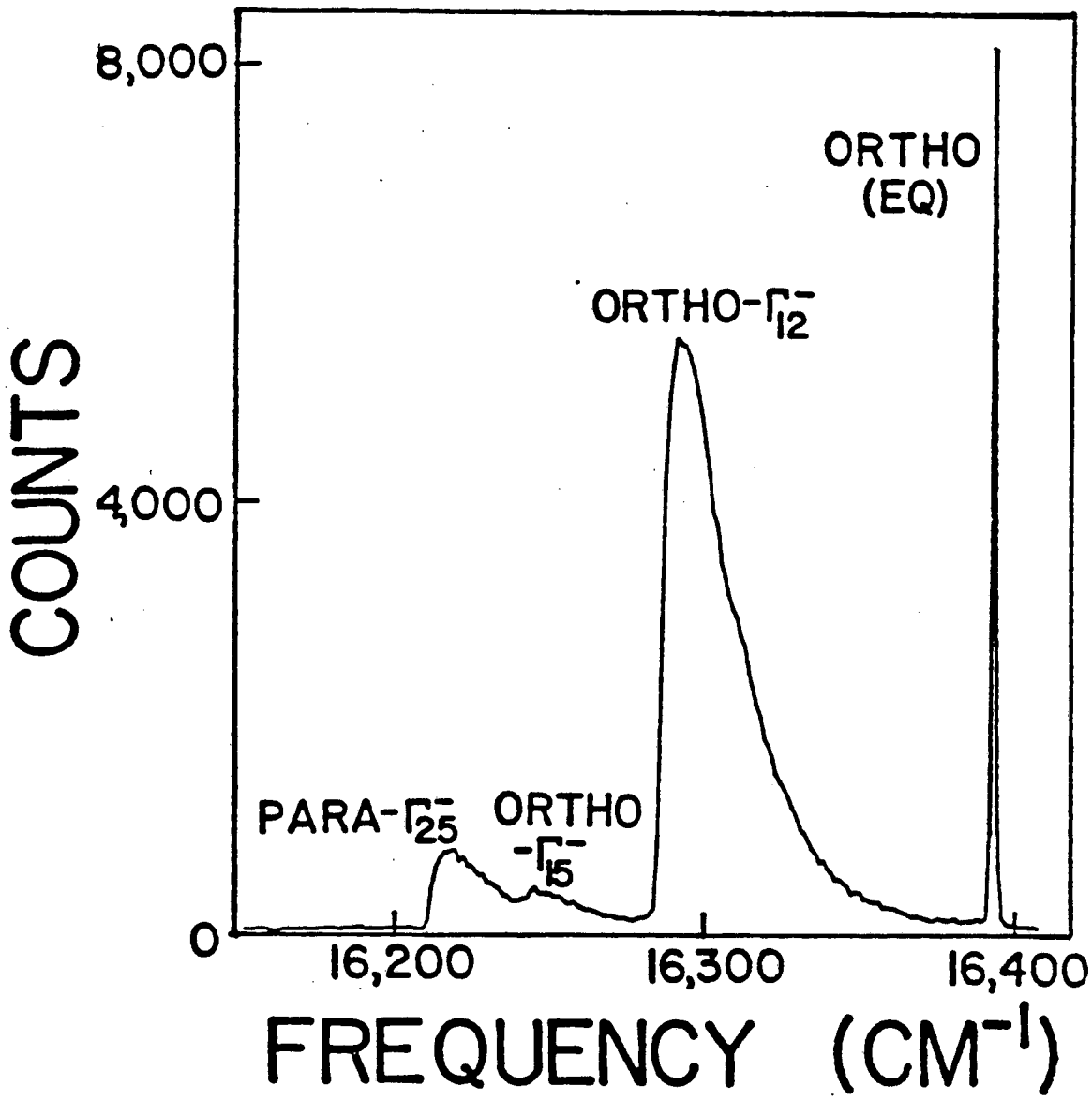
8,000
4,000
0
COUNTS
ORTHO
(EQ)
ORTHO-Γ_{12}^-
PARA-Γ_{25}^-
ORTHO
-Γ_{15}^-
16,200
16,300
16,400
FREQUENCY (CM^{-1})

Fig. 6

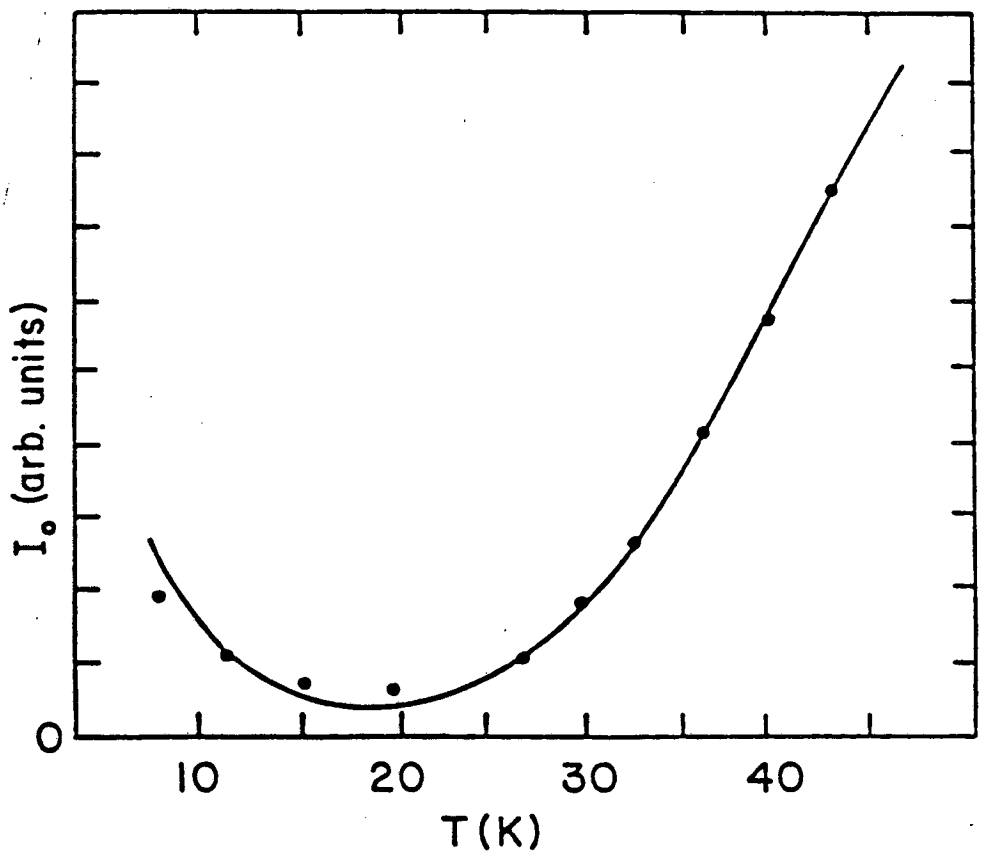

Fig. 7

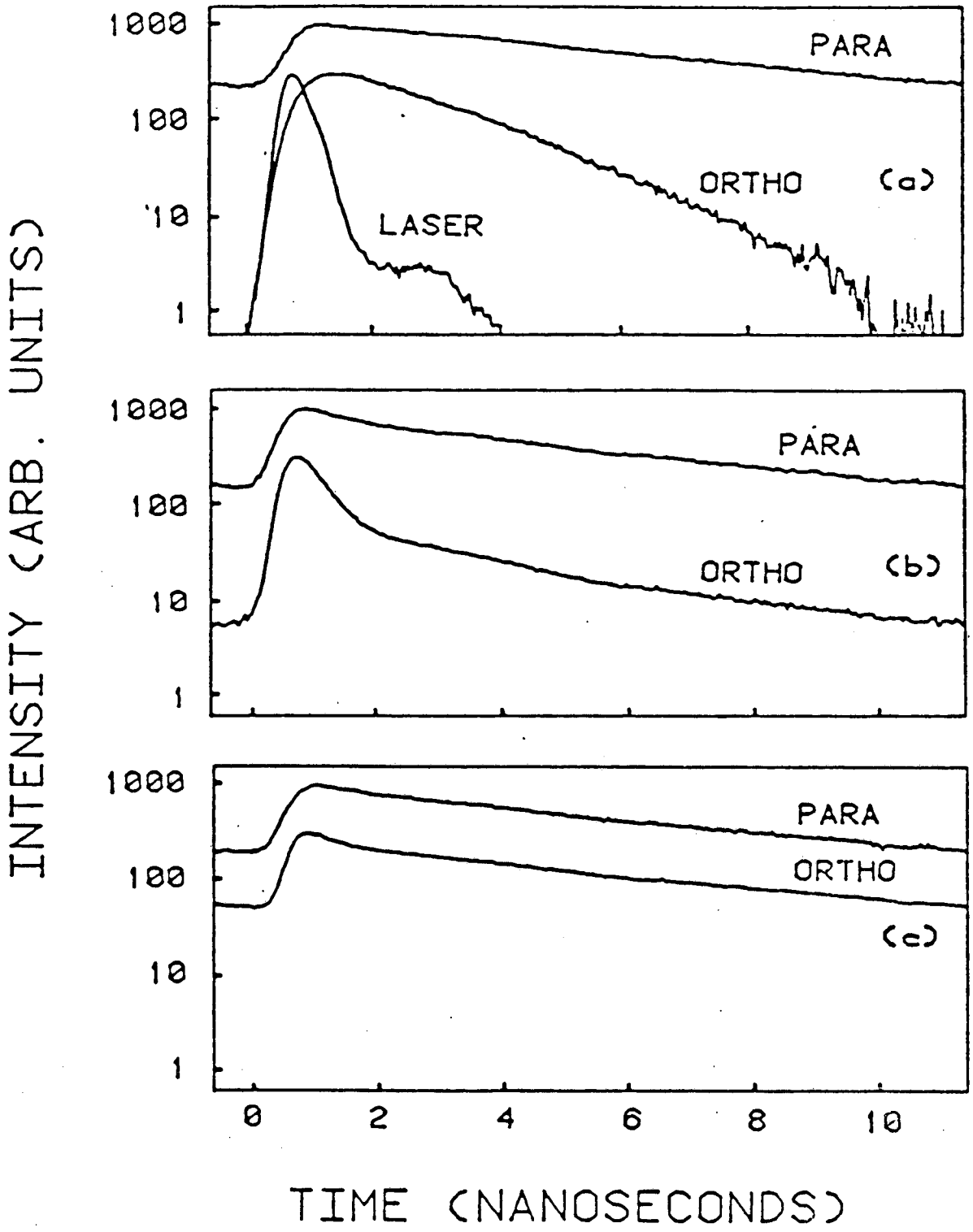
1000
100
10
1
PARA
ORTHO
(a)
LASER
1000
100
10
1
PARA
ORTHO
(b)
1000
100
10
1
PARA
ORTHO
(c)
0
2
4
6
8
10
INTENSITY (ARB. UNITS)
TIME (NANOSECONDS)

Fig. 8

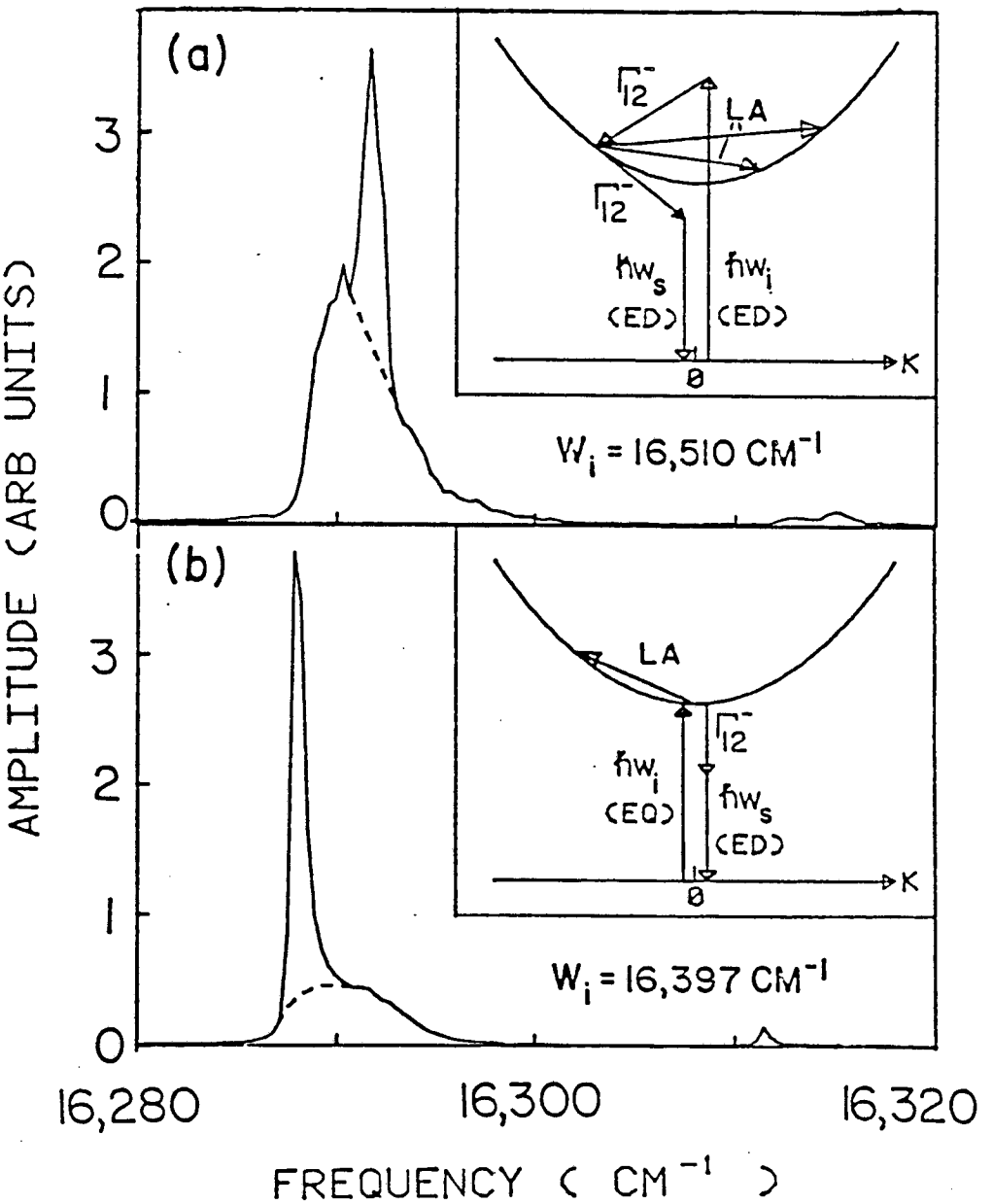
(a)
(b)
AMPLITUDE (ARB UNITS)
0
1
2
3
16,280
16,300
16,320
FREQUENCY (CM⁻¹)
Γ12⁻
LA
ħωs (ED)
ħωi (ED)
K
0
Wi = 16,510 CM⁻¹
ħωi (EQ)
ħωs (ED)
Wi = 16,397 CM⁻¹

Fig. 9

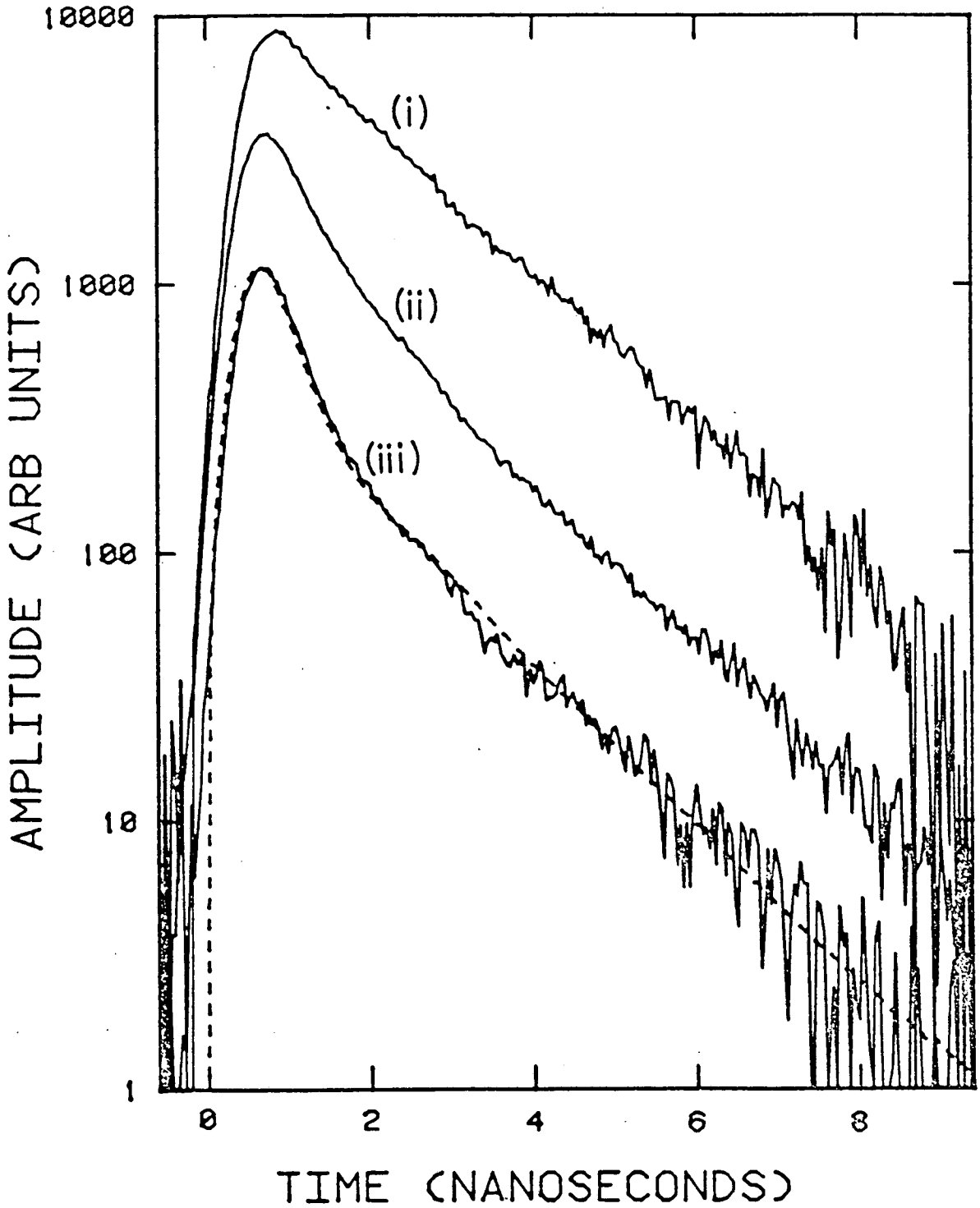
10000
1000
100
10
1
AMPLITUDE (ARB UNITS)
(i)
(ii)
(iii)
0
2
4
6
8
TIME (NANOSECONDS)

Fig. 10

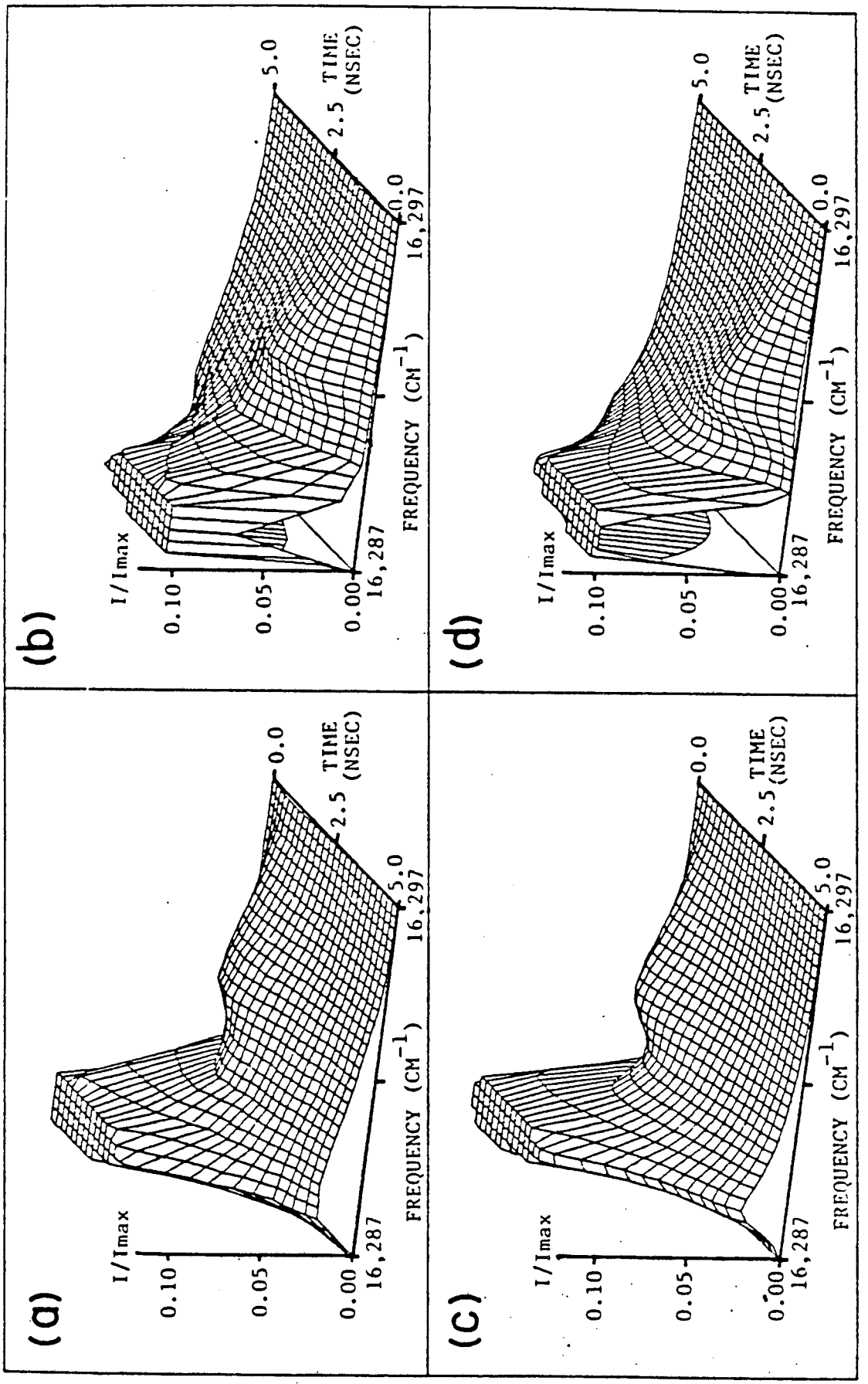
(a)
(b)
(c)
(d)
I/Imax
0.10
0.05
0.00
16,287
16,297
FREQUENCY (CM^{-1})
0.0
2.5
5.0
TIME (NSEC)

Fig. 11

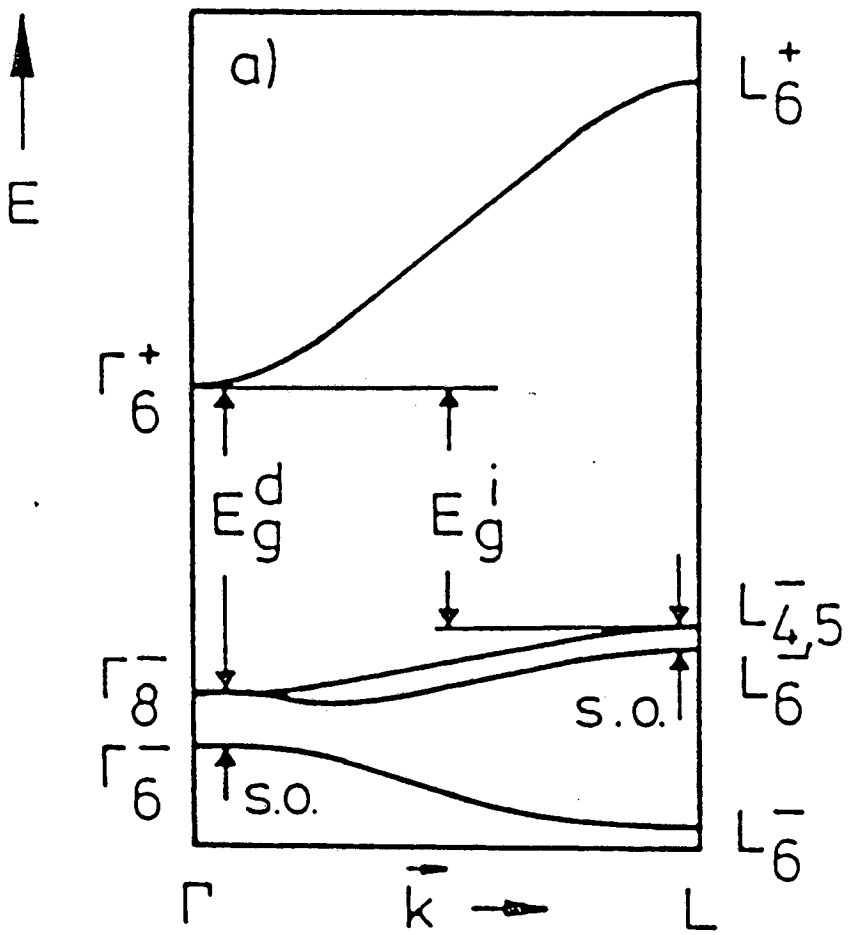

Fig. 12

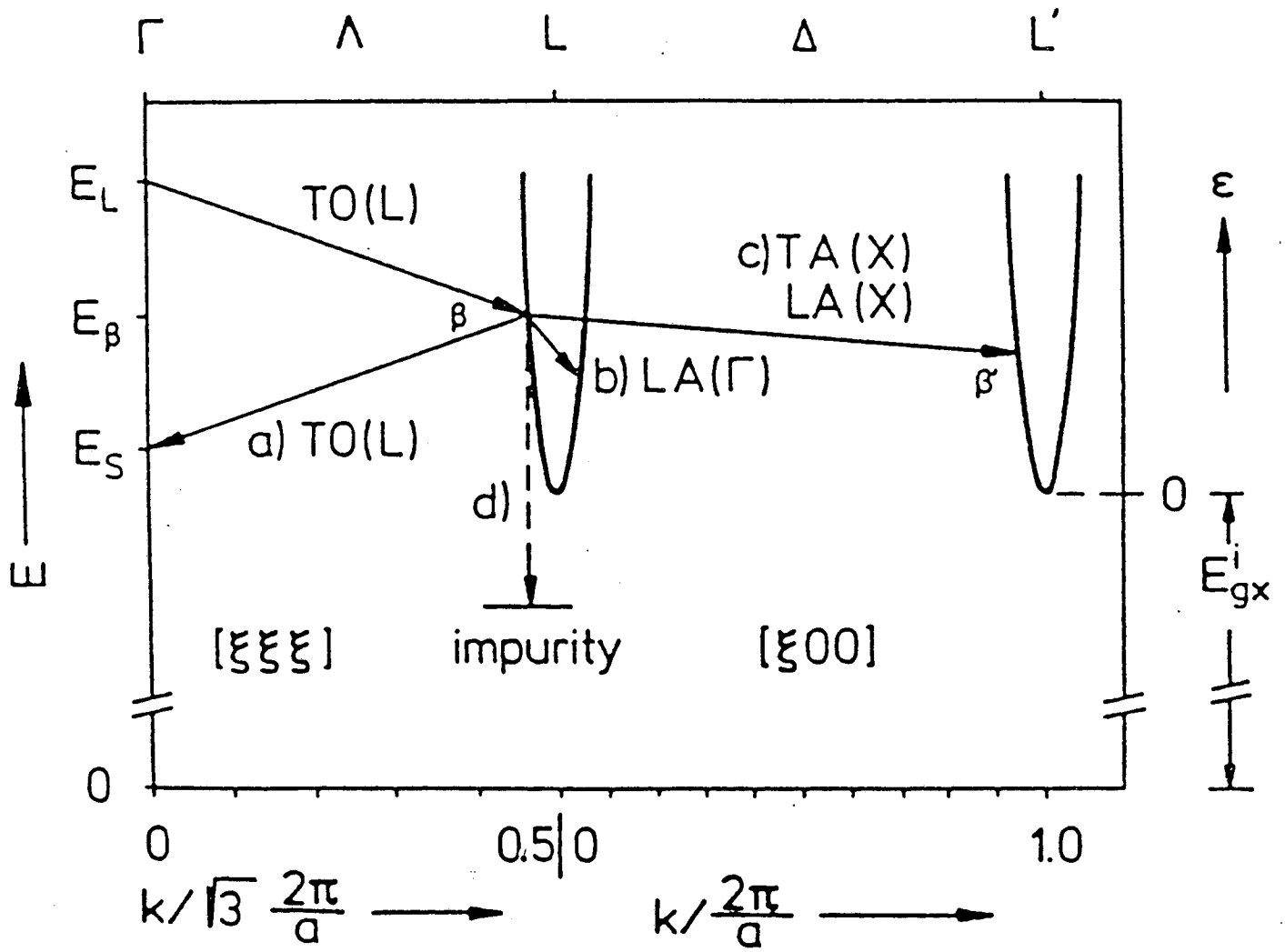
Γ
Λ
L
Δ
L'
E_L
E_β
E_S
TO(L)
β
c) TA(X)
LA(X)
b) LA(Γ)
β'
a) TO(L)
d)
0
E
ε
E^i_gx
[ξξξ]
impurity
[ξ00]
0
0
0.5
0
1.0
k/√3 2π/a
k/2π/a

Fig. 13

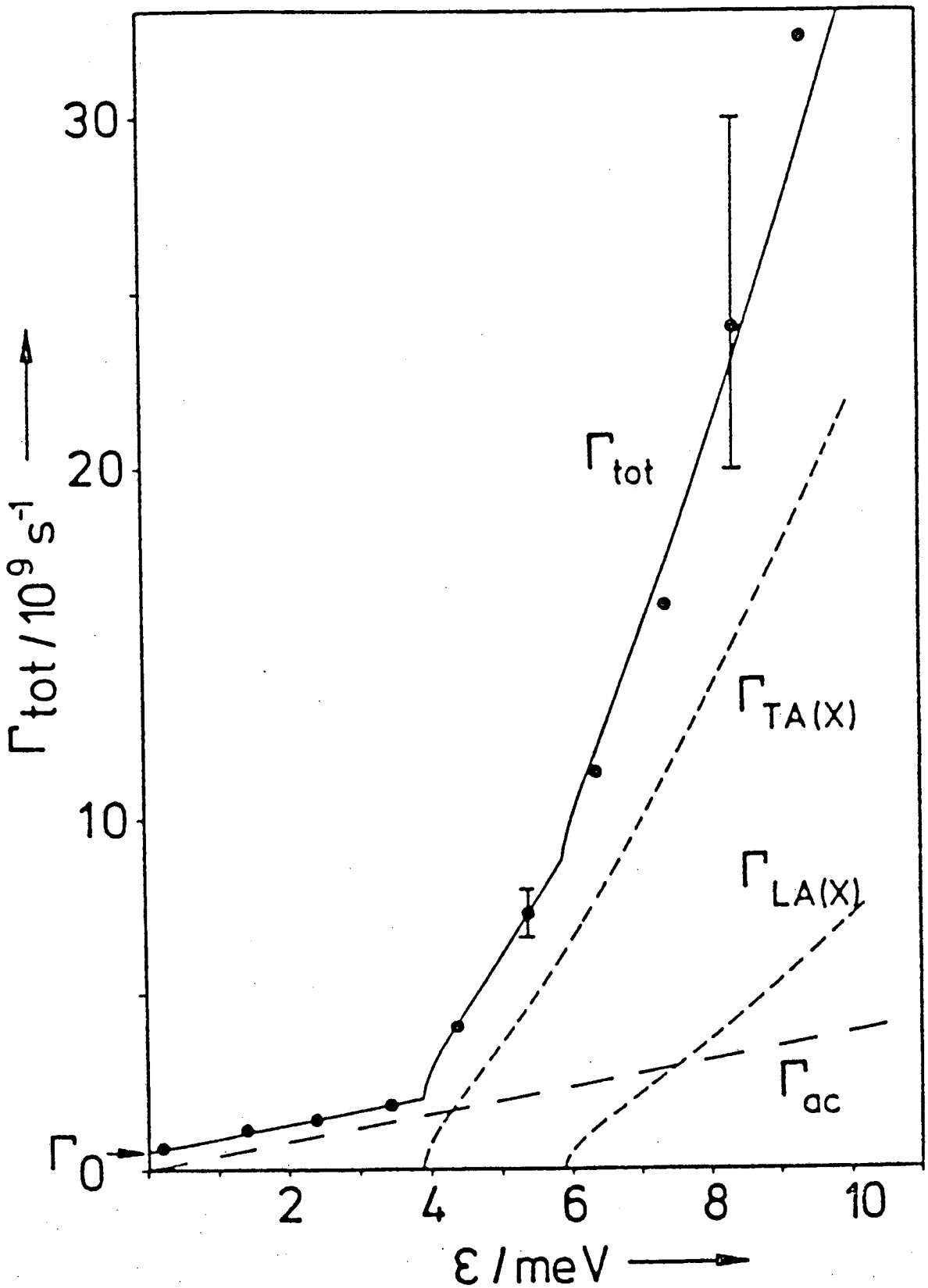
30
20
10
Γ_0
Γ_{tot}
$\Gamma_{TA(X)}$
$\Gamma_{LA(X)}$
Γ_{ac}
Γ_{tot} / 10^9 s^{-1}
2
4
6
8
10
ε / meV

Fig. 14

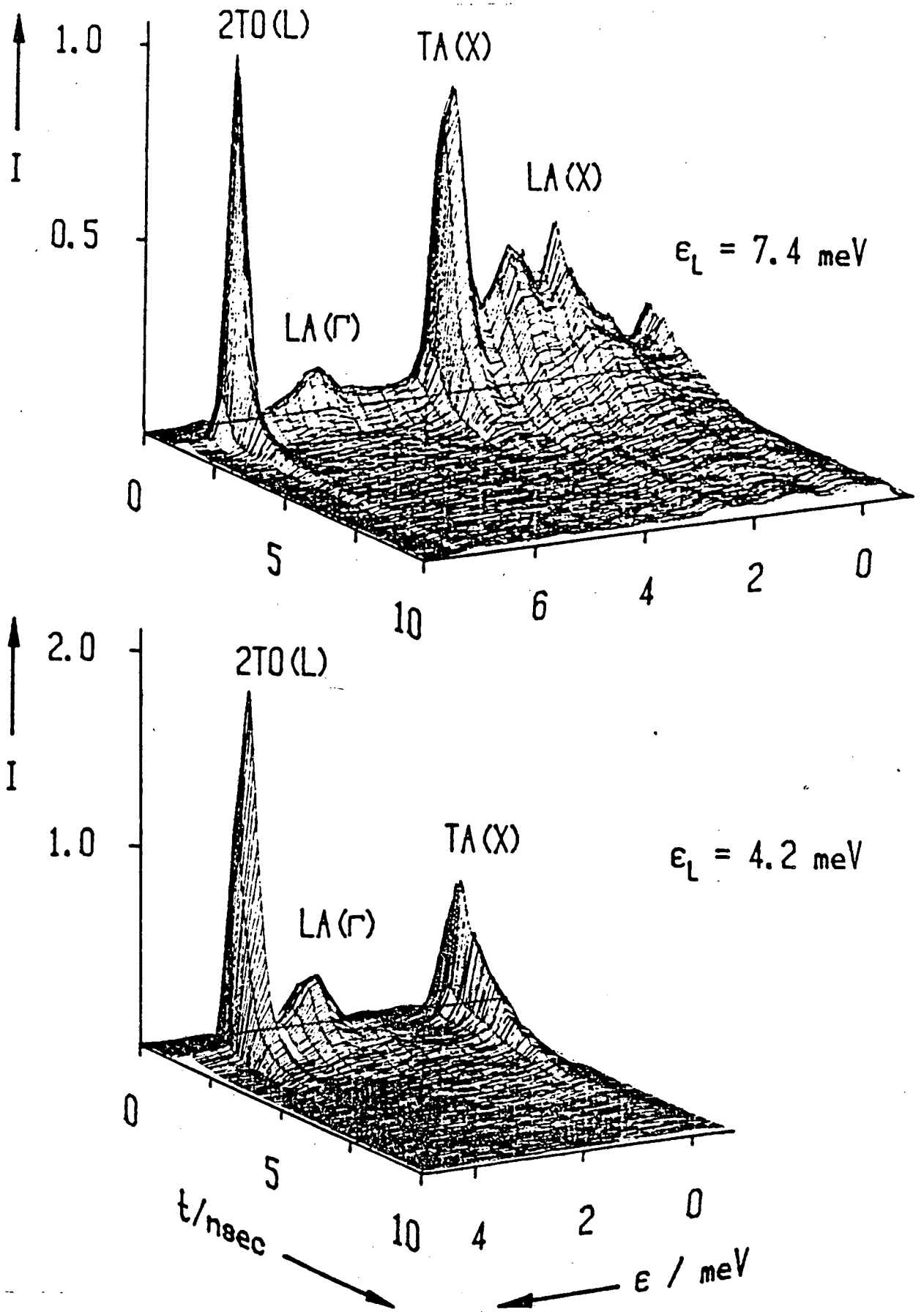
1.0
I
0.5
2TO(L)
TA(X)
LA(X)
LA(Γ)
ϵ_L = 7.4 meV
0
5
10
6
4
2
0
2.0
I
1.0
2TO(L)
TA(X)
LA(Γ)
ϵ_L = 4.2 meV
0
5
t/naec
10
4
2
0
ε / meV

Fig. 15

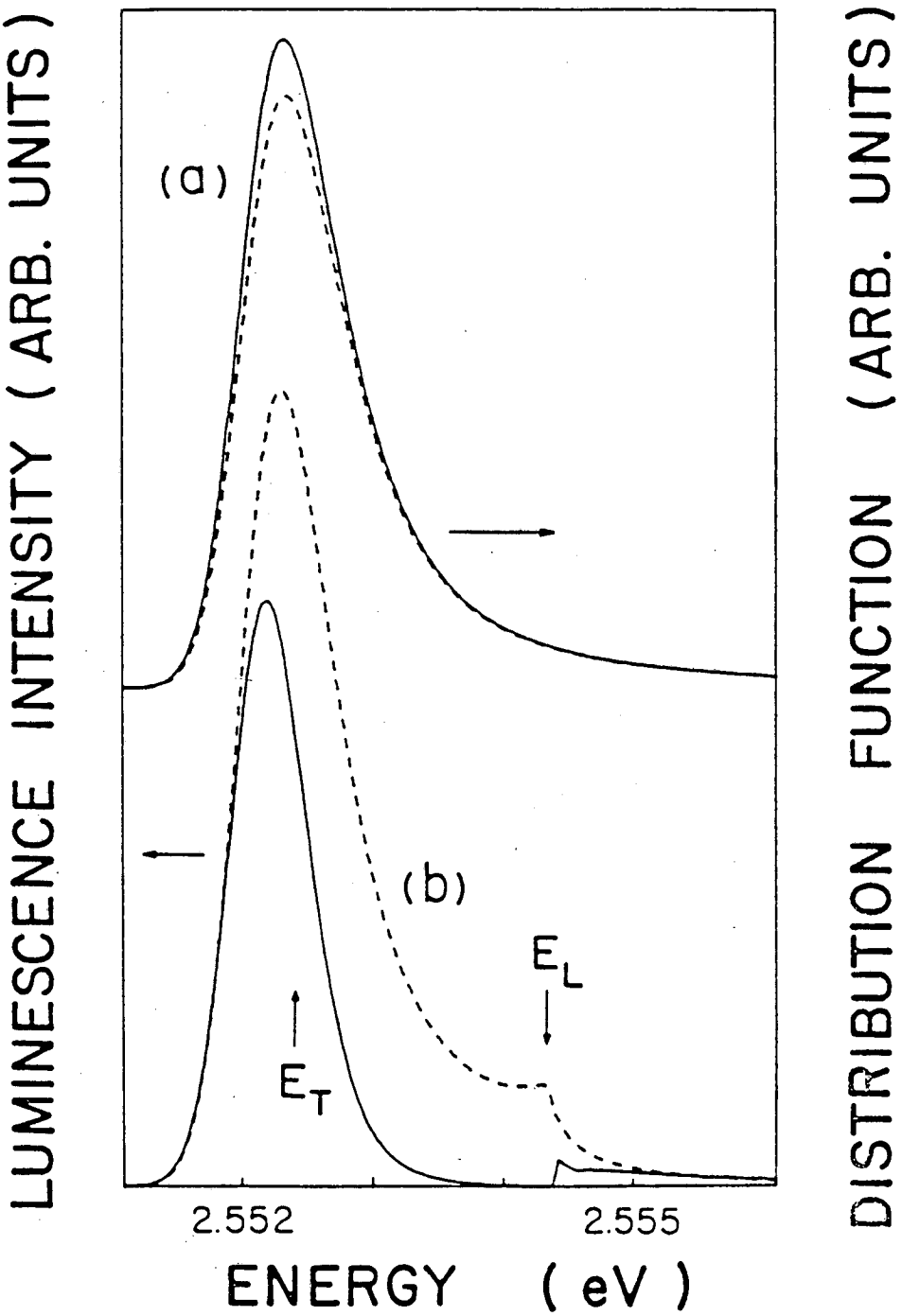
LUMINESCENCE INTENSITY (ARB. UNITS)
DISTRIBUTION FUNCTION (ARB. UNITS)
(a)
(b)
E_L
E_T
2.552
2.555
ENERGY (eV)

Fig. 16

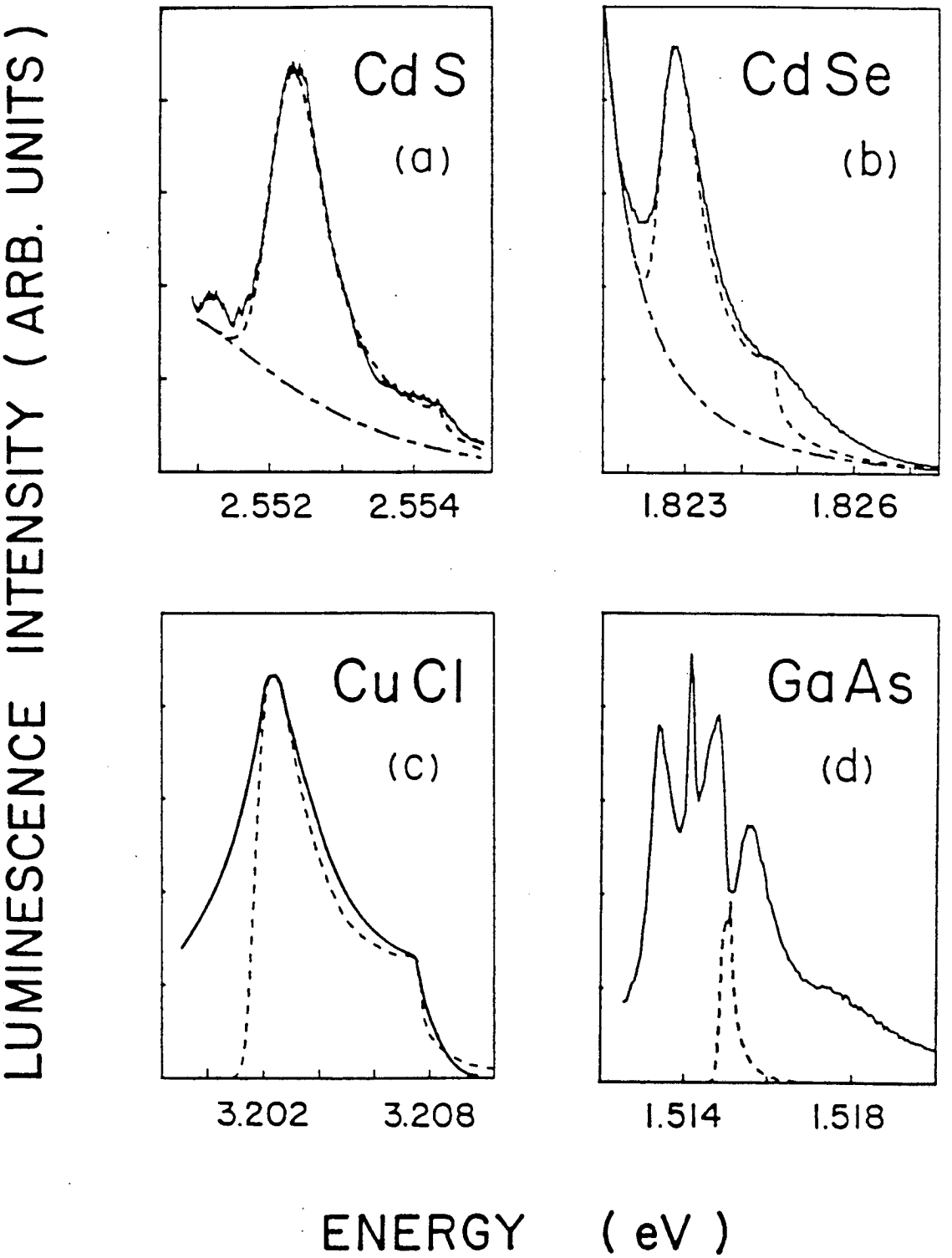
LUMINESCENCE INTENSITY (ARB. UNITS)
CdS
(a)
2.552
2.554
CdSe
(b)
1.823
1.826
CuCl
(c)
3.202
3.208
GaAs
(d)
1.514
1.518
ENERGY (eV)

Fig. 17

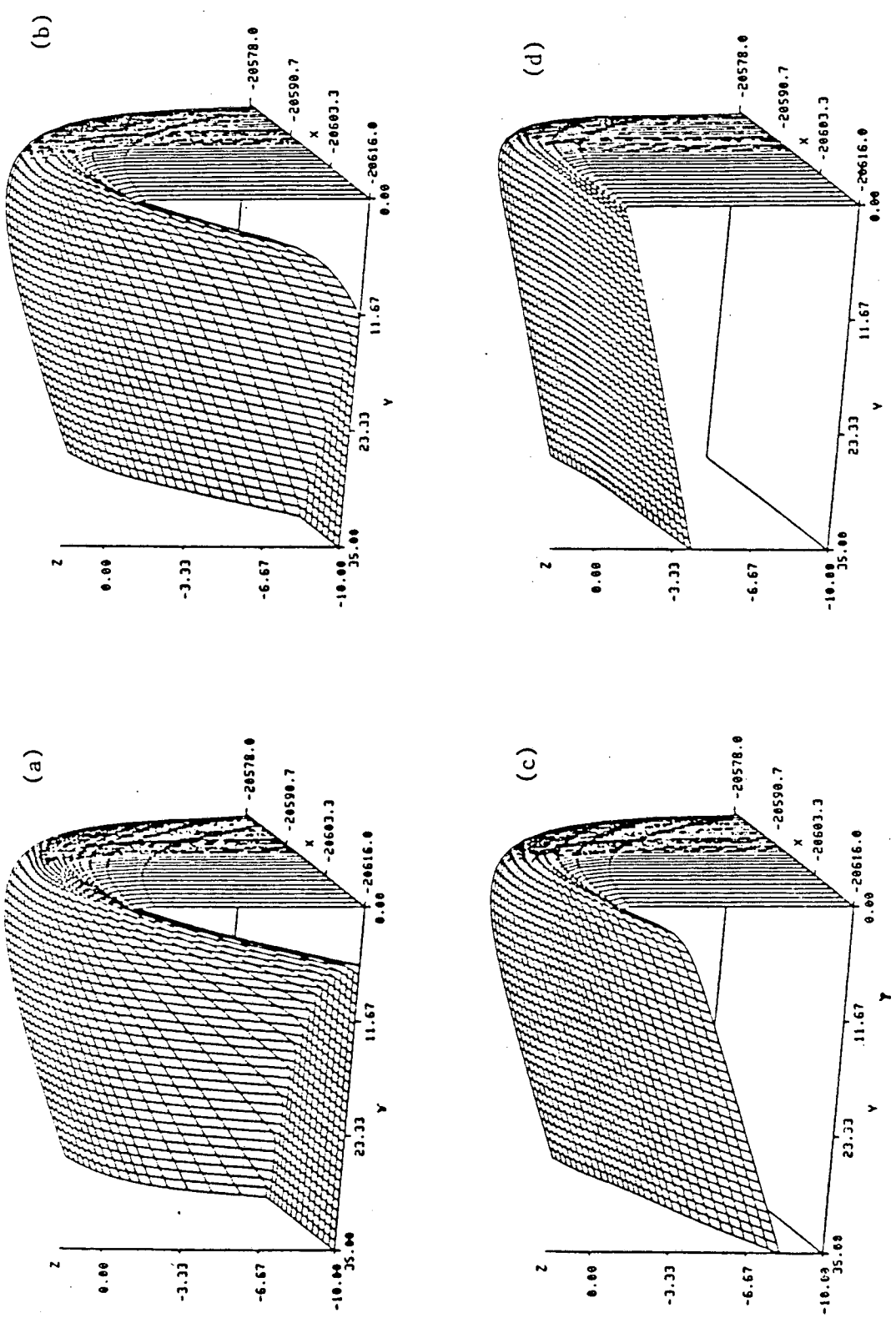
(a)
(b)
(c)
(d)
-20578.0
-20590.7
-20603.3
-20616.0
X
0.00
11.67
23.33
Y
0.00
-3.33
-6.67
-10.00
35.00
Z

Fig. 18

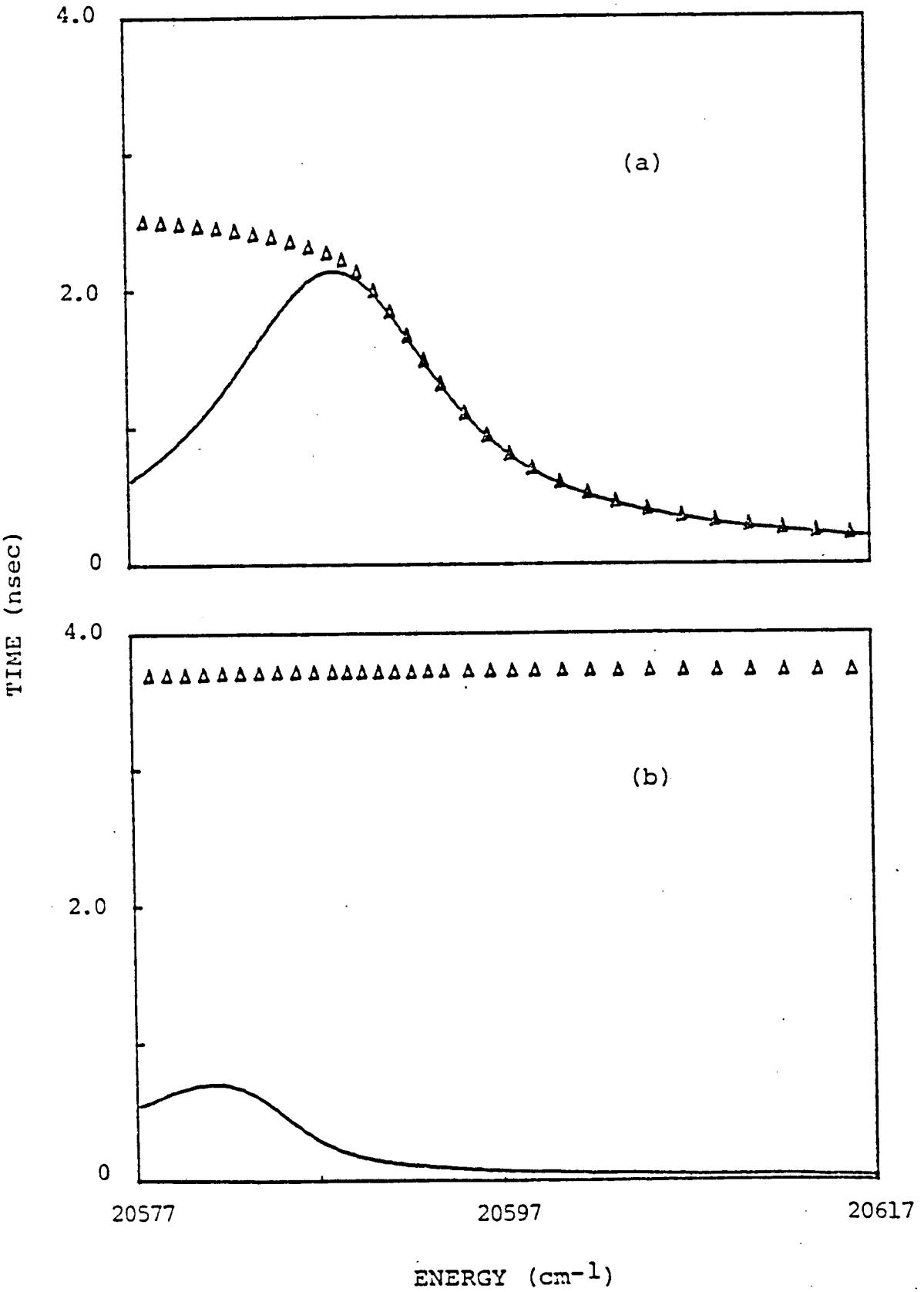

Fig. 19

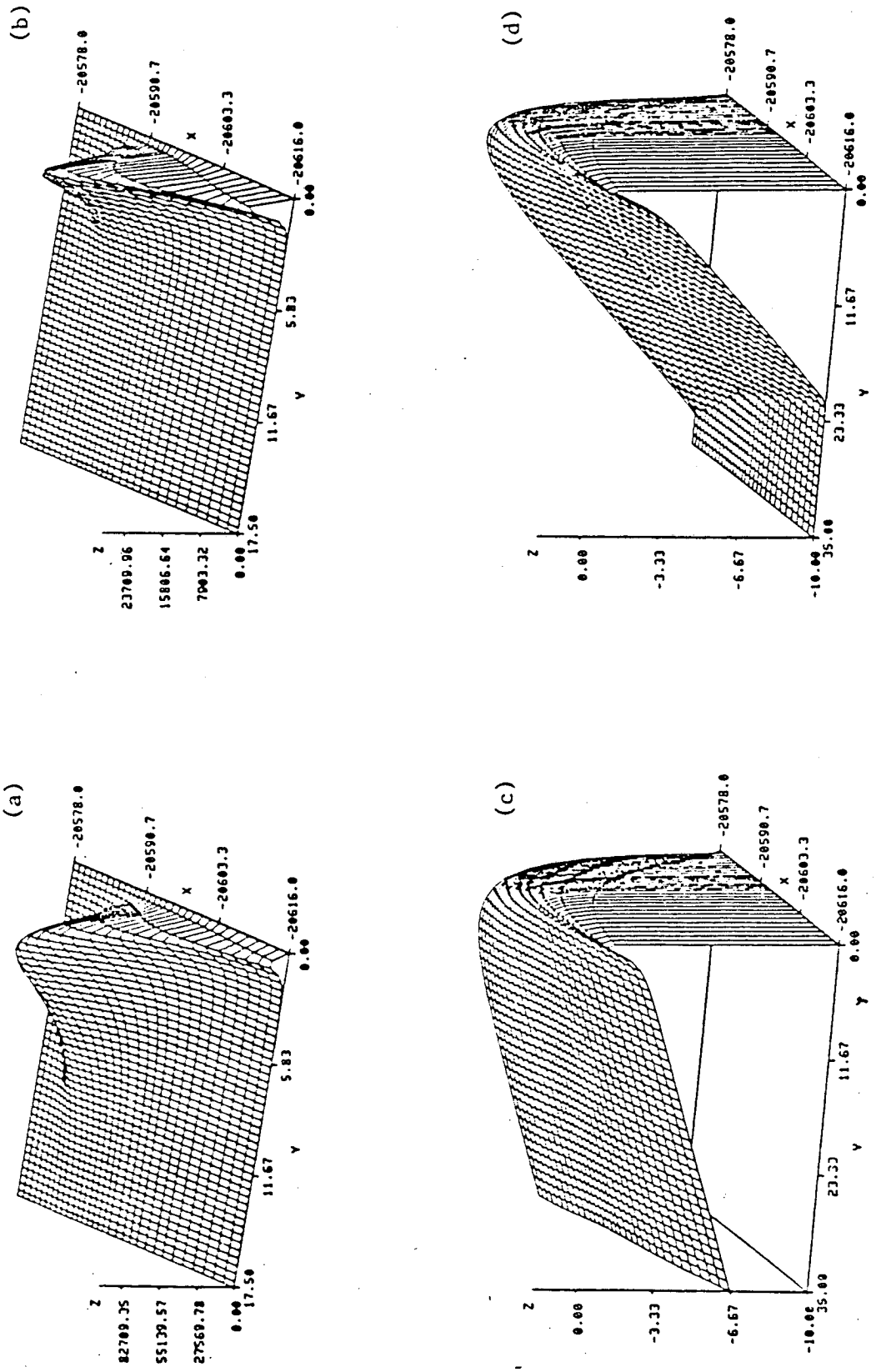
(a)
(b)
(c)
(d)
-20578.0
-20590.7
-20603.3
-20616.0
X
Y
Z
5.83
11.67
17.50
23.33
35.00
0.00
-3.33
-6.67
-10.00
82709.35
55139.57
27569.78
23709.96
15806.64
7903.32

Fig. 20

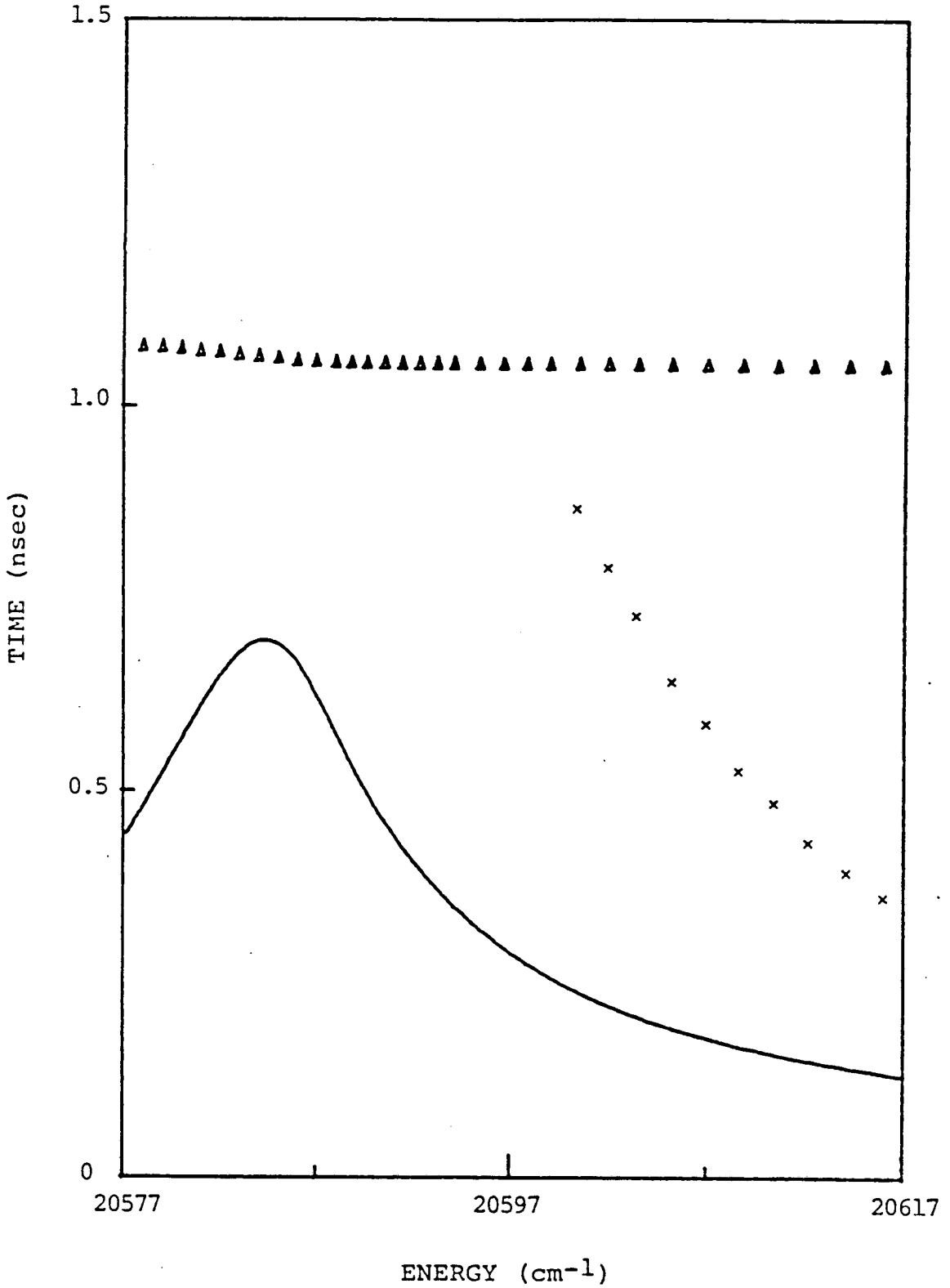

Fig. 21

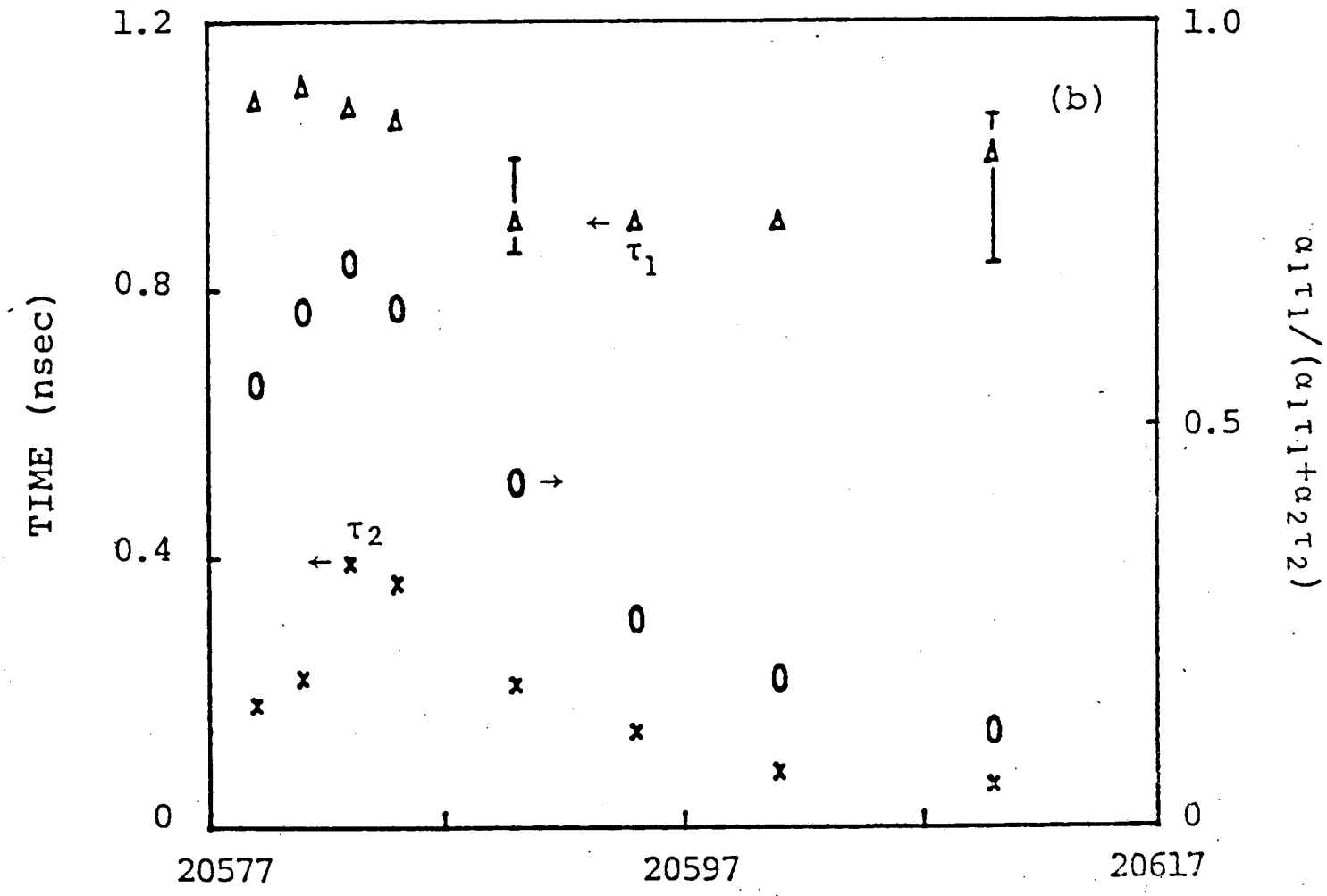
1.2
0.8
0.4
0
TIME (nsec)
1.0
0.5
0
$\alpha_1\tau_1/(\alpha_1\tau_1+\alpha_2\tau_2)$
(b)
τ_1
τ_2
20577
20597
20617

Fig. 22

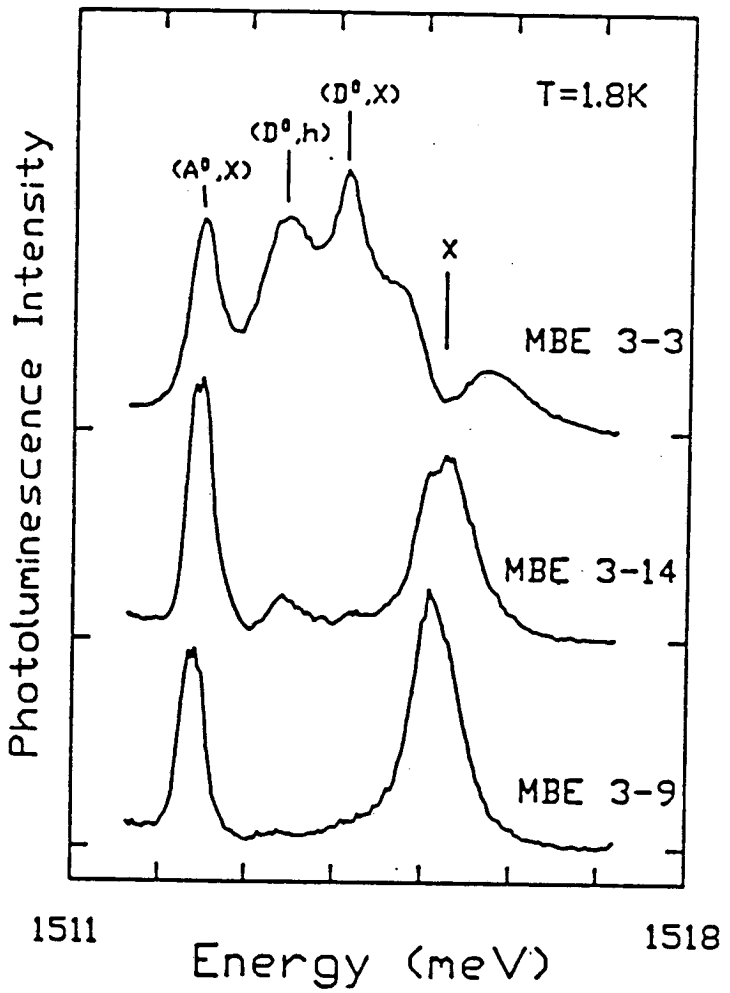
(D°,X)
T=1.8K
(D°,h)
(A°,X)
X
MBE 3-3
MBE 3-14
MBE 3-9
Photoluminescence Intensity
1511
1518
Energy (meV)

Fig. 23

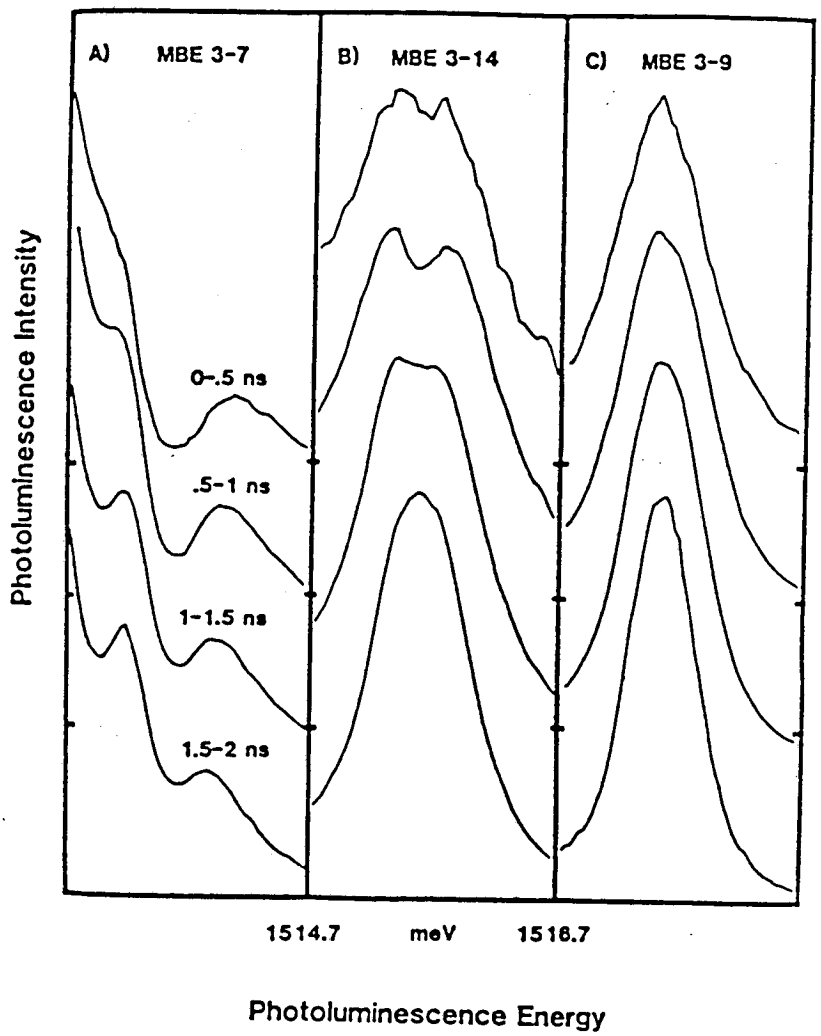
A) MBE 3-7
B) MBE 3-14
C) MBE 3-9
0-.5 ns
.5-1 ns
1-1.5 ns
1.5-2 ns
Photoluminescence Intensity
1514.7
meV
1516.7
Photoluminescence Energy

Fig. 24

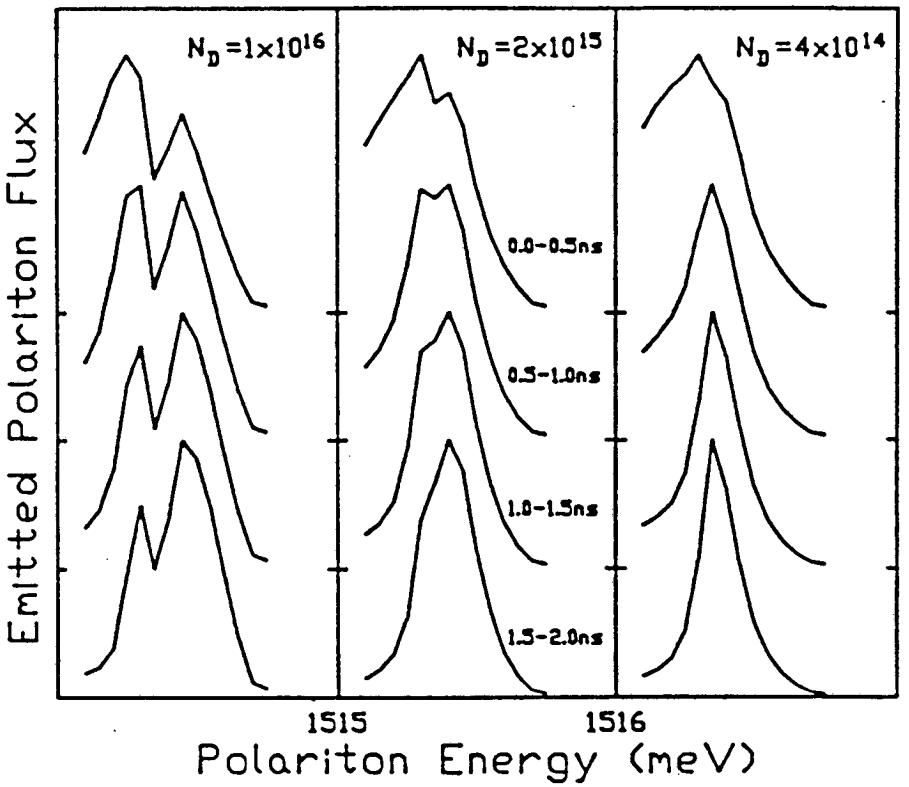
$N_D=1\times10^{16}$
$N_D=2\times10^{15}$
$N_D=4\times10^{14}$
0.0-0.5ns
0.5-1.0ns
1.0-1.5ns
1.5-2.0ns
Emitted Polariton Flux
1515
1516
Polariton Energy (meV)

Fig. 25

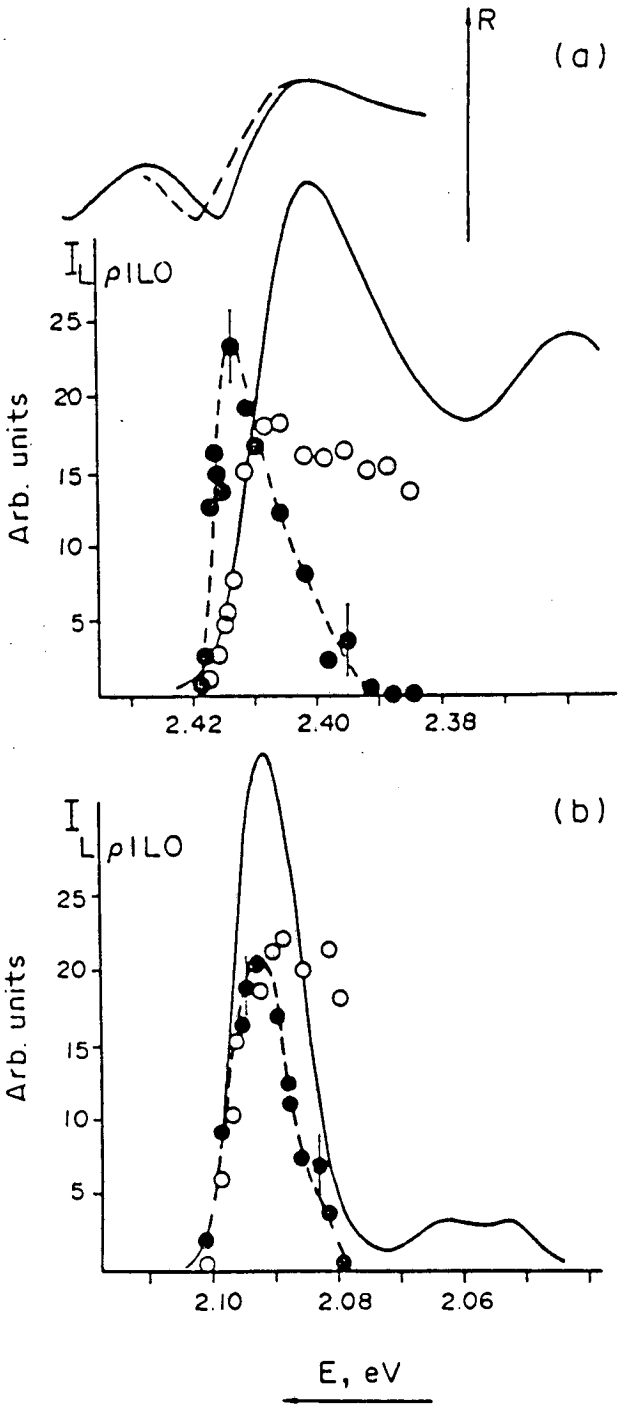
R
(a)
I_L ρ1LO
Arb. units
25
20
15
10
5
2.42
2.40
2.38
(b)
I_L ρ1LO
Arb. units
25
20
15
10
5
2.10
2.08
2.06
E, eV

Fig. 26

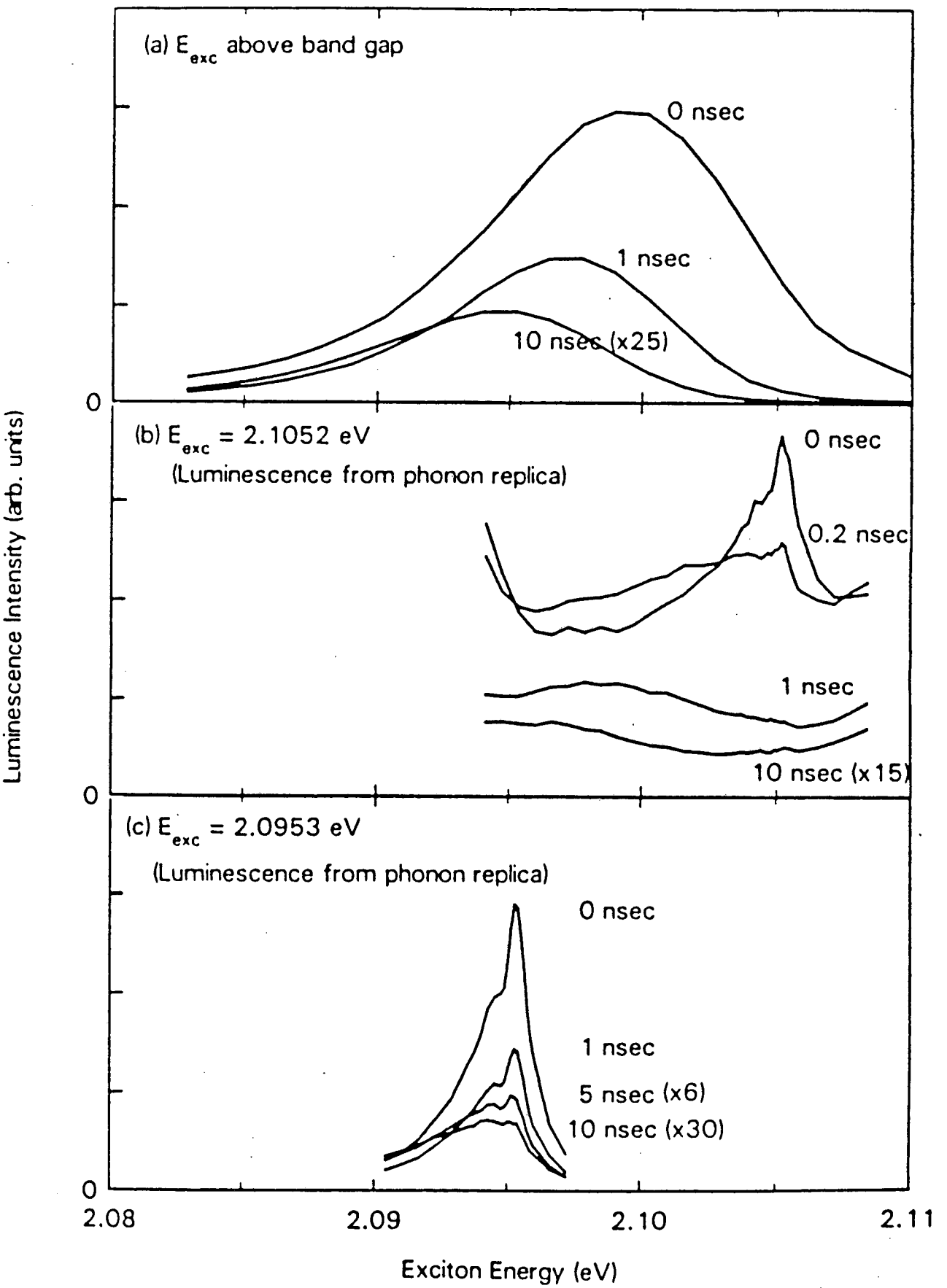
(a) E_{exc} above band gap
0 nsec
1 nsec
10 nsec (x25)
0
(b) E_{exc} = 2.1052 eV
(Luminescence from phonon replica)
0 nsec
0.2 nsec
1 nsec
10 nsec (x15)
0
(c) E_{exc} = 2.0953 eV
(Luminescence from phonon replica)
0 nsec
1 nsec
5 nsec (x6)
10 nsec (x30)
0
2.08
2.09
2.10
2.11
Exciton Energy (eV)
Luminescence Intensity (arb. units)

Fig. 27

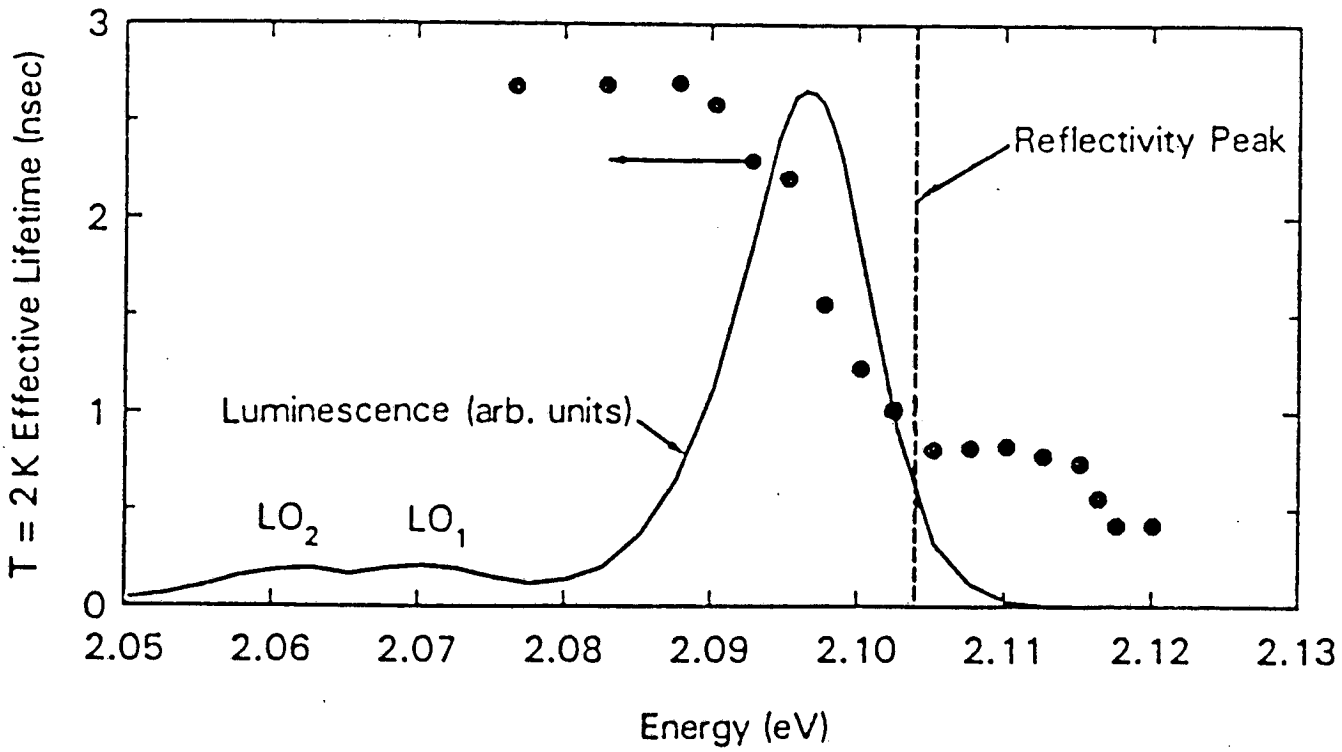
T = 2 K Effective Lifetime (nsec)
3
2
1
0
Luminescence (arb. units)
LO2
LO1
Reflectivity Peak
2.05
2.06
2.07
2.08
2.09
2.10
2.11
2.12
2.13
Energy (eV)

Fig. 28

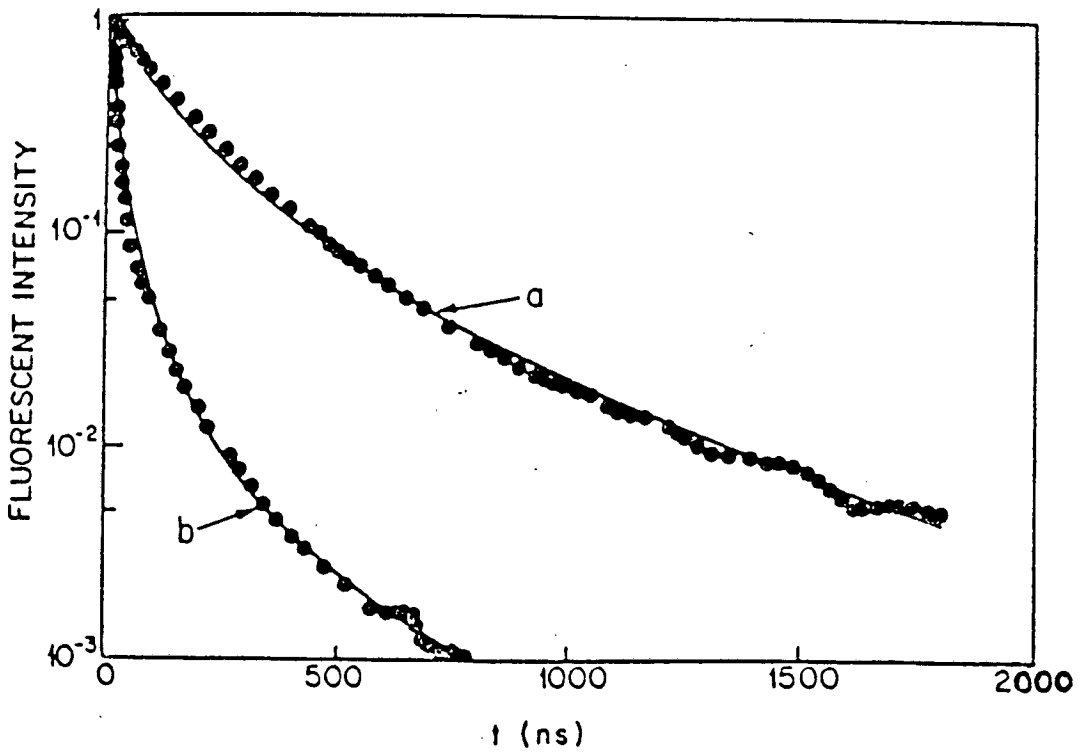
FLUORESCENT INTENSITY
1
10^{-1}
10^{-2}
10^{-3}
a
b
0
500
1000
1500
2000
t (ns)

Fig. 29

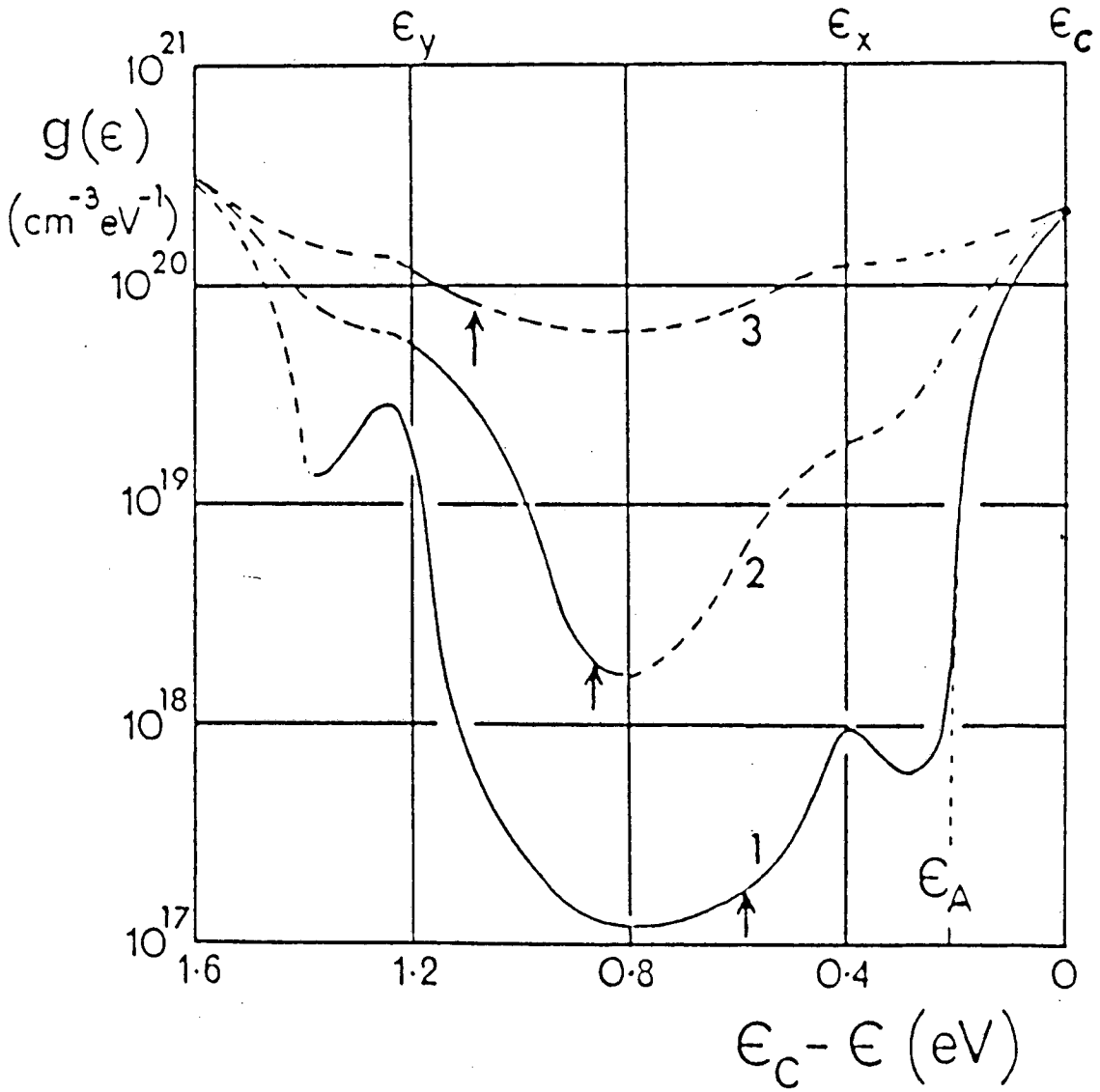
ϵ_y
ϵ_x
ϵ_c
10^{21}
$g(\epsilon)$
$(cm^{-3}eV^{-1})$
10^{20}
10^{19}
10^{18}
10^{17}
3
2
1
ϵ_A
1·6
1·2
0·8
0·4
0
$\epsilon_c - \epsilon$ (eV)

Fig. 30

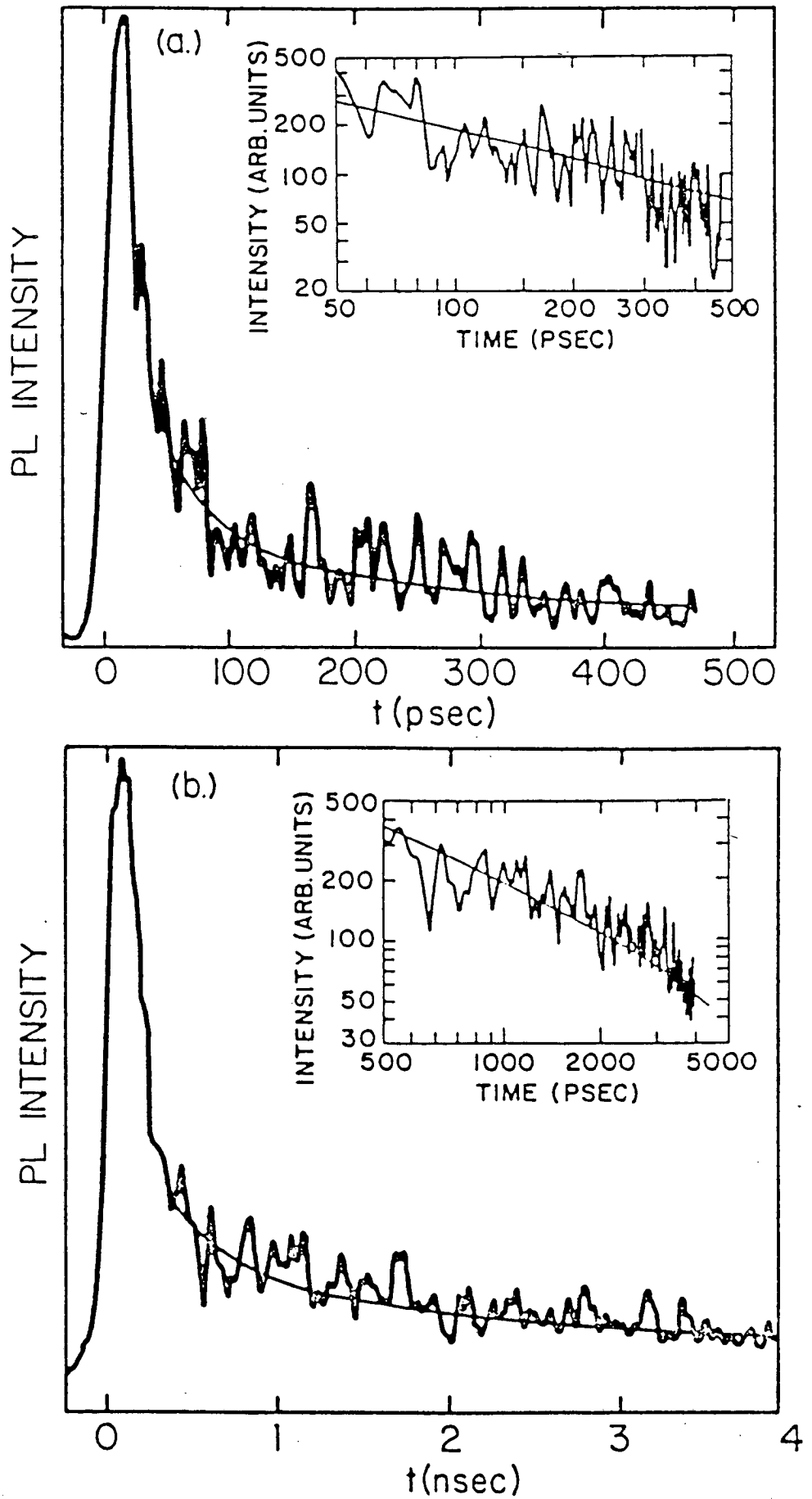
(a.)
PL INTENSITY
INTENSITY (ARB.UNITS)
500
200
100
50
20
50
100
200
300
500
TIME (PSEC)
0
100
200
300
400
500
t (psec)
(b.)
PL INTENSITY
INTENSITY (ARB.UNITS)
500
200
100
50
30
500
1000
2000
5000
TIME (PSEC)
0
1
2
3
4
t(nsec)

Fig. 31

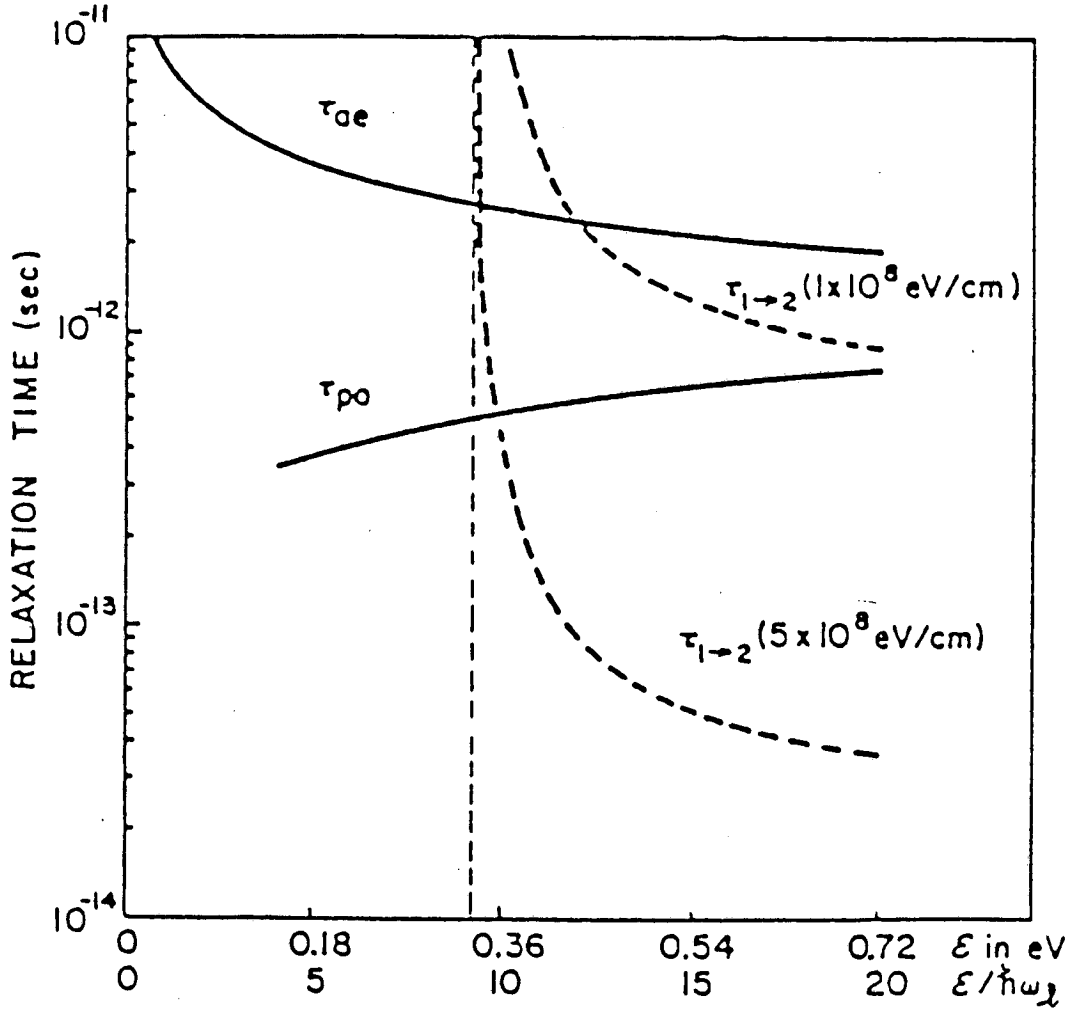
RELAXATION TIME (sec)
10^{-11}
10^{-12}
10^{-13}
10^{-14}
τ_{ae}
τ_{po}
$\tau_{1\to2}(1\times10^{8}$ eV/cm)
$\tau_{1\to2}(5\times10^{8}$ eV/cm)
0
0.18
0.36
0.54
0.72
$\mathcal{E}$ in eV
0
5
10
15
20
$\mathcal{E}/\hbar\omega_\ell$

Fig. 32

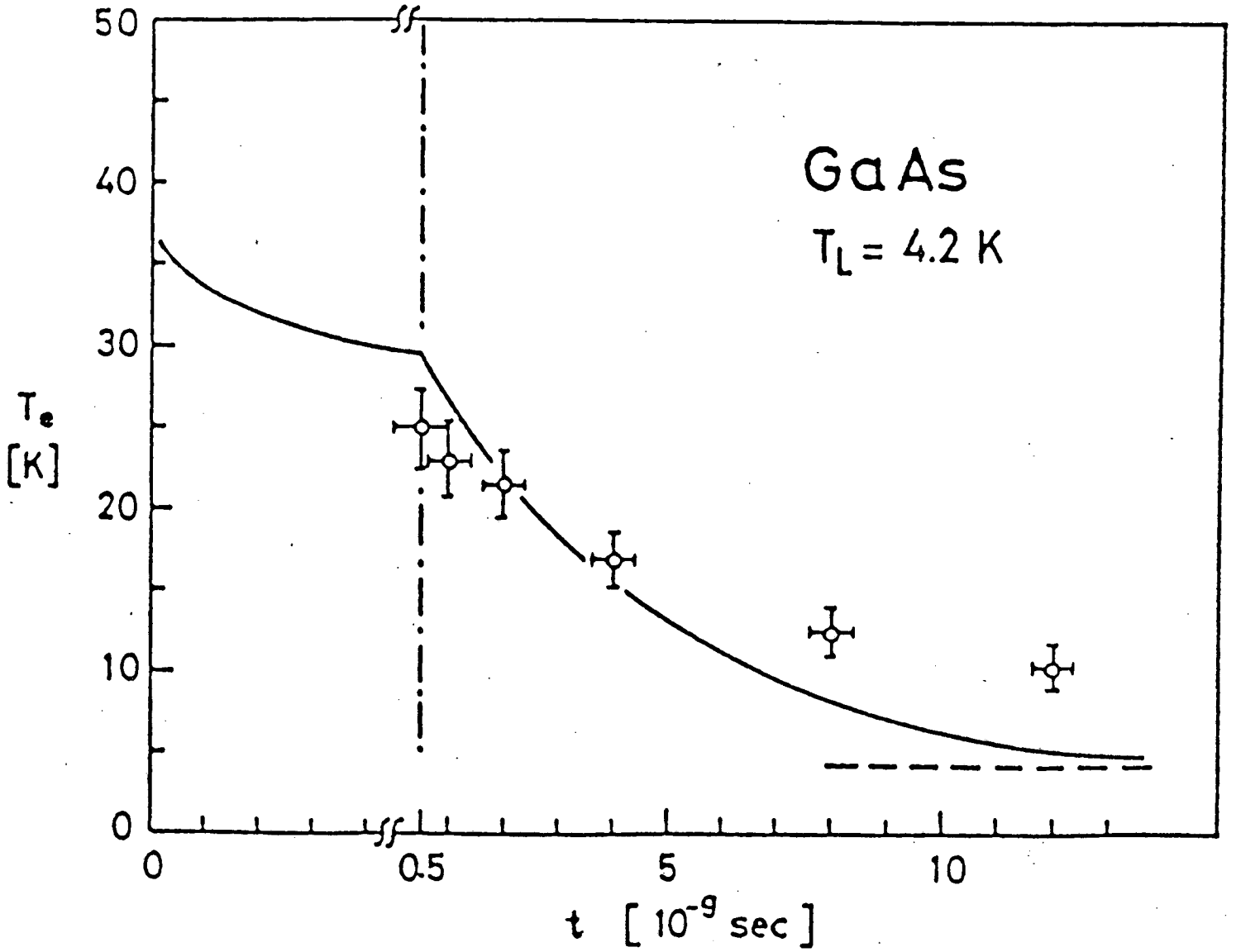

Fig. 33

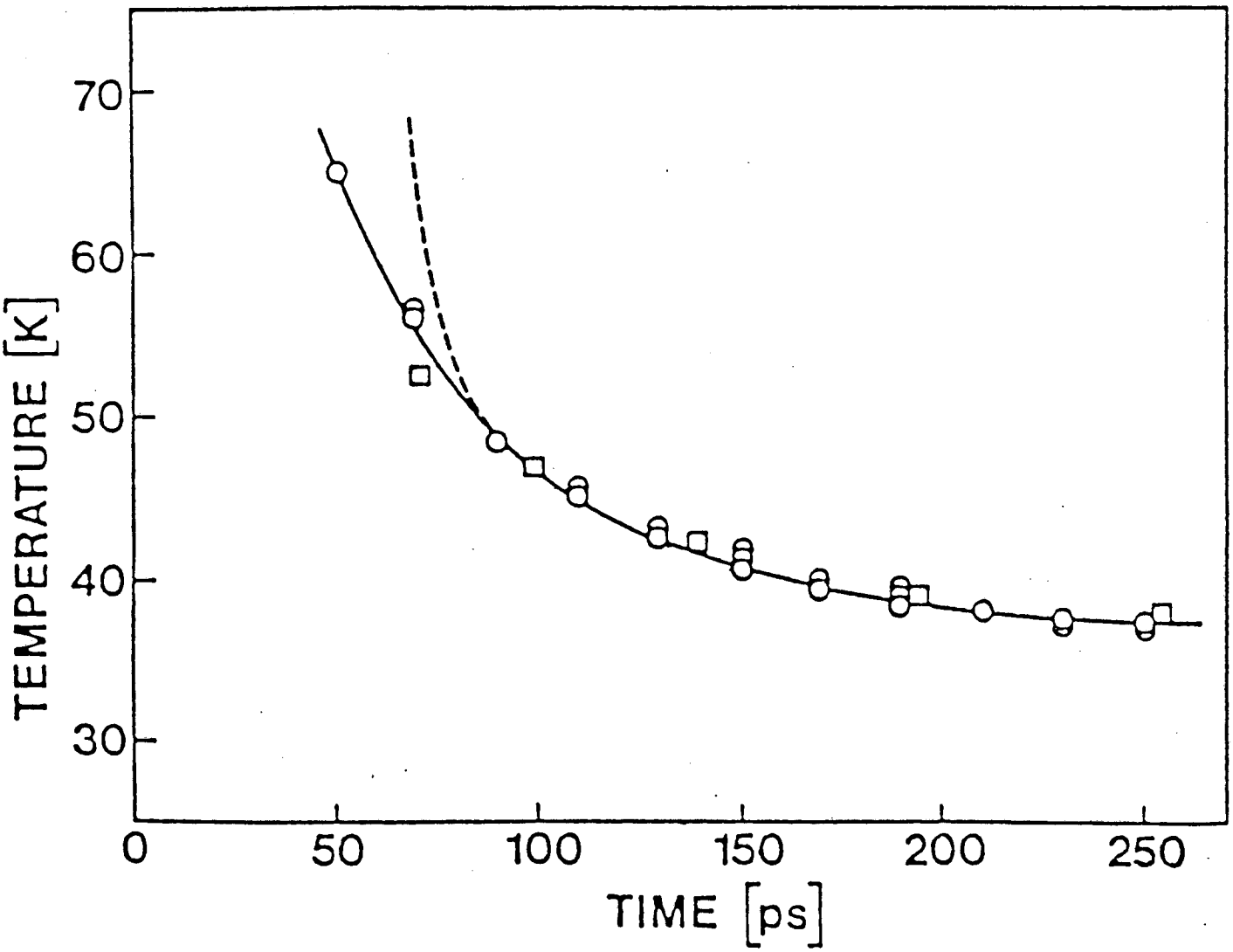

Fig. 34

LAWRENCE BERKELEY LABORATORY
TECHNICAL INFORMATION DEPARTMENT
UNIVERSITY OF CALIFORNIA
BERKELEY, CALIFORNIA 94720